1-1-2014

Characterization Of Initial Iron Binding Location And The Structure/iron Binding Site On S.cerevisiae Isu And On D.melanogaster Frataxin

Andria V. Rodrigues
Wayne State University,

CHARACTERIZATION OF INITIAL IRON BINDING LOCATION AND THE STRUCTURE/IRON BINDING SITE ON *S. CEREVISIAE* ISU AND ON *D. MELANOGASTER* FRATAXIN

by

ANDRIA V. RODRIGUES

DISSERTATION

Submitted to the Graduate School

of Wayne State University,

Detroit, Michigan

in partial fulfillment of the requirements

for the degree of

DOCTOR OF PHILOSOPHY

2015

MAJOR: BIOCHEMISTRY AND
MOLECULAR BIOLOGY

Approved by:

Advisor Date

DEDICATION

To my Family

ACKNOWLEDEMENTS

When I finished my Masters degree in 2007 I was certain that I was done with higher education. Moving across continents to get a PhD. seemed absurd. Through two years of having a regular job, the idea of attempting a PhD. seemed to get better and better. I remember boarding my flight to Detroit in 2009 wondering if things would work out. When I look back now, 5 years later, I am thankful that it did and there have been several wonderful people along my journey who I would like to thank right now:

I would like to begin by thanking my PhD. advisor Dr. Timothy Stemmler for giving me the opportunity to work in your laboratory. The art of scientific thinking took a while for me to develop (and is still a work in progress) and I would like to thank you for your patience and mentorship. This journey has been an immense learning experience for me and when I look back now at the years gone by, I am filled with nothing but gratitude. I would also like to thank my committee members Dr. Pamela Riggs-Gelasco, Dr. Brian Edwards and Dr. David Evans for agreeing to be a part of my committee and providing me with great suggestions and encouragement through the years. All three of you have also taught me at some point, be it learning to run XAS beamlines at the synchrotron (with Dr. Riggs-Gelasco), being guided at journal club (with Dr. Edwards) and learning to solve massive enzyme kinetics problems (with Dr. Evans), I thank each of you for your time. I would especially like to thank Dr. Marilynn Doscher, our department graduate officer during the year I joined, not just for accepting me into the program but also for making sure I settled into Detroit well and had everything I needed to embark on this long journey. For a foreign person like me in a new country, her

warmth and welcoming attitude was immensely comforting. I would also like to thank Dr. C.P. Lee for being a strong supporter of all-round student development and for advocating and making it possible for us students to present our work at good conferences. On the same note, I would like to thank all faculty and students in the BMB Department, each who have at some point either taught me and/ or provided me with valuable suggestions and encouragement. In addition, I would also like to thank the administrative staff in the BMB office: Yanna Marsh, Rose Cooper, Joe Fiore and April Wolak for their support, the WSU Graduate school and the WSU Office of International Students for their support through the years. I would also like to thank Dr. Stemmler's collaborators Dr. Andrew Dancis (U. Pennsylvania), Dr. Todd Harrop (U. Georgia), Dr. Sarah Michel (U. Maryland) and Dr. Joseph Brunzelle (Northwestern U.) for the opportunity to work with you and contribute to some great scientific work.

Next, I would like to thank my awesome lab-mates, past and present. I have learned much from you all and I would especially like to thank each of you for making the lab environment a fun place to work in. I would also like to thank Lindsey Thompson for being an awesome lab manager. I would like to thank my friends and fellow PhD. graduates who have gone ahead of me: Sandhya Muralidharan, who has been a good friend and mentor even until today, Amruta Jambekar with whom I explored the ins & outs and happenings around the city of Detroit and Poorna Subramanian who became a complex mix of a friend, a lab-mate and then next-door-neighbor all rolled into one. In short, it was a blast with you all and I miss your presence in Detroit. I would also like to thank my friends Shyamalee Kandegedara and Asmita Vaishnav who have been great

sources of both: practical scientific knowledge and basic life-lessons. I thank you both for your care and being a listening ear.

I'd like to thank my family; my parents Lazaro and Ana-Maria for ready words of encouragement in all circumstances of my life, and, my brother Oliver & sister Mercedes who have been pseudo parent-like creatures to me, yet friends and who have always been great sources of advice and support. I would also like to thank my extended family, my late grandmothers, aunts, uncles and cousins, all who have been a positive influence in my life.

Finally, I thank God for this life and the strength to face each new day.

TABLE OF CONTENTS

Dedication ii

Acknowledgements iii

List of Tables x

List of Figures xi

CHAPTER 1 – IRON CHAPERONES FOR MITOCHONDRIAL IRON-SULFUR CLUSTER BIOSYNTHESIS AND FERRITIN IRON STORAGE 1

1.1 Prelude 1

1.1.1 The need for metallochaperone proteins 3

1.2 Abstract 5

1.3 Introduction 5

1.4 Fe-S cluster biosynthesis iron chaperones 8

1.5 Ferritin iron chaperones 14

1.6 Conclusions 17

1.7 Acknowledgements 18

1.8 References 18

CHAPTER 2 – IRON BINDING AND INITIAL METAL LOADING SITE ON THE ISU SCAFFOLD PROTEINS 27

2.1 Prelude 27

2.2 Abstract 28

2.3 Introduction 29

2.4 Materials & Methods 31

2.4.1 Protein Expression & Purification 31

2.4.2 Isothermal Titration Calorimetry experiments & analysis 34

2.4.3 XAS sample preparation & analysis 35

2.4.4 Mössbauer Spectroscopy sample preparation & data analysis 37

2.5 Results 38

2.5.1 Isu proteins directly bind iron 38

2.5.2 Iron coordination geometry of ISU proteins 41

2.5.3 Metal site electronic structure by Mössbauer Spectroscopy 46

2.6 Discussion 46

2.7 Acknowledgements 52

2.8 References 53

CHAPTER 3 – IDENTIFICATION OF A PUTATIVE IRON BINDING SITE ON THE C-TERMINUS OF YEAST IRON SULFUR CLUSTER SCAFFOLD PROTEIN ISU & IMPLICATIONS FOR IRON DELIVERY BY FRATAXIN 57

3.1 Prelude 57

3.2 Abstract 58

3.3 Introduction 59

3.4 Materials & methods 62

3.4.1 Site directed mutagenesis & protein expression 63

3.4.2 Protein purification 63

3.4.3 Far UV circular dichroism experiments & analysis 66

3.4.4 Isothermal titration calorimetry experiments & analysis 68

3.4.5 Competition assay & analysis.....69

3.4.6 Differential scanning calorimetry experiments & analysis 70

3.4.7 Near UV circular dichroism for assembly activity 71

3.5 Results.....72

3.5.1 Mutant proteins have a similar fold as wild-type (WT) Yisu1.....72

3.5.2 Yisu1 mutants show a decreased Fe(II) binding affinity 75

3.5.3 Thermal stability of Yisu1 proteins by differential scanning calorimetry 79

3.5.4 Yisu1 mutants show altered holo-Yfh1WT binding.....83

3.5.5 Yisu1 mutant shows altered Fe-S assembly activity 87

3.6 Discussion 89

3.7 Acknowledgements 96

3.8 References 97

CHAPTER 4 – DROSOPHILA FRATAXIN CRYSTAL STRUCTURE, RESONANCE ASSIGNMENTS AND PUTATIVE IRON BINDING RESIDUES..... 102

4.1 Prelude 102

4.2 Abstract..... 103

4.3 Introduction..... 104

4.4 Materials and methods 106

4.4.1 Labeling, expression and purification of Drosophila frataxin (Dfh) 106

4.4.2 Crystallization and determination of apo Dfh structure..... 108

4.4.3 NMR Spectroscopy on apo and holo Dfh 111

4.4.4 Assignments and data deposition 112
4.5 Results 113
4.5.1 Crystal structure of Dfh 113
4.5.2 Dfh backbone resonance assignments 117
4.5.3 Mapping of the putative iron binding residues on Dfh 122
4.6 Discussion 125
4.7 Acknowledgements 128
4.8 References 129

CHAPTER 5 – SUMMARY & CONCLUSIONS 134
5.1 Significance of Iron in health 134
5.2 Summary & Future Directions 135
5.3 Conclusion 142
5.4 References 143

ABSTRACT 146
AUTOBIOGRAPHICAL STATEMENT 148

LIST OF TABLES

Table 2.1 Fe(II) binding affinities of ISU proteins 40

Table 2.2 Summary of EXAFS fitting results for Fe bound ISU proteins 43

Table 2.3 Analysis of Mössbauer parameters for Fe(II) bound to ISU proteins 48

Table 3.1 List of primers used for site directed mutageneses 65

Table 3.2 Masses of WT YIsu1 and mutants 67

Table 3.3 Secondary structural features for YIsu1 proteins from simulated raw CD spectra 74

Table 3.4 K_D values obtained from Mag-fura-2 values for Fe(II) binding YIsu1 proteins 78

Table 3.5 Thermodynamic parameters of melting of WT YIsu1 and mutant proteins 82

Table 3.6 Average simulation results using ITC analysis for WT YIsu1 and mutant proteins 85

Table 4.1 Dfh crystallography data collection and refinement statistics 110

LIST OF FIGURES

Figure 1.1 Major pathways for iron incorporation/ utilization within a cell.....9

Figure 1.2 Molecular details of the two Fe^{2+} binding sites on Yfh1 and Isu1.....13

Figure 1.3 Structural Details of PCBP as a ferritin iron chaperone.....16

Figure 2.1 Sequence alignment of Isu proteins.....33

Figure 2.2 Fe (II) binding to ISU proteins by Isothermal Titration Calorimetry.....39

Figure 2.3 EXAFS and fourier transforms of iron loaded ISU XAS data.....42

Figure 2.4 XANES spectrum of Fe (II) bound to WT YIsu1.....45

Figure 2.5 Mössbauer spectra of ISU proteins.....47

Figure 3.1 Amino acid sequence comparison of C-terminal region of Isu orthologs.....64

Figure 3.2 Far UV circular dichroism spectra of apo WT YIsu1 and mutants.....73

Figure 3.3 Fe (II) titration of Mag-fura-2 and YIsu1 proteins.....77

Figure 3.4 Denaturation curves for apo & holo YIsu1 proteins.....81

Figure 3.5 Isothermal Titration Calorimetry of Holo Yfh1WT with YIsu1 proteins.....84

Figure 3.6 Fe-S assembly activity of WT YIsu1 and mutant D145A.....88

Figure 4.1 SDS-PAGE gel showing purified *Drosophila* frataxin..... 109

Figure 4.2 Crystal structure of *Drosophila* frataxin homolog (Dfh)..... 114

Figure 4.3 Clustal- ω sequence alignment between frataxin orthologs..... 115

Figure 4.4 Assigned ^{15}N HSQC spectrum of Dfh..... 118

Figure 4.5 Summary of proposed secondary structural elements for Dfh..... 120

Figure 4.6 Consensus secondary structure prediction..... 121

Figure 4.7 Overlay of 2D ^{1}H-^{15}N HSQC spectra for Dfh 123

Figure 4.8 Putative Fe (II) binding residues on Dfh 124

Figure 5.1 Multiple sequence alignments of YIsu1 C-terminal truncation mutants..... 140

CHAPTER 1
IRON CHAPERONES FOR MITOCHONDRIAL IRON-SULFUR CLUSTER BIOSYNTHESIS AND FERRITIN IRON STORAGE

1.1 Prelude:

The need for transition metals spans every living organism from viruses to human beings. Cells traffic several transition metals to meet their dietary demand, but the minerals that are absolutely required include the essential metals Fe, Zn, Cu, Mo, Co, Mn, Cr, V and Ni [1]. Cells can also traffic additional metals, including Cd, Hg, Au and Ag, however these are not required for cellular vitality and are effectively cleared out of the cell to prevent toxicity [2]. The complement of metals required by cells is generally influenced by their geochemical availability [3], and it has been estimated that approximately a third to a fourth of all characterized proteins require metals for function [2]. The unique physical and chemical properties of each metal are exploited during their incorporation into metalloproteins, and the coordination chemistry specific to the metal drives formation of the protein-metal complex. This permits metal bound proteins to participate in several capacities that may be structural, catalytic or regulatory in nature [4].

Although indispensible to sustain life, metals are also cytotoxic, owing to their ability to initiate free radical reactions that can harm cellular components. Therefore metal concentrations are tightly regulated by a battery of proteins that accomplish metal homeostasis. Proteins that serve in this capacity include integral membrane transporters, metalloregulatory sensors, diffusible metallochaperone proteins and metal

storage proteins. Studies of the amount of transition metals in *E. coli* have shown that Zn & Fe are the most abundant with concentrations maintained at 0.1M, while Cu, Mn and Se are maintained at 0.01M and V, Co & Ni are much lower in abundance [4]. Protein affinities for divalent metal ions follow the Irving Williams series, beginning with the weakest binding to the tightest, in the following order: $Mn^{2+}<Fe^{2+}<Co^{2+}<Ni^{2+}<Cu^{2+}>Zn^{2+}$ [5]. In spite of the fact that higher affinity metals can outcompete others for protein binding sites, in most cases proteins are loaded with the correct metal. Loading is accomplished by several factors including:

A) Geometry: The metal may be inclined to bind the protein due to the availability of the correct ligands, the right size of metal binding site and matching charges & solvation energy that provide the metal bound protein with greater stability.

B) Function: In many cases proteins attain their biologically active conformation only after binding the correct metal. Often, proteins improperly loaded with the wrong metal exhibit an incorrect fold, exposing residues that are recognized by chaperone proteins that bring about insertion of the correct metal or, they may be targeted for degradation.

C) Compartmentation of Proteins: The compartment/organelle that the protein folds within also influences its metal binding as the complement of proteins involved in metal insertion may differ between compartments. Once folded, the metal binding site may be buried within the protein to prevent metal exchange with higher affinity metals.

D) Protein delivery by metallochaperones: Some proteins are metallated via specific protein-protein interactions directed by metallochaperone proteins that deliver the specific metal to the protein [2, 4, 6].

1.1.1 The need for metallochaperone proteins:

Efficient and selective metal delivery is essential for proper metal homeostasis and this chapter specifically highlights the role of metallochaperone proteins in this process. Metallochaperones are diffusible proteins that bind metal ions and escort them to partner proteins where they are delivered and transferred for incorporation as metal cofactors into the apoprotein [4]. Chaperone proteins protect the metal from participating in the generation of free radicals and hence protect the cell from potential damage caused by free radicals. Metallochaperone proteins may operate in the cytosol or in a subcellular compartment and they may even be found in circulation. As an example, iron chaperones described so far include the human cytosolic PCBP family of proteins, the mitochondrial iron chaperone protein frataxin (both of which have been described in the review below), and the protein transferrin that 'chaperones' Fe^{3+} in the blood [7]. Chaperones may activate proteins through direct metal insertion converting the protein into its active holoform [8]. In addition, metallochaperones may interact with metal import proteins from which they acquire their metal ions by specific ligand exchange reactions rather than by scavenging metal released into the cytosol [2].

It has been suggested that metal ions are always in the bound form inside the cell. Metals are believed to be either bound to proteins or nucleic acids and other small molecules such that the availability of free metal ions within the cell is far too low for apoproteins to directly acquire them via passive diffusion. Their concentrations are also reported to be 'buffered' keeping the amount of metal constant. For example, in case of high affinity metals such as Cu & Zn, the pool of 'free' Cu has been reported to be about one free ion per cell. Zn efflux pumps are activated when the intracellular Zn concentration reaches 0.5 fM, which corresponds to about one free Zn ion per cell. Under such stringent conditions, cells employ metallochaperone proteins that can incorporate metals using atypical coordination chemistry such that metals are bound with a high affinity, yet can be delivered to recipients via specific protein-protein interactions [4]. However, exchangeable cellular metal pools have also been described for lower affinity metals like iron [6]. How these pools are maintained to achieve metal homeostasis is currently under investigation.

The first chapter of my dissertation is a review that specifically outlines iron homeostasis in health & disease. This chapter provides in-depth insight into the structure-function role of the iron metallochaperone frataxin, that operates in the mitochondria & potentially serves as a source of iron for heme and iron-sulfur cluster biogenesis, and the PCBP family of proteins, that operate in the cytosol and serve as chaperones to Ferritin and other proteins. As my dissertation work is focused on the Fe-S assembly pathway, this review provides the necessary background information

regarding metal delivery for Fe-S cluster bioassembly and relates to the chapters that follow. The bulk of this chapter been published in the following review: *Subramanian, P., Rodrigues, A.V., Ghimire-Rijal, S. and Stemmler, T.L. "Iron chaperones for mitochondrial Fe-S cluster biosynthesis and ferritin iron storage" Curr. Opin. Chem. Biol., 2011 15(2): 312-318.*

1.2 Abstract:

Protein controlled iron homeostasis is essential for maintaining appropriate levels and availability of metal within cells. Recently, two iron chaperones have been discovered that direct metal within two unique pathways: 1) mitochondrial iron-sulfur (Fe-S) cluster assembly and 2) within the ferritin iron storage system. Although structural and functional details describing how these iron chaperones operate are emerging, both share similar iron binding affinities and metal-ligand site structures that enable them to bind and release Fe^{2+} to specific protein partners. Molecular details related to iron binding and delivery by these chaperones will be explored within this review.

1.3 Introduction:

Iron is essential for life and its unique chemical characteristics are often exploited in nature to assist cells in performing inherently complex oxidation chemistry, promote oxygen transport/storage and drive electron transfer pathways [9]. Iron is typically

absorbed into the body through diet [10] and on average, humans absorb 1 to 2 mg of iron from diet each day [11]. Although the amount of iron abstracted from the diet is low, tight regulation of absorbed iron is critical, as humans have no physiologic pathway to excrete metal. Once consumed, over 60% of the iron is incorporated into hemoglobin through developing erythroid precursors and finally into mature red blood cells. A second and third possible fate for Fe includes being directed towards the iron storage protein ferritin or being transferred throughout the body for incorporation into metalloprotein iron cofactor sites. As a cofactor, Fe is often found associated within iron-sulfur (Fe-S) clusters, found as mononuclear Fe-S, 2Fe-2S, 4Fe-4S and other higher nuclearity clusters common to nature [12]. Given the body's need to absorb and maintain appropriate iron levels, Fe reuse and recycling from degraded sources is another method the body uses to maintain iron homeostasis. A simple breakdown in any of these pathways can lead to conditions that are detrimental to human health.

When maintained at balanced levels, iron is essential for cellular and organism viability, however excess is toxic and deficiency leads to a variety of physiological and developmental irregularities[11]. Disorders related to a breakdown in iron homeostasis are among the most common human diseases. Diseases of iron overload are highly prevalent, with the hepatological disorder hereditary hemochromatosis being one of the most common [13]. Hemochromatosis patients absorb two to three times more iron than normal dietary iron levels. Excess iron is often deposited in the liver and redox chemistry performed by unregulated metal can kill the cell/organism. Neuronal iron

accumulation is a phenotype of numerous neurodegenerative disorders (Parkinson's disease, Alzheimer's disease, Friedreich's ataxia, others). In these disorders, unregulated but redox active metal is pooled within specific regions of the brain generating oxidative stress through iron produced reactive oxygen species (ROS) formation [14]. ROS can damage membrane phospholipids and generate reactive aldehydes that damage proteins, leading to accumulation of misfolded protein aggregates. While examples of the toxic effects of iron overload are prevalent, iron deficiency is an even larger human health issue affecting billions [15]. While iron deficiency leads to decreased cognitive development in children [16], continual long-term deficiency leads to numerous other health related issues [11]. It is clear that biological pathways controlling iron reactivity are essential, however it is equally clear that pathways ensuring metal delivery occurs are equally important for maintaining cell viability.

Many pathways that regulate cellular iron homeostasis are controlled at the genetic and at the protein level [17, 18]. As outlined in the transferrin cycle, iron is imported through endocytosis of Fe^{3+} loaded transferrin (Tf) interacting with the transferrin receptor (Tf-R), in a tightly regulated feedback loop controlled at the genetic and protein level **(Figure 1.1).** In eukaryotes, iron can be diverted to the mitochondria where it can be utilized during heme production or during Fe-S cluster assembly (pathway #1 in Figure 1.1). During mitochondrial Fe-S cluster assembly, the ISC machinery proteins work together to form clusters that can be loaded onto apo-

mitochondrial proteins or pumped out of the mitochondria in some manner (labeled X) to be used by the cytosolic Fe-S cluster assembly machinery (CIA). Cytosolic iron can also be directed for storage into ferritin in an inert form for future use (pathway #2 in Figure 1). While there are obviously other fates for cellular iron, recently two iron chaperones have been discovered that control iron delivery in the pathways highlighted above. An overview of the structure and biophysical properties leading to iron binding by these two chaperones is the basis of this review.

1.4 Fe-S cluster biosynthesis iron chaperones:

In eukaryotes, the mitochondrial ISC assembly is the major pathway for Fe-S cluster production. Key players in the yeast ISC machinery include the assembly scaffold protein (either Isu1 or 2, for clarity we will refer to only Isu1), the cysteine desulfurase (Nfs1) that provides sulfur to Isu1, the accessory protein (Isd11) that works in complex with Nfs1, a ferredoxin (Yah1) working with a ferredoxin reductase (Arh1) to provide electrons for the reaction, and the putative iron chaperone protein frataxin (Yfh1) [19]. Protein orthologs are highly conserved and found in all eukaryotes, while in prokaryotes most are found within the ISC pathway while variants of these proteins exist within the sulfur mobilization (SUF) and the nitrogen fixation (NIF) assembly pathways [20]. Isu1 is one of the most conserved proteins [21, 22], containing three conserved cysteines critical for de novo Fe-S cluster assembly [23, 24]. Sulfur transfer between Nfs1 and Isu1 occurs as a persulfide (-SSH) through a direct interaction between

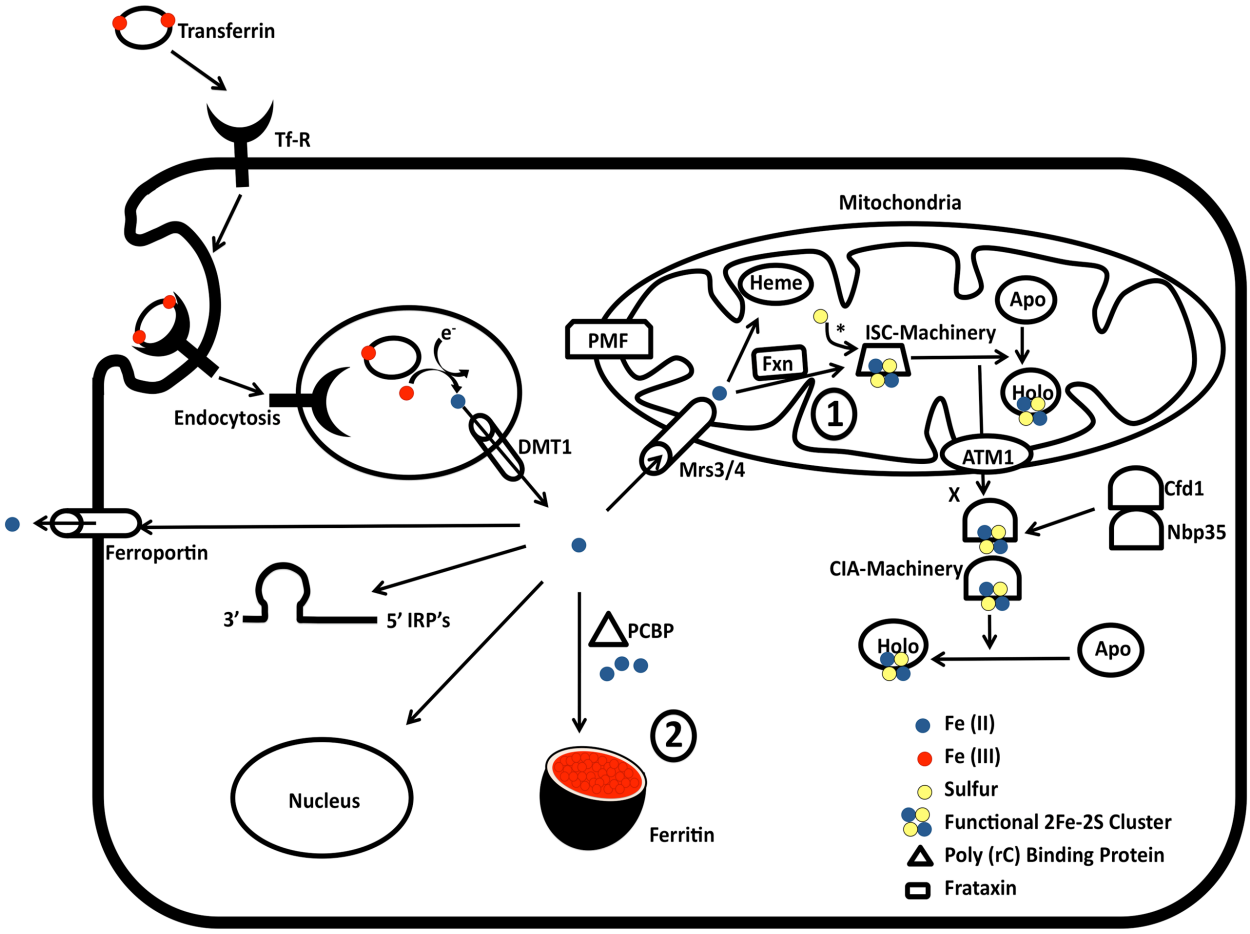

Figure 1.1: Major pathways for iron incorporation/utilization within a cell. Two pathways for Fe^{2+} utilization highlighted within the review include: 1) Frataxin and its role in mitochondrial Fe-S cluster assembly via the ISC-Machinery (* including the cysteine desulfurase/Isd11 complex that provides sulfur); 2) PCBP and its role in ferritin associated iron storage.

partners [25]; insight into the nature of this interaction has come from a recent structural characterization of bacterial orthologs [26]. *In vivo*, Yfh1 is essential for Fe-S cluster maturation [27], and an interaction between Yfh1 and Isu1/Nfs1/Isd11 is critical for cluster biosynthesis [28]. *In vitro,* frataxin was shown to deliver iron to the scaffold protein to stimulate Fe-S cluster assembly [29]. Based on these and additional reports (see review [19]), frataxin was shown to play a direct role in mitochondrial Fe-S cluster assembly, possibly by serving as the iron chaperone[28, 30], deficiency of which has direct consequences regarding cellular oxidative stress [31].

Insight into frataxin's function has come from investigating the structure and iron binding abilities of numerous orthologs [32]. Frataxin is a member of the a-b sandwich motif family, with N- and C-terminal helices constructing one molecular plane and the second constructed by at least five anti-parallel *b*-strands [33-38]. Key structural features for the frataxin orthologs include highly conserved surface exposed acidic residues lining the helix-1/strand-1 junction, a short predominately unstructured N-terminal region in eukaryotic orthologs only, and a C-terminal region in the human and bacterial proteins that confer stability [39]. The iron binding ability of frataxin was first identified in the yeast ortholog associated with iron induced aggregation stabilized by low salt/high oxygen solution conditions [40]. Monomeric bacterial, yeast, fly and human frataxin have since been shown to bind iron with micromolar affinity [29, 36, 41-44], and *in vivo* mutations preventing Yfh1 aggregation show no Fe-S cluster phenotypes under normal growth conditions [45], indicating while protein aggregation

may be important under oxidative stress, monomeric frataxin is active during Fe-S cluster assembly. Experimental data verify conserved acidic residues on frataxin's helix-1/strand-1 junction are directly involved in iron binding [36, 41, 43]. Structural studies confirm monomeric frataxin binds high spin Fe^{2+} in a symmetric 6-coordinate ligand environment constructed of only oxygen and nitrogen ligands, in agreement with the conserved acidic residue identified by NMR as iron ligands [43, 44, 46]. These data suggest as a starting point for iron delivery, frataxin binds iron using carboxylate side chain oxygens from conserved Asp and Glu residues from the helix-1/strand-1 iron binding sites, most likely with assistance from water molecules. Binding in this manner would predispose iron for delivery to Isu1 (Figure 2) since the exposed metal would be positioned for delivery to the protein partner and the charged surface surrounding the metal would be amenable for forming an interaction with a complementary charged region of the protein partner.

Yfh1 undergoes an iron-stimulated interaction with Isu1/Nfs1 [28, 47, 48] in agreement with frataxin interacting directly with members of the ISC assembly machinery. In vivo mutational studies place frataxin's acidic helix-1/strand-1 ridge, with residues on the Yfh1 β-sheet surface, as interacting with Isu1 [47-51]. In vitro binding interactions show frataxin/scaffold binding is iron dependent and occurs at nM binding affinity [44, 52, 53]. Chemical shift mapping studies provide spectroscopic confirmation that Isu1 interacts with Yfh1 on frataxin's acidic helix-1/strand-1 ridge utilizing the protein's β-sheet surface, in close agreement with *in vivo* mutational analysis [53]. In eukaryotic systems, activity assays for Fe-S cluster production confirm iron loaded

frataxin stimulates *in vitro* Fe-S cluster assembly, possibly by delivering the Fe^{2+} required for cluster production [29, 44, 54]. Direct structural details of the frataxin/scaffold interaction are however lacking. Two recent structural papers shed light on the potential binding interaction between these protein partners. Crystallographic data on the *Aquifex aeolicus* IscU ortholog, with cluster bound, confirm the three conserved Cys residues implicated in assembly form the active site of IscU [55]. An even more exciting result comes from the structure of the bacterial cysteine desulfurase (IscS) in complex with IscU [26]. This structure shows IscU binds to IscS such that the IscU Cys active site is in close contact with the IscS Cys residue implicated in forming the persulfide used for sulfur transfer. Binding of Isu1 to Nfs1 in this manner would prevent frataxin from interacting in this region, assuming sulfur delivery happens before iron delivery. Irrespective of this assumption, mounting evidence suggests all proteins in the ISC machinery form a complex that promotes the formation of a stable macromolecular complex used to accomplish cluster assembly, so the frataxin piece of this puzzle would need to fit in a unique location on Isu1. A likely candidate for where Yfh1 could bind to Isu1 is on the scaffold protein's C-terminal helix **(Figure 1.2)** [53]. The charge distribution from the electrostatic potential surface of Isu1 in this region matches nicely to the Yfh1 b-sheet surface. Conserved acidic/basic residues on Isu1's C-terminal helix could serve as the initial Fe^{2+} binding residues, metal could then translocate to the scaffold's active site [53]. Positional orientation of bacterial frataxin on the IscS/U from small angle X-ray scattering studies [56] suggest that such an orientation may be possible, although this orientation is likely to be altered between

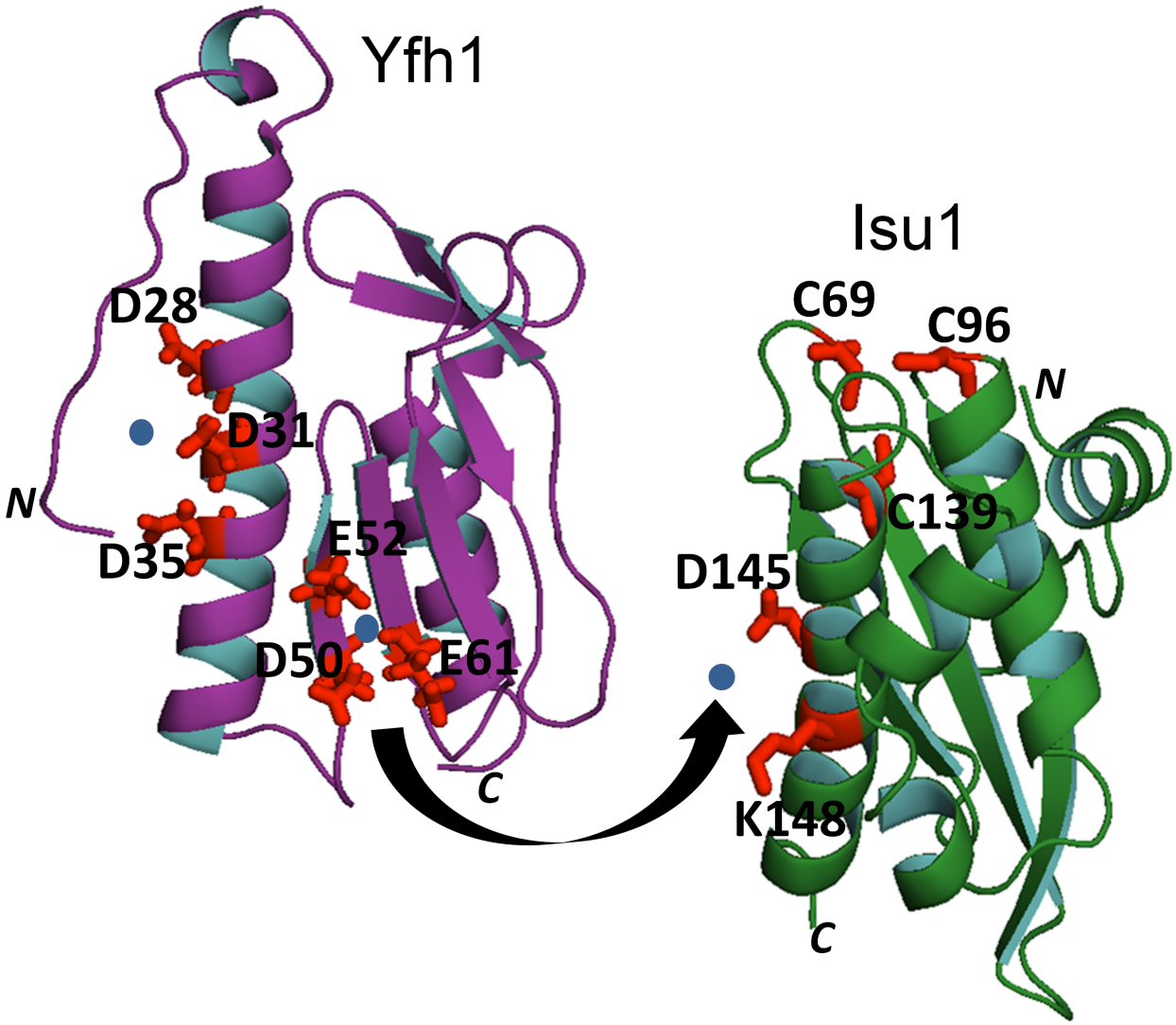

Figure 1.2: Molecular details of the 2 Fe^{2+} binding sites on Yfh1 (PDB #2GA5), and the Cys rich active site on Isu1 (modeled structure) coupled with possible Isu1 Fe^{2+} binding sites on the protein's C-terminus. Ferrous iron (blue dots) shown with arrow denoting Fe transfer events between the two proteins.

the prokaryotic and eukaryotic orthologs since the accessory protein Isd11 found only in eukaryotes is likely also positioned in this region. Following Fe delivery to Isu1 by Yfh1, the binding energetics are reduced, frataxin dissociates from its partner and Isu1 is primed for delivery of the second Fe atom required to make a 2Fe-2S cluster.

Recently it has been suggested frataxin may participate in Fe-S cluster biosynthesis by regulating activity of the cysteine desulfurase. NMR mapping studies of bacterial frataxin (CyaY) onto the bacterial IscS suggest residues lining frataxin's b-sheet ridge tangential to the C-terminus of helix 1, with helix-1 residues, participate in IscS binding [57]. Mutagenesis and binding studies implicate a region on one IscS monomer, in proximity to the persulfide site in the second molecule in the dimer, as the CyaY binding surface on IscS [26]. Recent studies suggest CyaY acts as an iron-dependent inhibitor of cluster formation by negatively regulating IscS activity [57]. In contrast, another recent report suggests human frataxin acts as an allosteric activator of Nfs1 [58]. Regardless, binding of frataxin to the ISC machinery is important during assembly and it will be interesting to see how this binding is finally correlated to iron delivery and assembly.

1.5 Ferritin iron chaperones

Cellular pathways directing iron storage are essential for preventing iron toxicity during overload and ensuring availability during deficiency. Storage is directed by the 4-helix bundle protein ferritin [59]. Mammalian cytoplasmic ferritins exist as a 24 subunits multimer of 2 ferritin subunit: H chain (21,000 kDa), which controls the ferroxidase

chemistry coupled to iron storage, and the L chain (19,000 kDa). Apo-ferritin H and L chains self-assemble to form a spherical protein shell that stores up to 4500 iron atoms as ferroxyhydrite within the central cavity. Iron storage involves two key steps: iron oxidation, leading to formation of a μ-oxo(hydroxo)-bridged di-Fe(III) intermediate, and mineralization, depositing the intermediate as inert ferrihydrite mineral. To proceed, iron must first be delivered to ferritin, and ferrous iron delivery occurs at a ferritin oligomer hydrophilic threefold (iron entry) channel. H-chain surface exposed residues H118 [60] and C130 [61], with threefold channel funnel-like forming residues Asp131 and Glu134 [62], are used during iron import. Binding of an iron chaperone must therefore proceed through direct contact with ferritin's three-fold iron entry site **(Figure 1.3).**

Recently, the human poly (rC)-binding protein (PCBP) was shown to function as a cytosolic iron chaperone that delivers Fe^{2+} to ferritin [63]. The RNA-binding PCBP protein family was originally shown to be important in mRNA stabilization and translational activation/silencing [64]. PCBPs have 3 KH (hnRNP K homology) domains, with structures of the two N-terminal domains and the third domain of PCBP2 being characterized [65, 66]. Expression of human PCBP1 recovered an iron loading deficiency for human ferritin expressed in yeast [63]. PCBP1 binds to ferritin *in vivo* and *in vitro* facilitates iron loading. PCBP1 binds 3 iron atoms at mM binding affinity comparable to frataxin's iron affinity [32]. Metal binding sites on PCBP are unknown, however recent iron structural data indicate PCBP1/2 bind ferrous iron in a 6-coordinate

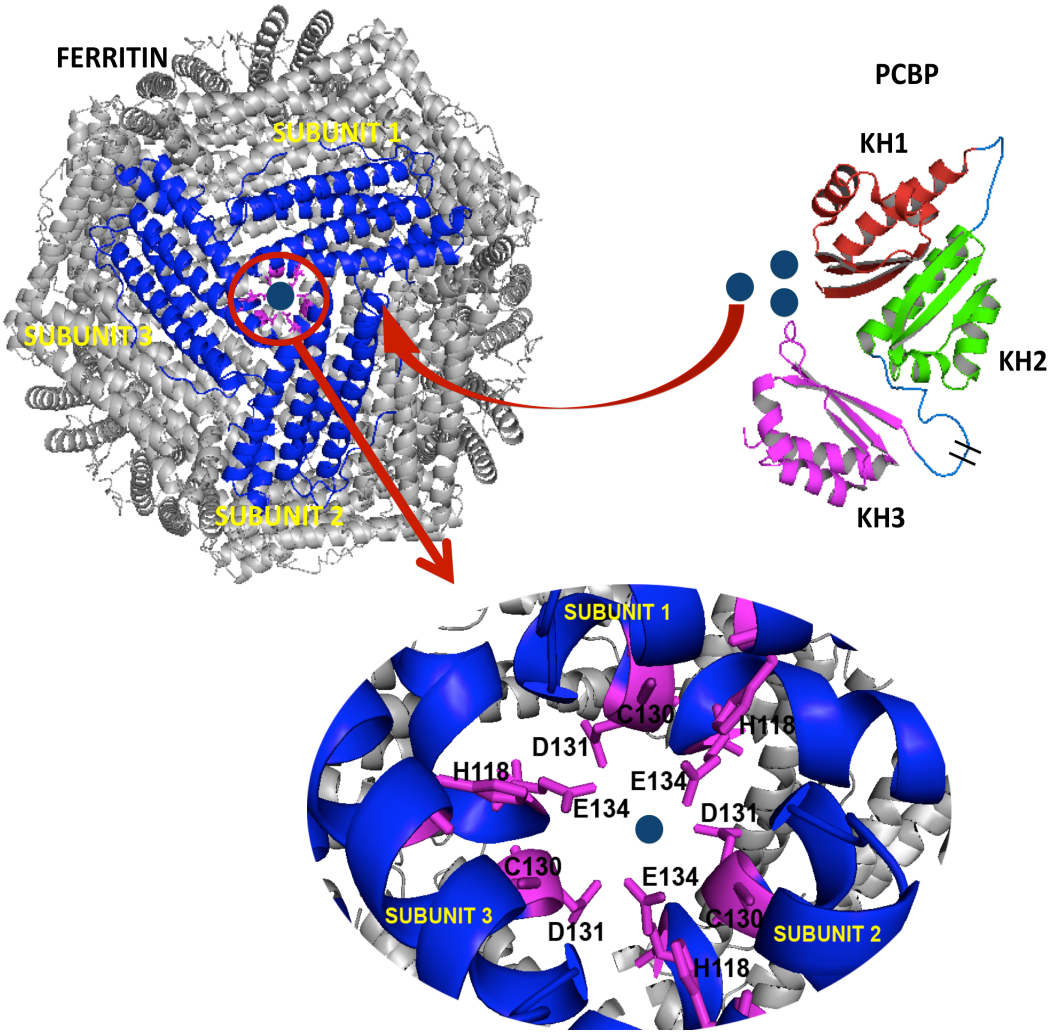

Figure 1.3: Structural details of PCBP as a ferritin iron chaperone. Top Right: PCBP2 total projected structure based on domains 1,2 (PDB #2JZX) and domain 3 (PDB #2P2R) structure linked together for visual clarity associated with 3 bound iron atoms (blue dots). Top Left: structure of the human ferritin 24-mer (PDB #3AJO) with iron loaded (blue dot) trimeric symmetry center. Bottom Left: expansion of the ferritin trimeric interface with residues from three subunits involved in Fe^{2+} loading (H118 and C130). In addition, residues (D131, E134) on the inner side of the iron incorporation gate that support metal exchange are also given.

oxygen/nitrogen ligand environment (author's unpublished results). Although molecular details of PCBP as an iron chaperone are still emerging, it is interesting to note that thermodynamic and structural data regarding PCBP iron binding are so similar to that of the Fe-S assembly iron chaperone.

1.6 Conclusions

Evidence that frataxin and PCBP are iron chaperones is compelling, although clarification of their function at the genetic, molecular and atomic levels will be important for understanding how they operate. There are still many questions that remain regarding the identity of other chaperones, how iron is loaded onto a chaperone and what promotes chaperone metal specificity? A possible candidate for the first question is the Glutaredoxins Grx3/ 4, members of the thioredoxin (Trx) fold family. Grx3/4 are central for cellular iron trafficking and a strong dependence of iron binding for Grx3/4 on core components in the ISC pathway indicate Grx3/4 bind iron as a Fe-S cluster [67]. The ability to form a bridging 2Fe-2S cluster with Fra1/2 for activation of Aft1 [68], coupled with the direct dependence of Grx3/4 on iron loading into heme, Fe-S clusters, into ribonucleotide reductase, etc. suggest iron activated by Grx3/4 may be utilized by other dedicated assembly factors [67]. Frataxin and PCBP are most likely the start of a soon to be recognized long list of iron chaperones.

1.7 Acknowledgements

We would like to thank Dennis Winge, Andy Dancis and Roland Lill for helpful discussions regarding the material. Work in the Stemmler laboratory is supported by the National Institute of Health (DK068139).

1.8 References

1. Theil, E.C. and K.N. Raymond, *Transition-metal storage, transport and biomineralization*. 1994, University Science Books: Mill Valley, CA. p. 1-37.
2. Waldron, K.J. and N.J. Robinson, *How do bacterial cells ensure that metalloproteins get the correct metal?* Nat Rev Microbiol, 2009. **7**(1): p. 25-35.
3. Dupont, C.L., et al., *Modern proteomes contain putative imprints of ancient shifts in trace metal geochemistry.* Proc Natl Acad Sci U S A, 2006. **103**(47): p. 17822-7.
4. Finney, L.A. and T.V. O'Halloran, *Transition metal speciation in the cell: insights from the chemistry of metal ion receptors.* Science, 2003. **300**(5621): p. 931-6.
5. Irving, H. and R. Williams, *Order of stability of metal complexes.* Nature, 1948. **162**: p. 746-747.
6. Waldron, K.J., et al., *Metalloproteins and metal sensing.* Nature, 2009. **460**(7257): p. 823-30.

7. Rouault, T.A., *How mammals acquire and distribute iron needed for oxygen-based metabolism.* PLoS Biol, 2003. **1**(3): p. E79.

8. Rae, T.D., et al., *Undetectable intracellular free copper: the requirement of a copper chaperone for superoxide dismutase.* Science, 1999. **284**(5415): p. 805-8.

9. Crichton, R., *Inorganic Biochemistry of Iron Metabolism: From Molecular Mechanisms to Clinical Consequences*. Second ed. 2001, West Sussex, England: John Whiler & Sons, Ltd.

10. Andrews, N.C. and P.J. Schmidt, *Iron homeostasis.* Annu Rev Physiol, 2007. **69**: p. 69-85.

11. Andrews, N.C., *Disorders of iron metabolism.* N Engl J Med, 1999. **341**(26): p. 1986-95.

12. Beinert, H., Holm,R.H., Munck,E., *Iron-sulfur clusters: nature's modular, multipurpose structures.* Science, 1997. **277**: p. 653-659.

13. Eisenstein, R.S., *Interaction of the hemochromatosis gene product HFE with transferrin receptor modulates cellular iron metabolism.* Nutr Rev, 1998. **56**(12): p. 356-8.

14. Crichton, R.R., D.T. Dexter, and R.J. Ward, *Brain iron metabolism and its perturbation in neurological diseases.* J Neural Transm, 2010.

15. Andrews, N.C., *Forging a field: the golden age of iron biology.* Blood, 2008. **112**(2): p. 219-30.

16. Pollitt, E., *Iron deficiency and cognitive function.* Annu Rev Nutr, 1993. **13**: p. 521-37.

17. Hentze, M.W., M.U. Muckenthaler, and N.C. Andrews, *Balancing acts: molecular control of mammalian iron metabolism.* Cell, 2004. **117**(3): p. 285-97.

18. Kaplan, C.D. and J. Kaplan, *Iron acquisition and transcriptional regulation.* Chem Rev., 2009. **109**: p. 4536-4552.

19. Lill, R., *Function and biogenesis of iron-sulphur proteins.* Nature, 2009. **460**(7257): p. 831-8.

20. Lill, R. and U. Muhlenhoff, *Maturation of iron-sulfur proteins in eukaryotes: mechanisms, connected processes, and diseases.* Annu Rev Biochem, 2008. **77**: p. 669-700.

21. Tokumoto, U., et al., *Interchangeability and distinct properties of bacterial Fe-S cluster assembly systems: functional replacement of the isc and suf operons in Escherichia coli with the nifSU-like operon from Helicobacter pylori.* J Biochem, 2004. **136**(2): p. 199-209.

22. Schilke, B., Voisine,C., Beinert,H., Craig,E., *Evidence for a conserved system for iron metabolism in the mitochondria of Saccharomydes cervisiae.* Proc. Natl. Adad. Aci, USA, 1999. **96**: p. 10206-10211.

23. Yuvaniyama, P., et al., *NifS-directed assembly of a transient [2Fe-2S] cluster within the NifU protein.* Proc Natl Acad Sci U S A, 2000. **97**(2): p. 599-604.

24. Frazzon, J. and D.R. Dean, *Formation of iron-sulfur clusters in bacteria: an emerging field in bioinorganic chemistry.* Curr Opin Chem Biol, 2003. **7**(2): p. 166-73.

25. Zheng, L., et al., *Assembly of iron-sulfur clusters. Identification of an iscSUA-hscBA-fdx gene cluster from Azotobacter vinelandii.* J Biol Chem, 1998. **273**(21): p. 13264-72.

26. Shi, R., et al., *Structural basis for Fe-S cluster assembly and tRNA thiolation mediated by IscS protein-protein interactions.* PLoS Biol, 2010. **8**(4): p. 1-18.

27. Muhlenhoff, U., et al., *The yeast frataxin homolog Yfh1p plays a specific role in the maturation of cellular Fe/S proteins.* Hum Mol Genet, 2002. **11**(17): p. 2025-36.

28. Gerber, J., U. Muhlenhoff, and R. Lill, *An interaction between frataxin and Isu1/Nfs1 that is crucial for Fe/S cluster synthesis on Isu1.* EMBO Rep, 2003. **4**(9): p. 906-11.

29. Yoon, T. and J.A. Cowan, *Iron-sulfur cluster biosynthesis. Characterization of frataxin as an iron donor for assembly of [2Fe-2S] clusters in ISU-type proteins.* J. Am. Chem. Soc., 2003. **125**: p. 6078-84.

30. Layer, G., et al., *Iron-sulfur cluster biosynthesis: characterization of Escherichia coli CYaY as an iron donor for the assembly of [2Fe-2S] clusters in the scaffold IscU.* J Biol Chem, 2006. **281**(24): p. 16256-63.

31. Moreno-Cermeno, A., et al., *Frataxin depletion in yeast triggers upregulation of iron transport systems before affecting iron-sulfur enzyme activities.* J Biol Chem.

32. Bencze, K.Z., et al., *The structure and function of frataxin.* Crit Rev Biochem Mol Biol, 2006. **41**(5): p. 269-91.

33. Dhe-Paganon, S., et al., *Crystal structure of human frataxin.* J Biol Chem, 2000. **275**(40): p. 30753-6.

34. Musco, G., et al., *Towards a Structural Understanding of Friedreich's Ataxia: The Solution Structure of Frataxin.* Structure, 2000. **8**(7): p. 695-707.

35. Cho, S.J., et al., *Crystal structure of Escherichia coli CyaY protein reveals a previously unidentified fold for the evolutionarily conserved frataxin family.* Proc Natl Acad Sci U S A, 2000. **97**(16): p. 8932-7.

36. He, Y., et al., *Yeast frataxin solution structure, iron binding, and ferrochelatase interaction.* Biochemistry, 2004. **43**(51): p. 16254-62.

37. Nair, M., et al., *Solution structure of the bacterial frataxin ortholog, CyaY: mapping the iron binding sites.* Structure (Camb), 2004. **12**(11): p. 2037-48.

38. Karlberg, T., et al., *The structures of frataxin oligomers reveal the mechanism for the delivery and detoxification of iron.* Structure, 2006. **14**(10): p. 1535-46.

39. Adinolfi, S., et al., *The Factors Governing the Thermal Stability of Frataxin Orthologues: How To Increase a Protein's Stability.* Biochemistry, 2004. **43**(21): p. 6511-6518.

40. Adamec, J., et al., *Iron-dependent self-assembly of recombinant yeast frataxin: implications for Friedreich ataxia.* Am J Hum Genet, 2000. **67**(3): p. 549-62.

41. Bou-Abdallah, F., et al., *Iron binding and oxidation kinetics in frataxin CyaY of Escherichia coli.* J Mol Biol, 2004. **341**(2): p. 605-15.

42. O'Neill, H.A., et al., *Assembly of human frataxin is a mechanism for detoxifying redox-active iron.* Biochemistry, 2005. **44**(2): p. 537-45.

43. Cook, J.D., et al., *Monomeric yeast frataxin is an iron-binding protein.* Biochemistry, 2006. **45**(25): p. 7767-77.

44. Kondapalli, K.C., et al., *Drosophila frataxin: an iron chaperone during cellular Fe-S cluster bioassembly.* Biochemistry, 2008. **47**(26): p. 6917-27.

45. Aloria, K., et al., *Iron-induced oligomerization of yeast frataxin homologue Yfh1 is dispensable in vivo.* EMBO Rep, 2004. **5**(11): p. 1096-101.

46. Bencze, K.Z., et al., *Human frataxin: iron and ferrochelatase binding surface.* Chem Commun (Camb), 2007(18): p. 1798-800.

47. Ramazzotti, A., V. Vanmansart, and F. Foury, *Mitochondrial functional interactions between frataxin and Isu1p, the iron-sulfur cluster scaffold protein, in Saccharomyces cerevisiae.* FEBS Lett, 2004. **557**(1-3): p. 215-20.

48. Wang, T. and E.A. Craig, *Binding of yeast frataxin to the scaffold for Fe-S cluster biogenesis, Isu.* J Biol Chem, 2008. **283**(18): p. 12674-9.

49. Correia, A.R., et al., *Iron-binding activity in yeast frataxin entails a trade off with stability in the alpha1/beta1 acidic ridge region.* Biochem J. **426**(2): p. 197-203.

50. Foury, F., A. Pastore, and M. Trincal, *Acidic residues of yeast frataxin have an essential role in Fe-S cluster assembly.* EMBO Rep, 2007. **8**(2): p. 194-9.

51. Leidgens, S., S. De Smet, and F. Foury, *Frataxin interacts with Isu1 through a conserved tryptophan in its beta-sheet.* Hum Mol Genet, 2010. **19**(2): p. 276-86.

52. Wu, S.P., et al., *Iron-sulfur cluster biosynthesis. Kinetic analysis of [2Fe-2S] cluster transfer from holo ISU to apo Fd: role of redox chemistry and a conserved aspartate.* Biochemistry, 2002. **41**(28): p. 8876-8885.

53. Cook, J.D., et al., *Molecular Details of the Yeast Frataxin-Isu1 Interaction during Mitochondrial Fe-S Cluster Assembly.* Biochemistry, 2010. **49**: p. 8756-65.

54. Li, H., et al., *Oligomeric yeast frataxin drives assembly of core machinery for mitochondrial iron-sulfur cluster synthesis.* J Biol Chem, 2009. **284**(33): p. 21971-80.

55. Shimomura, Y., et al., *The asymmetric trimeric architecture of [2Fe-2S] IscU: implications for its scaffolding during iron-sulfur cluster biosynthesis.* J Mol Biol, 2008. **383**(1): p. 133-43.

56. Prischi, F., et al., *Structural bases for the interaction of frataxin with the central components of iron-sulphur cluster assembly.* Nat Commun, 2010. **1**(7): p. 95.

57. Adinolfi, S., et al., *Bacterial frataxin CyaY is the gatekeeper of iron-sulfur cluster formation catalyzed by IscS.* Nat Struct Mol Biol, 2009. **16**(4): p. 390-6.

58. Tsai, C.L. and D.P. Barondeau, *Human frataxin is an allosteric switch that activates the Fe-S cluster biosynthetic complex.* Biochemistry, 2010. **49**(43): p. 9132-9.

59. Liu, X. and E.C. Theil, *Ferritin: dynamic management of biological iron and oxygen chemistry.* Acc. Chem. Res., 2005. **38**: p. 167-175.

60. Granier, T., et al., *Structural description of the active sites of mouse L-chain ferritin at 1.2 A resolution.* J Biol Inorg Chem, 2003. **8**(1-2): p. 105-11.

61. Takeda, S., et al., *Site-specific reactivities of cysteine residues in horse L-apoferritin.* J Biochem, 1995. **117**(2): p. 267-70.

62. Levi, S., et al., *Evidence that residues exposed on the three-fold channels have active roles in the mechanism of ferritin iron incorporation.* Biochem. J., 1996. **317**: p. 467-473.

63. Shi, H., et al., *A cytosolic iron chaperone that delivers iron to ferritin.* Science, 2008. **320**(5880): p. 1207-10.

64. Makeyev, A.V. and S.A. Liebhaber, *The poly(C)-binding proteins: a multiplicity of functions and a search for mechanisms.* RNA, 2002. **8**(3): p. 265-78.

65. Du, Z., et al., *Structure of a construct of a human poly(C)-binding protein containing the first and second KH domains reveals insights into its regulatory mechanisms.* J Biol Chem, 2008. **283**(42): p. 28757-66.

66. Fenn, S., et al., *Crystal structure of the third KH domain of human poly(C)-binding protein-2 in complex with a C-rich strand of human telomeric DNA at 1.6 A resolution.* Nucleic Acids Res, 2007. **35**(8): p. 2651-60.

67. Muhlenhoff, U., et al., *Cytosolic monothiol glutaredoxins function in intracellular iron sensing and trafficking via their bound iron-sulfur cluster.* Cell Metab, 2010. **12**(4): p. 373-85.

68. Li, H., et al., *The yeast iron regulatory proteins Grx3/4 and Fra2 form heterodimeric complexes containing a [2Fe-2S] cluster with cysteinyl and histidyl ligation.* Biochemistry, 2009. **48**(40): p. 9569-81.

CHAPTER 2
IRON BINDING AND INITIAL METAL LOADING SITE ON THE ISU SCAFFOLD PROTEINS

2.1 Prelude

The iron-sulfur (Fe-S) cluster scaffold protein, ISU drives the chemistry associated with mitochondrial Fe-S cluster assembly. This process is accomplished by an interaction of ISU with several protein partners, stimulating the process of ferrous iron delivery and sulfide delivery in the process. One of our early goals was to take an individual molecular approach to understand how cluster assembly is accomplished. Given the importance of ISU in the assembly process, we would like to deconstruct the substrate delivery events with the cluster assembly events in a step-wise manner, with the hope of determining mechanistic details that lead to the assembly process. Therefore, we began by looking at the iron loading events for how ISU is initially exposed to substrate. To accomplish this, we did a comprehensive characterization of ISU iron loading events.

The work described below, which is directed to accomplish this aim, was performed on four ISU orthologs: human, fly, yeast and bacteria. This work was initiated by previous graduate students in the Stemmler laboratory: Dr. Jeremy Cook and Dr. Swati Rawat, in collaboration with the Cowan laboratory (Ohio State) and the Lindahl laboratory (Texas A&M). *Saccharomyces cerevisiae* Isu1 (or YIsu1) used in

these studies was a variant that contained a D37A mutant that locked the synthesized cluster in place while the complementary experiments were performed on the wild type ISU orthologs. My goal was therefore to complete the complementary experiments on the wild type (WT) *Sc* Isu1 protein, to set the basis for comparison of orthologs under similar conditions. I have optimized expression & purification of the WT *Sc* Isu1 ortholog, and characterized the protein in detail in this and the subsequent chapter.

2.2 Abstract

Fe-S clusters are utilized in nearly every biochemical pathway. The chemistry of iron is modulated by incorporation of metal into Fe-S clusters, protein bound cofactors that drive biochemical pathways ranging from steroid biosynthesis to energy production. In eukaryotes, clusters are assembled by the Isu scaffold protein. The iron-sulfur (Fe-S) scaffold protein ISU occurs ubiquitously among all organisms. The ISU proteins have three conserved cysteine residues in the active site that coordinate iron and sulfur during the synthesis of a cluster. The source of sulfur for cluster assembly is the protein cysteine desulfurase that catalyzes the conversion of cysteine to alanine forming an active persulfide that appears to be transferred directly to ISU's active site. Frataxin, a potential mitochondrial iron chaperone protein, has been identified to provide the putative source of iron, however, the region of binding and/or delivery of iron onto ISU remains unknown. In this study the ISU iron binding properties of four orthologs

(human, fly, yeast and bacteria) have been characterized and compared to identify unifying factors for iron utilization. Isothermal titration calorimetry studies show ISU can bind iron alone with a nano- to micromolar binding affinity. X-ray absorption spectroscopy results show that the Fe(II)-ISU complex is composed of a ligand environment that is completely oxygen/nitrogen based in all orthologs, indicating Isu binds iron at a site distinct from its cysteine rich active site. Mössbauer spectroscopy confirmed the iron-oxygen/nitrogen ligand environment at this metal "acceptance" site. In addition to identifying a unique iron-binding site on ISU, a model for Fe delivery to ISU has been proposed.

2.3 Introduction

In the pre-biotic milieu of ancient earth, Fe-S clusters were most likely among the first chemical compounds to perform the chemistry essential to life processes [1]. Fe-S cofactors are used ubiquitously throughout biology to perform basic catalytic, electron transfer, and regulatory roles [2, 3]. Three dedicated pathways and upwards of at least 20 different proteins have been identified for the formation of these ancient cofactors [4]. The major pathway within the mitochondria responsible for general Fe-S cluster production is the iron-sulfur cluster (ISC) biosynthetic pathway [4]. Assembly of Fe-S clusters within the ISC pathway requires a highly conserved scaffold protein on which the cofactors are assembled (termed ISU or IscU in eukaryotes and prokaryotes,

respectively) [5-8]. Sulfide is provided by a cysteine desulfurase, NifS (along with an accessory protein, Isd11 in eukaryotes) [4, 6, 9]. Frataxin, a chaperone protein, is believed to be the putative iron donor [6, 10-14]. Although genetics studies have identified many of the players involved during assembly, many biochemical details of the pathway are still unclear. ISU proteins contain three highly conserved cysteine residues and a semiconserved histidine residue; in the active site [15, 16]. This finding was recently validated in prokaryotes by the crystal structure of IscU with a 2Fe-2S cluster bound [17]. However, the enzymatic mechanism for Fe-S cluster production remains unknown. In this report, we seek to characterize four highly homologous ISU orthologs (*Homo sapiens, Drosophila melanogaster, Saccharomyces cerevisiae and Thermatoga maritima*) in the hope of clarifying the initial steps of Fe binding to ISU proteins. Isu proteins studied in this report exhibit 80% (*Dm)*, 73% (*Sc)*, and 28% (*Tm)* sequence identity to the human homolog **(Figure 2.1).** We present both structural and biochemical data that suggest the presence of a metal binding site on the protein independent of the active site in each of the ISU proteins.

2.4 Materials and Methods:

2.4.1 Protein Expression and Purification

S. cerevisiae Isu1 containing a D37A mutation was subcloned into a pET21b expression vector (Novagen) with a C-terminal His tag and the sequence was confirmed by DNA sequencing. Plasmid was transfected into BL21(DE3) CodonPlus cells and grown by auto induction [18] at 25°C for ca. 24 hrs. before harvesting by centrifugation (5000 rpm, 45 min). All protein isolation steps were all performed at 4°C. Cells were re-suspended in 50 mM $NaPO_4$ (pH 7.5), 300 mM NaCl, 20 mM Imidazole, and 5 mM β-Me (5 mL/g cells) in the presence of Complete EDTA free protease inhibitor cocktail (Roche). Cells were lysed during two passes through a French press cell followed by 2 rounds of sonication (50% power), and spun at high speed (21000 rpm) for 1 hour. The crude soluble fraction was filtered (0.20 μm) and loaded onto a HisPrep FF Ni-column (Pharmacia) using an Imidazole gradient (20-500 mM, protein elutes ~ 120 mM). Active fractions were pooled and concentrated to ca. 1 mL using 3 kDa cutoff centricons (Millipore) and run over a Sephadex 75 size exclusion column (Pharmacia) equilibrated with 20 mM HEPES (pH 7.5), 150 mM NaCl and 5 mM β-Me. The protein eluted as a dimer at ≥ 95% purity (typical yields were 1 mg/L). *D. melanogaster* mature wild type ISU was subcloned into a pET151D-TOPO expression vector (Invitrogen) with cleavable His-tag and then sequenced. Plasmid was transfected into BL21(DE3) CodonPlus cells and grown by auto induction [18] at 25°C for ca. 24 hrs. before harvesting by

centrifugation. Protein was isolated as described above with typical yields of 27 mg/L. The plasmid containing the *Sc* Isu1 WT gene was transformed into BL21 codon plus RIL cells (Stratagene) for protein expression. Cells were grown at 37^0C in Luria-Bertani broth containing Ampicillin (0.1 µg/ µl) and Chloramphenicol (0.05 µg/ µl) with shaking speed set at 250rpm. At OD_{600} of 0.6 cells were induced for protein expression by the addition of 0.8mM IPTG. Post induction expression conditions were found to be optimum at a temperature of 37^0C, over a period of 3 hrs. following which the cells were harvested by centrifugation and stored at -80^0C until lysis. Protein purification followed methods similar to those described above. Wild type *Sc* Isu1 eluted as a dimer. Pure fractions were pooled and protein concentration was determined using IR Spectrometry (EMD Millipore Direct Detect). Purification yielded about 2.5 mg/ml of ≥ 95% pure protein from ~ 50gm cells. Purified samples of the *H. sapien* and *T. maritima* orthologs were generously provided by the Cowan lab (Evans Laboratory of Chemistry, Ohio State University), expression and isolation protocols are described elsewhere [10, 12, 19].

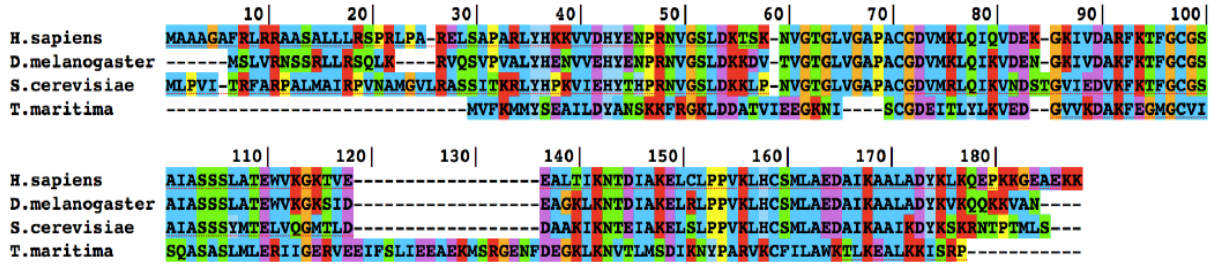

Figure 2.1. Sequence alignment of ISU proteins. Mature protein sequences from *H. sapiens, D. melanogaster, S. cerevisiae* and *T. maritima* were aligned using Kalign v2 software [20]. The conserved 3-Cysteine active site consists of C71, C98 and C159 according to the consensus ruler.

2.4.2 Isothermal Titration Calorimetry experiments & analysis:

Isothermal titration calorimetry (ITC) measurements were performed to measure the binding affinity and maximum stoichiometries of ferrous iron to each ISU protein. Experiments were performed at 30 °C on a VP-ITC titration microcalorimeter (Micro Cal Inc.). A solution containing 30 µM ISU (human, yeast and *Thermatoga*) was thoroughly degassed and loaded into the adiabatic cell and 500 µM buffered anaerobic ferrous iron solution was loaded into the syringe. The Fe into *Dm* Isu ITC experiment was conducted by titrating a 2.1 mM ferrous iron solution into 90 μM DIsu solution in small increments. An initial 2 µL injection was followed by 29 additional injections of 10 µL titrant allowing 10 min between each injection to allow for complete equilibration with constant stirring (500 rpm). Both sample and titrant were in matched 20 mM HEPES (pH 7.5), 150 mM NaCl and 5mM β-Me buffer. Data was collected in duplicate and protein samples were extensively degassed and buffers were purged with Ar (g) to help stabilize the iron in the ferrous state. Data was fit and analyzed using the Origin 5.0 software package supplied by Micro Cal (GE life sciences), which uses a non-linear least squares curve fitting algorithm, to determine the stoichiometric ratio, dissociation constant and change in enthalpy of the reaction.

Experimental parameters for the WT *Sc* Isu1 to Fe (II) titration was similar as described above. A 1 mM solution of Fe (II) was titrated into 50 μM solution of WT *Sc* Isu1 protein. Both solutions were prepared in the same buffer, which contained 20 mM, HEPES (pH: 7.5), 150 mM NaCl, 5 mM β-ME. The parameters of the ITC experiment are the same as described above.

2.4.3 XAS Sample Preparation and Analysis

X-ray absorption spectroscopy (XAS) was used to study the electronic properties and ligand coordination geometry of iron bound to different ISU orthologs. All samples were prepared anaerobically within a glove box (PlasLabs) using protein and iron solutions that were initially degassed on a Schlenk line and stored under an Ar(g) atmosphere. XAS samples were prepared at ~0.5 mM final protein concentrations in 20 mM HEPES (pH 7.0), 150 mM NaCl and 5 mM β-Me buffer. WT *Sc* Isu1 samples were prepared as described above in buffer containing 20 mM HEPES (pH: 7.5), 250 mM NaBr, 5 mM β-Me. Samples were diluted with 30% glycerol as a glassing agent and loaded into Lucite cells wrapped with Kapton tape, flash frozen in liquid nitrogen, removed from the glove box and stored in liquid nitrogen until data collection.

XAS data were collected at the Stanford Synchrotron Radiation Laboratory (SSRL), on beamlines 7-3 and 9-3, and at the National Synchrotron Light Source (NSLS), on beamline X3b. Beamlines were equipped with harmonic rejection mirrors and either Si(220) double crystal monochromators or a Si(111) single crystal monochromator, at SSRL and NSLS, respectively. Samples were maintained at 10 K using an Oxford Instruments continuous-flow liquid helium cryostats at SSRL and at ca. 24 K using a He Displex Cryostat at NSLS. Protein fluorescence excitation spectra were collected using 30-element Ge solid-state array detectors at SSRL and a 13-element Ge solid-state detector at NSLS. XAS spectra were measured using 5 eV steps in the pre-edge regions (6900-7094), 0.25 eV steps in the edge regions (7095-

7135 eV) and 0.05 $Å^{-1}$ increments in the extended X-ray absorption fine structure (EXAFS) region (to k = 13.5 $Å^{-1}$), integrating from 1 to 20 s in a k^3 weighted manner for a total scan length of approximately 40 minutes. X-ray energies were calibrated by collecting an iron foil absorption spectrum simultaneously with collection of the protein and model data. The first inflection point for the Fe foil edge was assigned at 7111.3 eV. Fluorescence channels for each scan was examined for spectral anomalies prior to averaging and spectra were closely monitored for photoreduction.

SSRL protein data represent the average of 5 to 6 scans, while NSLS protein data represent the average of 8 to 9 scans. XAS data were processed using the Macintosh OS X version of the EXAFSPAK program suite integrated with the Feff v7.2 software for theoretical model generation [21]. XAS data reduction utilized a Gaussian function in the pre-edge region and a three-region cubic spline in the x-ray absorption fine structure (EXAFS) region. EXAFS data were converted to k-space using an E_0 value of 7130 eV. The k^3 weighted EXAFS was truncated at 1.0 and 12.85 $Å^{-1}$ for filtering purposes and Fourier transformed. The final fitting results presented are from analysis of the raw unfiltered data.

EXAFS data fitting analysis performed on both Fourier filtered and raw/unfiltered data gave equivalent structural results. Model and protein EXAFS data were fit using both single and multiple scattering amplitude and phase functions calculated using Feff v7.2. Single scattering Feff v7.2 models were calculated for carbon, oxygen, sulfur and iron coordination to simulate possible iron-ligand environments in our systems. Fits to the crystallographically characterized model compounds were used to calibrate the

scale factor and ΔE0 values which we used in our protein fits. A scale factor of 0.95 and a threshold shift (ΔE0) -11.5 eV were used during our protein data analysis. The scale factor and E0 were not allowed to vary as they were calibrated from the Fe(II) model compounds matching the oxidation state of the ferrous iron we found in our protein samples. When simulating empirical data, metal-ligand coordination numbers were fixed at half-integer values while only the absorber-scatterer bond length (R) and Debye-Waller factor (σ^2) were allowed to freely vary. The criteria for judging the best fit simulation, and for adding ligand environments to the fit, included: (A) the lowest mean square deviation between data and fit (F'), a value corrected for number of degrees of freedom in the fit, (B) individual shell bond distances must be outside the spectral resolution (> 0.13 Å), and finally (C) all Debye-Waller factors in the ligand system must have values less than 0.006 s^2.

2.4.4 Mössbauer Spectroscopy Sample Preparation and Data Analysis

Mössbauer samples were prepared anaerobically in a glovebox (PlasLabs), and all proteins and solutions were first extensively degassed on a schlenk line. Ferric ^{57}Fe was dissolved in a mixture of HCl/HNO3 and reduced to the ferrous form using sodium hydrosulfite in a basic solution under anaerobic conditions. Iron oxidation state was confirmed using the Fe(II) specific chromophore bipyridine. The reduced iron was combined with ISU protein samples at a 1:1 stoichiometry and allowed to equilibrate for 10 min at room temperature prior to loading into the sample cells. Samples were frozen in the glovebox using an aluminum block bathed in liquid nitrogen. Mössbauer spectra

were also collected at Texas A&M University using a model MS4 WRC spectrometer (WEB Research, Edina, MN) with a 4.5 to 300 K closed-cycle helium refrigerated system and a W106 temperature controller. Data was analyzed using the WMOSS software package (WEB Research, Edina, MN). Isomer shifts are quoted relative to Fe metal at 298 K. Spectra were collected for 24 h at 4.5 K and 100 K with little distinguishable difference in spectral features.

2.5 Results

2.5.1 ISU Proteins Directly Bind Iron

In order for the protein-assisted assembly of Fe-S clusters to occur within the ISC pathway, ISU proteins must be capable of binding iron. Using ITC, we observed ISU proteins have a direct interaction with ferrous iron. It has been previously shown the *Tm and Hs* proteins are capable of binding ferrous iron at micromolar binding affinities [12, 15]. We observe similar results in the two additional species; *Dm* and *Sc* (D37A). Measurements of both *Dm* and *Sc* ISU were performed anaerobically in buffered solutions that helped increase protein stability (20 mM HEPES (pH 7.5), 150 mM NaCl and 5 mM β-Me). Addition of iron resulted in a strong single exothermic reaction shown in **Figure 2.2 A, C** for both *Dm* and *Sc* ISU. Plots of the integrated heat released vs. molar ratio are shown in **Figure 2.2 B and D** for *Dm* and *Sc* ISU, respectively. Data were best fit in both cases using a 2 binding-site model using the Origin 5.0 software. *Dm* Isu binds approximately 1.21± 0.25 Fe(II) atoms with an apparent KD1 of 475 ± 166 nM and 1.40 ± 0.07 Fe(II) atoms with a K_{D2} of 64.5 ± 17 nM. S*c* Isu1 (D37A) binds ca.

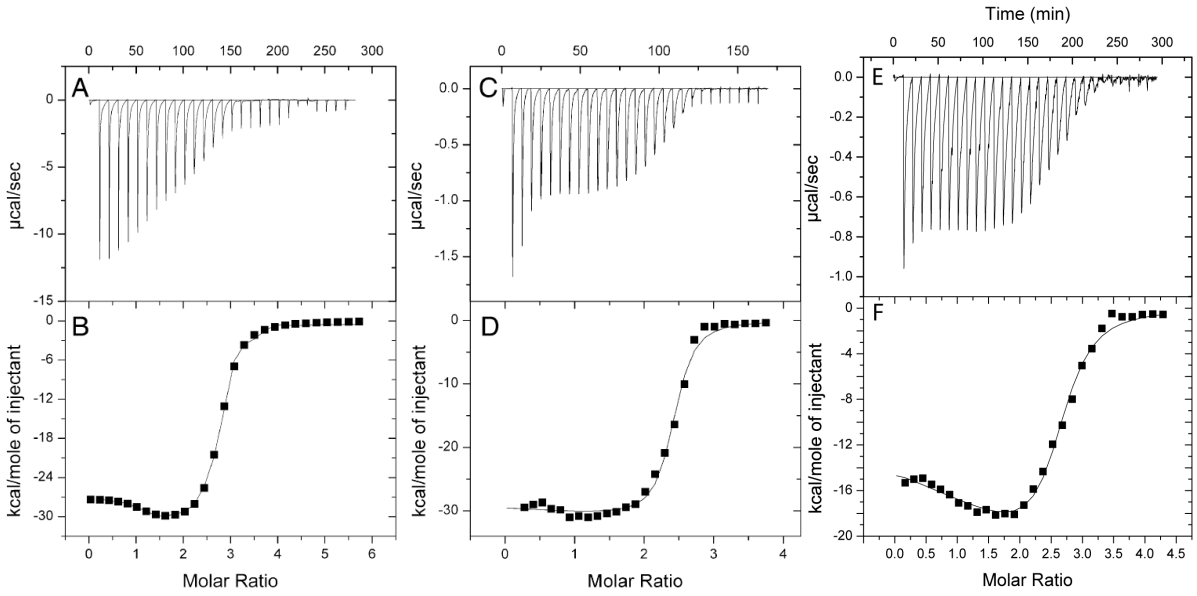

Figure 2.2. Fe(II) binding to ISU proteins by ITC. Raw isothermal titration calorimetry and binding isotherm data for ferrous iron binding to ISU proteins. Raw heat released data for *Dm* ISU (A) *Sc* Isu1 D37A (C) and *Sc* Isu1 WT (E) binding to ferrous iron, simulated fits to the binding isotherm data for *Dm* Isu (B), *Sc* Isu1 D37A (D) and *Sc* Isu1 WT (F). Data were collected anaerobically at 30°C in 20 mM HEPES (pH 7.5) and 150 mM NaCl and 5mM β-Me. Spacing between injections was 10 minutes. Syringe stirring speed was kept at 500 rpm.

Table 2.1. Fe (II) binding affinities of ISU proteins. ITC fitting parameters for ISU proteins binding ferrous iron. Averaged values for stoichiometry (N_1 and N_2) and dissociation constants (K_{D1} and K_{D2}) are provided with error bars.

Ortholog	N_1	K_{D1}	N_2	K_{D2}
H.sapien	1.0‡	2.0 ± 0.2 uM	---	---
D.melanogaster	1.21 ± 0.25	475 ± 166 nM	1.40 ± 0.07	64.5 ± 17 nM
S.cerevisiae (D37A)	1.19 ± 0.66	234 ± 35 nM	0.97 ± .31	6 ± 4 nM
T.maritima	1.0§	2.7uM	---	---
S.cerevisiae (WT)	1.61 ± 0.16	0.98 ± 0.75 uM	0.6 ± 0.16	18 ± 7.24 nm

‡ [16]
§ [15]

1.19 ± 0.66 atoms Fe(II) with a K_{D1} of 234 ± 35 nM and 0.97 ± 0.31 atoms Fe(II) with a slightly tighter K_{D2} of 6 ± 4 nM. These binding affinities are slightly tighter compared to previously published data for *Hs* and *Tm* ISU, of which both bound Fe(II) in the μM range **(Table 2.1);** however, the *Hs* and *Tm* data were collected under different buffer conditions [12, 15, 16]. The WT *Sc* Isu1 sample, as the D37A *Sc* Isu1 variant bound ca. 1.61 ± 0.16 atoms Fe (II) with a K_{D1} of 0.98 ± 0.75 μM and 0.6 ± 0.16 atoms Fe (II) with a tighter K_{D2} of 18 ± 7.24 nM shown in **Figure 2.2 E and F.**

2.5.2 Iron Coordination Geometry of ISU Proteins

XAS studies were used to probe the structural details of initial iron loading onto ISU type proteins. Full XAS data sets were collected on multiple independent samples of *Hs, Dm, Sc* and *Tm* ISU proteins with one iron bound. Samples were prepared anaerobically and loaded into each sample cell while the protein was inside a glove box. XANES analysis revealed iron was predominantly in the Fe(II) state as compared to ferrous iron controls, based on the analysis of the first inflection point of the edge feature for each spectrum. Raw EXAFS data for all 4 ISU samples show a predominant single frequency pattern centered at ca. 5-6 $Å^{-1}$ and this is suggestive of a nearest-neighbor coordination environment constructed of only O/N based ligands **(Figure 2.3 A, C, E, G black lines)**. An apparent 'camel back' feature is observed for the *Hs* and *Tm* samples **(Figure 2.3 A and G, respectively)** suggesting the presence of a Histidine ligand, but this feature is not present in the other samples. Fourier transforms of the data for *Hs, Dm, Sc* and *Tm* ISU proteins **(Figure 2.3 B, D, F, H,** black lines, respectively) indicate a predominant single nearest neighbor ligand environment feature

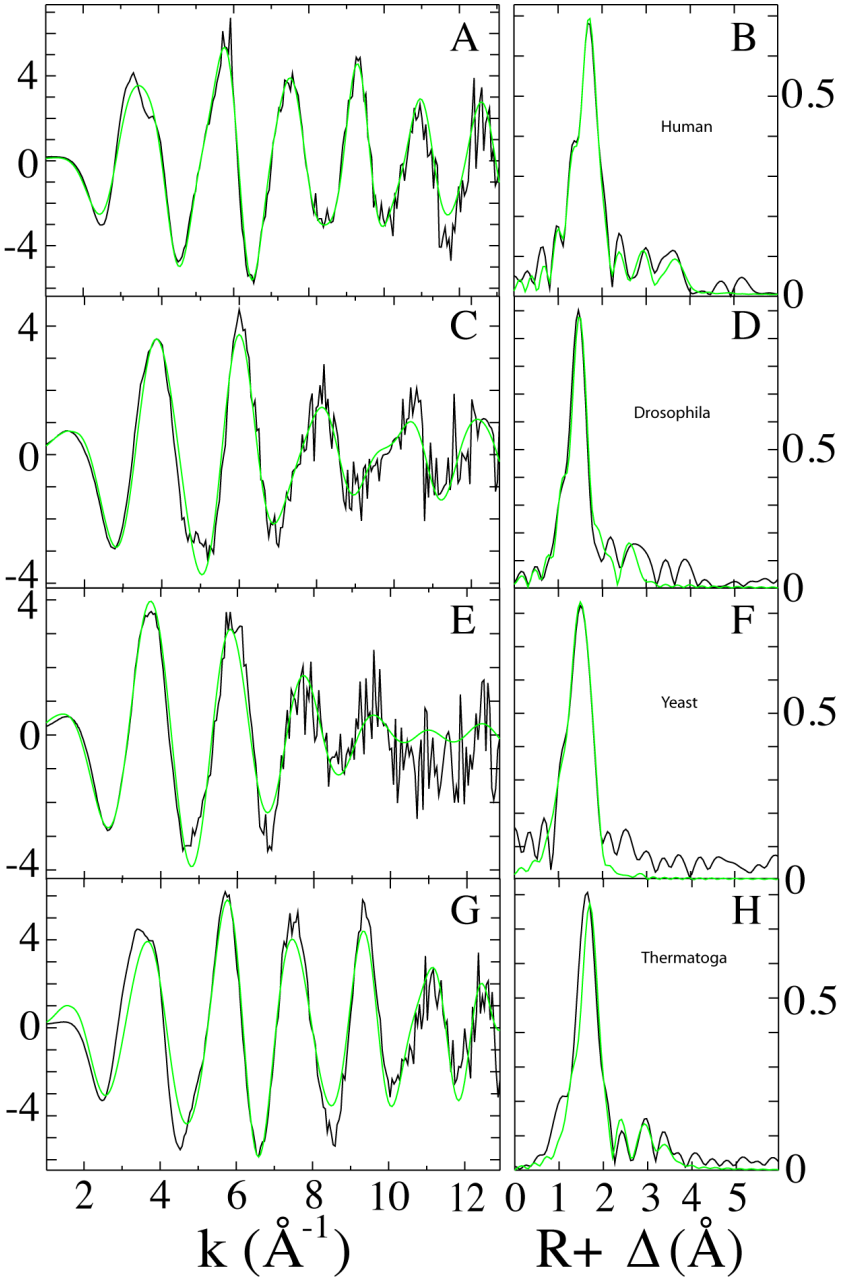

Figure 2.3. EXAFS and Fourier transforms of iron loaded ISU XAS data. EXAFSspectra in black (A,C,E,G) and FT (B,D,F,H) data, and best fit simulations shown in green of *H. sapiens* (A,B) *D. melanogaster* (C,D), *S. cerevisiae* (E,F) and *T. maritima* (G,H) ISU proteins bound to 1 Fe atom.

Table 2.2. Summary of EXAFS fitting results for Fe bound ISU proteins. Data fit over a *k* range of 1 to 12.5 $Å^{-1}$ using EXAFSPAK and feff7 theoretical models.

	Fe-Nearest Neighbor Ligands[a]				Fe···Long Range Ligands[a]				
Sample	**Atom[b]**	**R(Å)[c]**	**C.N.[d]**	**σ^{2} [e]**	**Atom[b]**	**R(Å)[c]**	**C.N.[d]**	**σ^{2} [e]**	**F' [f]**
H.sapien	O/N	2.01	1.5	2.02	C	3.13	3.0	5.83	0.45
	O/N	2.14	4.0	1.28	C	3.52	1.0	1.0	
					C	4.13	6.5	5.95	
D.melanogaster	O/N	1.99	3.0	3.78	C	3.13	1.5	3.01	0.32
	O/N	2.15	2.0	2.94					
S.cerevisiae	O/N	2.01	1.0	1.91	C	3.01	1.5	1.14	0.99
	O/N	2.14	4.5	3.25					
T.maritima	O/N	2.13	6.0	4.30	C	3.10	3	1.56	0.99
					C	3.27	4.5	1.20	
					C	3.49	4.5	1.66	
					C	3.71	3.5	3.9	

[a] Data were fit over a *k* range of 1 to 12.5 $Å^{-1}$.
[b] Independent metal-ligand scattering environment
[c] Scattering atoms: O (oxygen), N (nitrogen), S (sulfur) and C (carbon),
[d] Average metal-ligand bond length from two independent samples
[e] Average metal-ligand coordination number from two independent samples
[f] Average Debye-Waller factor in $Å^2$ x 10^3 from two independent sample

centered around a phase-shifted bond length (R + Δ) of ca. 1.8 Å, with minimal scattering from long distance ligands. *Hs, Dm,* and *Sc* data were best fit using 2 O/N shell nearest neighbor simulations **(Figure 2.3 A, C, E,** green lines) while *Tm* samples could only be fit using a single O/N shell **(Figure 2.3 F)**. Long-range scattering could only be fit with carbon scattering, attempts with fits using sulfur or iron atoms decreased the quality of the fit. The best-fit simulations are summarized in **Table 2.2**. All samples show partially disordered ligand environments with total coordination around 6, as would be expected for an Fe(II) with octahedral symmetry. Interestingly, there is no evidence for sulfur ligation in any of the samples. All orthologs studied appear to have similar but not identical metal binding characteristics using O/N based ligands.

The x-ray absorption near edge (XANES) plot for WT *Sc* Isu1 is plotted with two octahedral iron model complexes, ferrous and ferric sulfate (**Figure 2.4)**. When compared to the models, pre-edge and edge features of the WT protein are similar to that of an octahedral oxygen/ nitrogen containing environment**.** Edge energy at half height of the rising edge for the WT sample is 7120 eV, and that for ferrous sulfate control is 7119.5 eV, indicating a ferrous iron-containing complex. These results confirm the presence of an octahedral Fe (ll) complex bound to WT *Sc* Isu1.

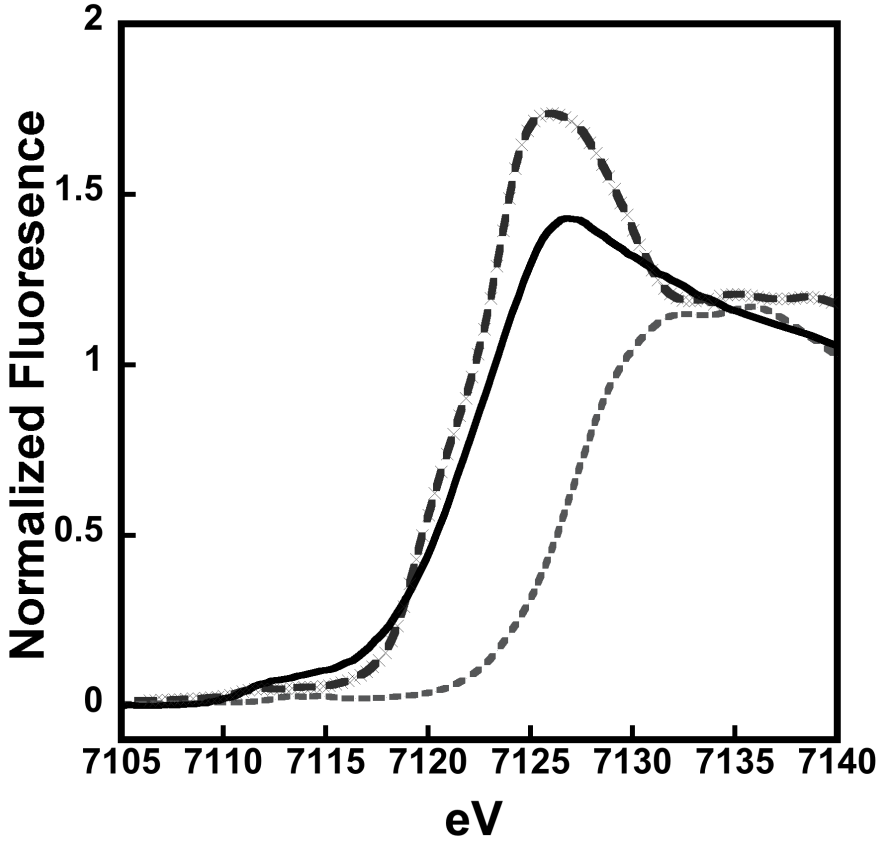

Figure 2.4: XANES spectrum of Fe (II) bound to WT *Sc* Isu1. Spectrum for WT *Sc* Isu1 shown in black solid line compared with two octahedral oxygen/nitrogen model complexes: Ferrous sulfate (-x-) and ferric sulfate (--). Spectrum was collected at NSLS X3B in buffer containing 20 mM HEPES (pH: 7.5), 250 mM NaBr, 5 mM β-Me. Two equivalents of Fe(II) was added to protein. Samples were prepared after overnight incubation of protein & reagents in an anaerobic glove box.

2.5.3 Metal Site Electronic Structure by Mössbauer Spectroscopy

Mössbauer spectroscopy was utilized as an alternative technique to probe the metal site electronic structure of ferrous iron bound to ISU proteins. The 4.5 K Mössbauer spectra of each ISU protein anaerobically loaded with ferrous iron are shown in **Figure 2.5** and each was consistent with high spin ferrous iron constrained within an octahedral ligand environment. A single major quadrupole doublet was observed for all samples, with δ values of 1.24, 1.20, and 1.27 mm/s for *Hs, Dm* and *Tm,* respectively, and corresponding ΔEQ values of 2.35,1.94 and 2.76 mm/s **(Table 2.3).**

2.6 Discussion

The ISU family of proteins is essential for cellular Fe-S cluster assembly. This family is highly conserved in their amino acid sequence, indicating a common and ancient evolution. In this report, we characterize the structural and electronic properties of ferrous iron bound to four members of the ISU family of proteins. Although ISU has been shown at both a genetic and biochemical level to be the scaffold upon which Fe-S cluster biosynthesis is orchestrated [5, 7, 15], the mechanistic details of Fe-S cluster assembly still remain elusive and have been the subject of intense research efforts by many research groups. Although cluster formation is chemically a simple task, it is still unclear how these events occur in a strictly controlled protein environment. Both the sulfide and iron donors have been identified which promote transfer of these substrates to the scaffold protein however the subsequent cluster formation is difficult to observe

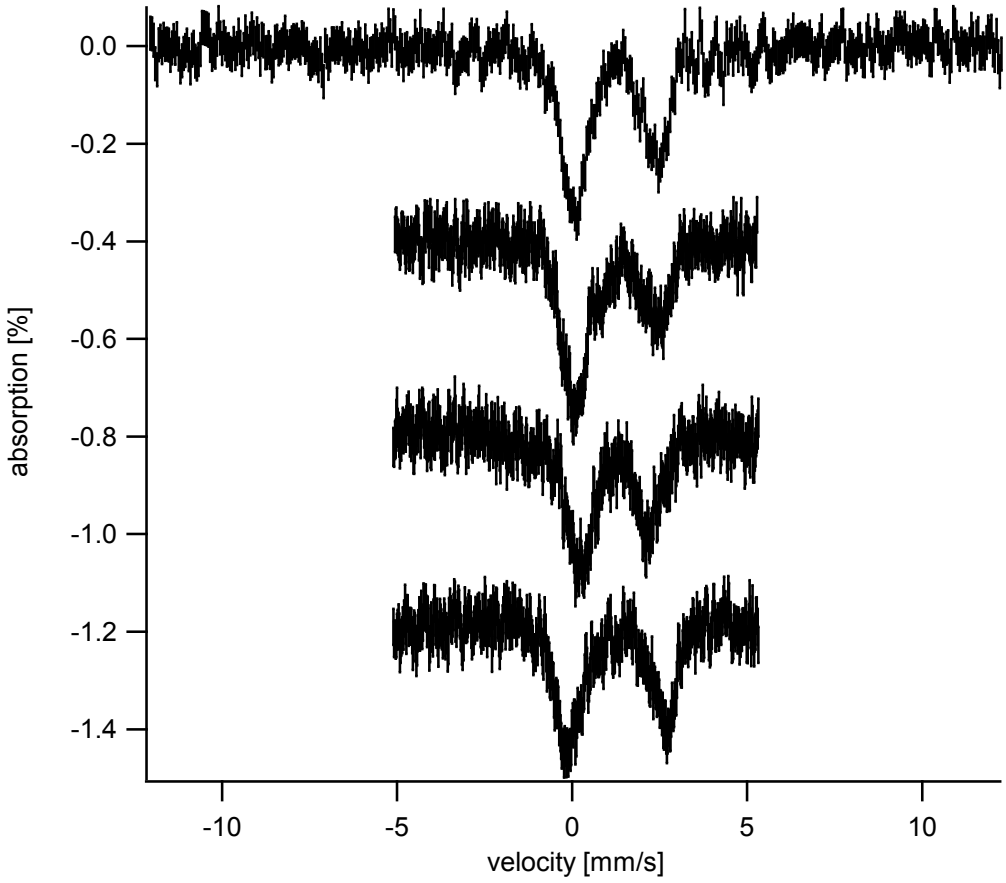

Figure 2.5. Mössbauer spectra of ISU proteins. Top to bottom: Human Isu 4.5K 700G parallel field, Human Isu 100K 700G parallel field, Drosophila Isu 4.5K 400G parallel field, *Thermatoga* Isu 4.5K 400G applied field. All samples have been collected ~24h for about 3-4 M counts of radiation.

Table 2.3. Analysis of Mössbauer parameters for Fe(II) bound ISU proteins.

Sample	δ (mm/sec)	ΔE_Q (mm/sec)	L_w (mm/sec)
H.sapien	1.26	2.60	0.768
D.melanogaster	1.24	2.83	0.801
S.cerevesiae	NA	NA	NA
T.maritima	1.26	2.61	0.742
Aq Fe (II)	1.35	3.06	

δ – Isomer shift
ΔEQ – Electric quadrupole
Lw – Line width at full width half maximum of signal

directly at a molecular level. It has been shown structurally that the product of cluster formation is bound at the 3-Cys site and these 3 Cys residues are implicated as being active site residues [17]. ISU proteins have previously been shown to bind iron, but biophysical analysis of the metal center has always been after an intact cluster has been formed [15, 16]. To help further elucidate the mechanistic details of cluster formation by the ISU proteins, we characterized iron binding of ISU proteins across a variety of species. A comparison of iron binding to ISU proteins by ITC shows these proteins are able to bind ferrous iron with low nanomolar and sub-micromolar affinities. These binding affinities are consistent with the copper chaperones have been studied to date [23].

Frataxin, the proposed iron donor within the Fe-S assembly pathway has been extensively studied using the human, fly, yeast and bacterial systems. To date, all frataxin homologs studied have been observed to bind iron with binding affinities also in the low micromolar range [13, 24-26]. Binding affinities for iron by the ISU proteins that are tighter than the chaperones themselves suggests metal transfer is energetically favorable. The process is most likely however much more complicated than simple inter-residue transfer, with multiple proteins and conformational changes ultimately leading to cluster formation. The K_D values reported by the Cowan group for Hs (K_D= 2.0 μM) and Tm (K_D= 2.7μM) ISU proteins are lower than those reported here for Dm (K_{D1}= 475 nM, K_{D2}= 64.5 nM) and Sc (K_{D1}= 234 nM, K_{D2}= 6 nM), but this may be attributable to the fact that different solution conditions were tested during the

experiments. It is clear that the different ISU proteins are capable of directly binding ferrous iron and this certainly has direct mechanistic implications regarding the protein's enzymatic function. We therefore probed the metal binding characteristic of these family members to further explore how clusters are assembled.

XAS and Mössbauer studies of ferrous iron bound to ISU proteins are consistent with a metal-ligand coordination environments constructed of only oxygen and nitrogen based ligands. XANES analysis of the iron edge for each ISU ortholog is consistent with iron being stable in the ferrous state based on the first inflection point of the edge and the primary energy feature of the 1s→3d transitions. In addition, the 1s→3d transitions areas and energies are consistent with the ferrous iron being stable in the high-spin state. A quadrupole doublet observed in each Fe-ISU sample by Mössbauer spectroscopy, with δ values at ca. 1.25 mm/s and ΔE_Q ~2 mm/s, also supports the presence of high spin ferrous iron. Both Mössbauer and EXAFS analysis indicate the metal is coordinated to only O/N based ligands, these coordination environments differ slightly between species. Best fit nearest neighbor environments for *Hs* ISU yield two O/N shells with coordination numbers of 1.5 and 4 at distances of 2.01 and 2.15 Å, respectively. Long-range ligand interactions at distances of 3.13, 3.52 and 4.13 Å are most likely due to carbon atoms. *Dm* Isu was also best-fit using two O/N ligand environment with 3 O/N atoms at 1.99 Å and 2 O/N atoms at 2.14 Å. Long-range interactions were also best fit with a carbon shell at 3.13Å. Similarly, *Sc* Isu1 was best fit with two shells, the first composed of 1 O/N at 2.01 Å and the second composed of

4.5 O/N at a distance of 2.14 Å. The long-range interaction at 3.01 Å was best fit with carbon. Iron bound *Tm* IscU show a slightly different coordination geometry with only a single O/N shell composed of 6 ligands at 2.13 Å, long-range carbon scattering was best fit at 3.27, 3.49 and 3.71 Å.

Simulations to the different Mössbauer data qualitatively support these XAS results. The ISU proteins from different sources have somewhat different isomer shift and quadrupole splitting values, which suggests that the ligands are not precisely the same in each. The isomer shift arises from differences in s-electron densities between source and absorber nuclei and is sensitive to oxidation and spin state. Here we observe relatively high values (δ = 1.20-1.27) due to shielding of the outer s-electron charge density by the inner 3d electron charge density indicating a metal center in the S=2 high spin ferrous state. Additionally this shielding leads to the high quadropole splittings of around 2-3 mm s^{-1}. Although line widths are not extraordinarily large it is possible they may indicate multiple spectral features, and therefore multiple species or binding sites. Interestingly, the δ and ΔE_Q for the different ISU proteins are not exactly the same. This suggests some variation in coordinating ligands, with *Tm* having more oxygen and *Dm* having the most nitrogen with *Hs* and *Sc* in between.

In summary, these data report clear evidence that the ISU proteins have an iron binding site that is distinct from the Cys rich active site. In particular, these data indicate: 1) ISU orthologs are able to bind iron with high affinity and 2) ferrous iron is bound initially via O/N based ligands. In this report, we focused solely on the initial

process of iron binding to the ISU orthologs to gain insight into the Fe-S cluster assembly pathway. It was originally assumed that both iron and sulfur addition to ISU scaffold proteins occurred at the 3 Cys active site. Our data indicate ISU initially bind iron in a step prior to cluster assembly at a distinctly separate site composed entirely of non-cysteine ligands. The techniques used in this study do not provide any information as to the identification of the residues that make up this initial metal binding site, nor how the metal is transferred from the iron binding site to the active site. Insight into the conserved sequences may provide further clarification into how these proteins bind iron. Acidic residues are highly conserved in approximately 11 positions (9 of which are completely conserved in our alignment) and 3 partially conserved His residues. We therefore plan to target each of these residues in the future to provide better clarification into which are at the Fe binding site.

2.7 Acknowledgements

This work was supported by the National Institutes of Health (TLS DK068139) and by the American Heart Association (AHA12PRE11720005). Portions of this research were carried out at both the Stanford Synchrotron Radiation Laboratory (SSRL) and at the National Synchrotron Light Source (NSLS). SSRL is a national user facility operated by Stanford University on behalf of the U.S. Department of Energy, Office of Basic Energy Sciences. The SSRL Structural Molecular Biology Program is supported by the Department of Energy, Office of Biological and Environmental

Research, and by the NIH, National Center for Research Resources, Biomedical Technology Program. NSLS, located at Brookhaven National Laboratory, is supported by the U.S. Department of Energy, Division of Materials Sciences and Division of Chemical Sciences, under Contract No. DE-AC02-98CH10886.

2.8 References

1. Huber, C. and G. Wachtershauser, *Peptides by activation of amino acids with CO on (Ni,Fe)S surfaces: implications for the origin of life.* Science, 1998. **281**(5377): p. 670-2.
2. Beinert, H., Holm,R.H., Munck,E., *Iron-sulfur clusters: nature's modular, multipurpose structures.* Science, 1997. **277**: p. 653-659.
3. Johnson, D.C., et al., *Structure, function, and formation of biological iron-sulfur clusters.* Annu Rev Biochem, 2005. **74**: p. 247-81.
4. Lill, R., *Function and biogenesis of iron-sulphur proteins.* Nature, 2009. **460**(7257): p. 831-8.
5. Garland, S.A., et al., *Saccharomyces cerevisiae ISU1 and ISU2: members of a well-conserved gene family for iron-sulfur cluster assembly.* J Mol Biol, 1999. **294**(4): p. 897-907.
6. Gerber, J., U. Muhlenhoff, and R. Lill, *An interaction between frataxin and Isu1/Nfs1 that is crucial for Fe/S cluster synthesis on Isu1.* EMBO Rep, 2003. **4**(9): p. 906-11.

7. Gerber, J., et al., *The yeast scaffold proteins Isu1p and Isu2p are required inside mitochondria for maturation of cytosolic Fe/S proteins.* Mol Cell Biol, 2004. **24**(11): p. 4848-57.

8. Muhlenhoff, U., et al., *Components involved in assembly and dislocation of iron-sulfur clusters on the scaffold protein Isu1p.* Embo J, 2003. **22**(18): p. 4815-25.

9. Wiedemann, N., et al., *Essential role of Isd11 in mitochondrial iron-sulfur cluster synthesis on Isu scaffold proteins.* Embo J, 2006. **25**(1): p. 184-95.

10. Mansy, S.S. and J.A. Cowan, *Iron-sulfur cluster biosynthesis: toward an understanding of cellular machinery and molecular mechanism.* Acc Chem Res, 2004. **37**(9): p. 719-25.

11. Foury, F., A. Pastore, and M. Trincal, *Acidic residues of yeast frataxin have an essential role in Fe-S cluster assembly.* EMBO Rep, 2007. **8**(2): p. 194-9.

12. Huang, J., E. Dizin, and J.A. Cowan, *Mapping iron binding sites on human frataxin: implications for cluster assembly on the ISU Fe-S cluster scaffold protein.* J Biol Inorg Chem, 2008. **13**(5): p. 825-36.

13. Kondapalli, K.C., et al., *Drosophila frataxin: an iron chaperone during cellular Fe-S cluster bioassembly.* Biochemistry, 2008. **47**(26): p. 6917-27.

14. Wang, T. and E.A. Craig, *Binding of yeast frataxin to the scaffold for Fe-S cluster biogenesis, Isu.* J Biol Chem, 2008. **283**(18): p. 12674-9.

15. Nuth, M., T. Yoon, and J.A. Cowan, *Iron-sulfur cluster biosynthesis: characterization of iron nucleation sites for assembly of the [2Fe-2S]2+ cluster*

core in IscU proteins. Journal of the American Chemical Society, 2002. **124**(30): p. 8774-8775.

16. Huang, M.L., et al., *Elucidation of the mechanism of mitochondrial iron loading in Friedreich's ataxia by analysis of a mouse mutant.* Proc Natl Acad Sci U S A, 2009. **106**(38): p. 16381-6.
17. Shimomura, Y., et al., *The asymmetric trimeric architecture of [2Fe-2S] IscU: implications for its scaffolding during iron-sulfur cluster biosynthesis.* J Mol Biol, 2008. **383**(1): p. 133-43.
18. Studier, F.W., *Protein production by auto-induction in high density shaking cultures.* Protein Expr Purif, 2005. **41**(1): p. 207-34.
19. Foster, M.W., et al., *A Mutant Human IscU Protein Contains a Stable [2Fe-2S]2+ Center of Possible Functional Significance.* J. Am. Chem. Soc., 2000. **122**: p. 6805-6.
20. Lassmann, T., O. Frings, and E.L. Sonnhammer, *Kalign2: high-performance multiple alignment of protein and nucleotide sequences allowing external features.* Nucleic Acids Res, 2009. **37**(3): p. 858-65.
21. George, G.N., S.J. George, and I.J. Pickering, *EXAFSPAK*. 2001, http://www-ssrl.slac.stanford.edu/~george/exafspak/exafs.htm: Menlo Park, CA.
22. Randall, C.R., et al., *X-ray absorption pre-edge studies of high-spin iron (II) complexes.* Inorg Chem, 1995. **34**(5): p. 1036-1039.

23. Kim, B.E., T. Nevitt, and D.J. Thiele, *Mechanisms for copper acquisition, distribution and regulation.* Nat Chem Biol, 2008. **4**(3): p. 176-85.

24. Yoon, T. and J.A. Cowan, *Iron-sulfur cluster biosynthesis. Characterization of frataxin as an iron donor for assembly of [2Fe-2S] clusters in ISU-type proteins.* J. Am. Chem. Soc., 2003. **125**: p. 6078-84.

25. Bou-Abdallah, F., et al., *Iron binding and oxidation kinetics in frataxin CyaY of Escherichia coli.* J Mol Biol, 2004. **341**(2): p. 605-15.

26. Cook, J.D., et al., *Monomeric yeast frataxin is an iron-binding protein.* Biochemistry, 2006. **45**(25): p. 7767-77.

CHAPTER 3
IDENTIFICATION OF A PUTATIVE IRON BINDING SITE ON THE C-TERMINUS OF YEAST IRON-SULFUR SCAFFOLD PROTEIN ISU & IMPLICATIONS FOR IRON DELIVERY BY FRATAXIN

3.1 Prelude

This chapter describes my work directed at the identification and characterization of the ISU Fe binding site described in Chapter 2. X-ray absorption spectroscopy (XAS) studies showed that this site was found to be composed entirely of oxygen/nitrogen based ligands, distinct from the protein's thiol rich active site. The goal of this work is therefore, to identify the region & and residues on ISU, in the yeast model (YIsu1), that constitute this initial Fe binding site. Site directed mutagenesis and subsequent spectroscopic, calorimetric and kinetic analysis of the mutant proteins in comparison to the wild-type (WT) and in the presence/absence of Frataxin were employed in this study. These results aim to provide insight, at the atomic level, into the delivery of iron to YIsu1 and, subsequent loading of its cysteine rich active site. Contributors to this work were Dr. Ashoka Kandegedara, a postdoctoral researcher in the Stemmler lab who designed and performed a competition assay to determine Fe(II) binding affinities of wild type (WT) YIsu1 and mutants, graduate student Stephen Dzul, who aided in development of a time-dependent Circular Dichroism assay to determine activity of Fe-S synthesis of YIsu1 proteins, and a summer undergraduate student (2011-13), John Rotondo who aided in protein purification and collection of Far UV CD experiments. This work is being prepared for submission to the journal Biochemistry.

3.2 Abstract

Eukaryotes utilize the protein ISU as a scaffold for the assembly of iron-sulfur clusters within the mitochondria. Yeast Isu1 (YIsu1) contains three conserved cysteine residues at its active site that coordinate the utilization of ferrous iron, Fe(II) and inorganic sulfide, S^{2-} for assembly into a 2Fe-2S cluster. We have previously shown that YIsu1 binds two iron atoms with sub-micromolar to nanomolar affinity and that YIsu1 interacts with the yeast Frataxin homologue 1 protein (Yfh1) in an iron-dependent manner. Frataxin has since been described to participate in cluster assembly as an iron donor and a pathway modulator. Although its function is essential, atomic details of its interactions with partner proteins are still lacking. Recently, we have found by X-ray absorption spectroscopy (XAS) and Mössbauer spectroscopy (manuscript in preparation) that YIsu1 binds iron in a 6 coordinate octahedral oxygen/nitrogen (O/N) based ligand environment free of thiol ligation, indicating that YIsu1 binds Fe initially at a site independent of the protein's cysteine rich active site. In this report, we demonstrate that the C-terminal residues of YIsu1 participate in iron loading leading to a possible molecular rearrangement that drives a structural switch to enable iron translocation to the thiol rich protein active site in order to accomplish Fe-S cluster assembly. Iron binding competition assays and isothermal titration calorimetry experiments show a reduction in the Fe(II) and Frataxin binding affinity for mutant YIsu1 forms (E144A and D145A). Differential scanning calorimetry studies, comparing holo-WT YIsu1 to mutants, show a change in stability and associated thermodynamic parameters. Finally, our *in*

vitro Fe-S assembly assay shows mutant Yfh1 has a dramatically perturbed ability to complete Fe-S cluster biosynthesis, as compared to the WT protein. Based on these results, we speculate that the residues E144 and D145 on the Yfh1 C-terminal α-helix serves as a possible initial iron-binding site on the scaffold protein, and that metal delivered to this site can then be utilized for Fe-S cluster assembly.

3.3 Introduction

Iron sulfur (Fe-S) clusters are indispensible for life [1]. These inorganic cofactors have a high degree of chemical versatility which allows them to participate, when bound to proteins, in several reactions that include electron transfer (complex 1 & 2 of the electron transport chain) [2], enzyme catalysis (mitochondrial Aconitase that functions in glycolysis) [3], signal transduction (DinG that participates in DNA repair) [4] and sensing of cellular metabolites such as oxygen and Fe content (Cytosolic Aconitase/IRP) [5, 6]. As these pathways are essential to sustain life**,** an inability to synthesize these clusters is a condition that is incompatible to life [7].

The assembly of iron sulfur clusters occurs by a highly regulated protein controlled process owing to the instability of the cofactor in aerobic environments and the inherent toxicity of free iron and sulfide [8-10]. The formation of a multiprotein complex ensures efficient production and delivery of clusters, while at the same time actively suppresses free radical formation by free iron and the cyanide-like effects of free sulfide [11]. In yeast, this complex is found within the mitochondria and is

composed of the cluster assembly scaffold protein (Isu1), the cysteine desulfurase that provides sulfur for cluster assembly (Nfs1), the Nfs1 accessory protein (Isd11), a ferredoxin that provides reducing equivalents for cluster assembly (Yah1) and the protein frataxin (Yfh1), which has been suggested to serve as an iron chaperone that delivers Fe(II) for cluster assembly, a regulator of Nfs1 activity [12]. Defects or deficiencies in these proteins have been associated with several human diseases [7, 13]. A deficiency of Frataxin causes the debilitating disease Friedreich's Ataxia (FRDA), associated with pooling of iron in the mitochondria of nerve and muscle tissues of affected individuals leading to progressive neurodegeneration and cell death [14, 15]. In addition to disrupted iron homeostasis, cardiac biopsies of FRDA patients exhibited decreased activity of several Fe-S containing proteins, such as Aconitase, and proteins of the electron transport chain involved in respiration, such as Complexes I, II & III [13, 16]. A genetic deficiency of ISU, caused by a splice-defect, has been reported to be associated with muscular dystrophy in humans, due to a deficiency of Fe-S containing proteins Succinate dehydrogenase and Aconitase [17, 18]. In yeast, Isu1 and 2 are YIsu paralogs that show a combined deletion mutant lethality [19].

The active site of all Isu orthologs contains conserved cysteine residues that coordinate the assembled iron-sulfur cluster [20]. Our XAS studies have shown that YIsu1 binds iron at a site comprising a 6 coordinate O/N ligand environment [8]. In addition, our XAS and Mössbauer studies on Fe(II) bound to ISU proteins in the human, fly and *T. maritima* orthologs show the same trend (chapter 2). This suggests ISU must

bind iron at an initial acceptor site that is distinct from its Cysteine rich active site. The occurrence of a distinction between a metal acceptance site from a substrate binding site has been described previously for iron delivery to the protein Ferrochelatase that participates in heme biosynthesis [21].

The crystal structure of IscU from *Aquiflex aeolicus* has shown distinct structural differences in the IscU C-terminus dependent on the presence and absence of bound cluster [20]. There appears to be an increase in order of the N-terminal region of the IscU C-terminal helix coupled to cluster formation. Our previous studies have shown that YIsu1 undergoes changes in fold upon substrate binding. Using the ANS chromophore, we have shown that binding of both Fe(II) and S^{2-} to Isu1 is associated with an increase in order of the protein's fold [8]. Recently, solution structural studies by the Markley lab have shown that Isu does indeed exist in equilibrium between two structural conformations: a "structured" (S) and "disordered" (D) states [22]. The D state has been reported to be the substrate for Nfs binding. Cluster synthesis then drives the protein to the S state, which is the substrate for co-chaperone proteins that remove the cluster and drive the downstream delivery of cofactor to target apoproteins [23].

In this report, we study the properties of charged and conserved amino acid residues on the YIsu1 C-terminus (residues E144 and D145) with regards to iron binding, their interaction with Frataxin and Fe-S assembly. Using site directed mutagenesis, these residues were mutated to alanine. Using competition-binding studies, mutated proteins show a decrease in Fe(II) binding affinity by up to 8 fold, in

case of the E144A mutant, and up to 5 fold, in case of the D145A mutant. In addition, interactions between these mutant proteins and holo-Frataxin, measured using isothermal titration calorimetry (ITC), showed pronounced changes in binding energetics. Differential scanning calorimetry (DSC) was used to test the stability of the apo and holo forms of both WT and mutant protein. Finally circular dichroism (CD) spectroscopy was used to test the overall fold of the mutants and to test the ability of these mutants to synthesize Fe-S clusters. For Fe-S assembly, although WT YIsu1 showed an increased activity upon Frataxin binding, the D145A mutant protein behaved differently in the presence of Frataxin, possibly due to changes in associated energetics permitting assembly by an alternative mechanism. The involvement of these residues in initial iron loading of YIsu1 is explored in detail below.

3.4 Materials & Methods

3.4.1 Site Directed Mutagenesis & Protein Expression:

Characteristics of expression and isolation of wild type YIsu1 have been outlined within Chapter 2. The Quickchange site directed mutagenesis kit (Stratagene) was used to make point mutations (E144A, D145A, and double mutant E144A, D145A) on the pET21b plasmid containing the YIsu1 gene without the N-terminal targeting sequence (Δ1-32 YIsu1). Forward and reverse primers were designed using Quickchange primer design program and were purchased from Invitrogen (**Table 3.1**). Mutations were confirmed by DNA sequencing (Genewiz). Plasmids containing the

Ylsu1 wild type (WT Ylsu1) and mutant genes were transformed into BL21 codon plus RIL cells (Stratagene) for protein expression. Cells were grown at 37^0C in Luria-Bertani broth containing Ampicillin (0.1 µg/µl) and Chloramphenicol (0.05 µg/µl) with shaking speed set at 250 rpm. At OD_{600} of 0.6, cells were induced for protein expression by the addition of 0.8 mM IPTG. Post induction expression conditions were found to be optimum at a temperature of 37 ^{0}C, over a period of 3 hrs. following which the cells were harvested by centrifugation and stored at -80 ^{0}C until lysis.

3.4.2 Protein Purification:

All protein isolation steps were carried out at 4^0C. Cells were re-suspended in buffer containing 50 mM $NaPO_4$ (pH 7.4), 300 mM NaCl, 10 mM Imidazole, 5 mM β-Me (5 ml buffer/g cells) in the presence of lysozyme (100 µg/µl), a complete EDTA free protease inhibitor tablet (1 tablet/ 50 ml, Roche), DNAse (10 µg/ml) and $MgCl_2$ (5 mM), and then allowed to incubate for ~15 mins. Cells were lysed by three passes through a high-pressure homogenizer (Emulsiflex C3, Avestin) and centrifuged at 21,000 rpm for one hour. The supernatant was separated and filtered using a 0.2 µm filter and the crude soluble fraction was loaded onto a bench top column filled with Ni-NTA (Qiagen) affinity resin. Using a stepwise imidazole gradient (20-500 mM), Ylsu1 eluted at a concentration of ~200 mM Imidazole. Fractions containing protein were pooled and treated with 5 mM EDTA (overnight), followed by concentration to 1 ml using 10 KDa cutoff Amicon filters and then loaded onto a Sephadex 75 gel filtration column (GE)

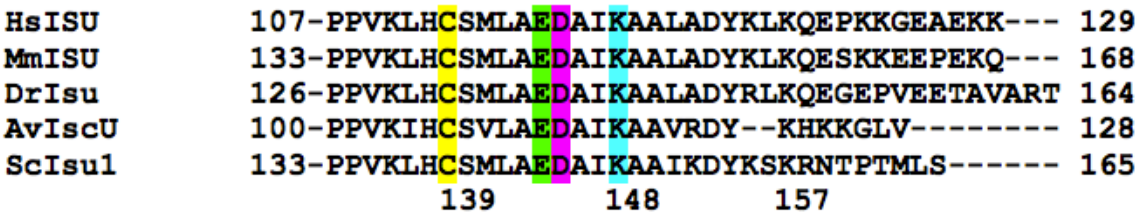

Figure 3.1: Amino acid sequence comparison of the C-terminal region of Isu1 orthologs. Human (*Hs*ISU), Mouse (*Mm*ISU), Zebrafish (*Dr*Isu), Bacteria (*Av*IscU) and yeast (*Sc*Isu1). Conserved residues in the proposed Fe binding site are in green and pink while the c-terminal most conserved cysteine residues at the Isu active site is in yellow.

Table 3.1: **List of primers used for Site Directed Mutagenesis**

Primer Name	Primer Sequence[a]
Ylsu1 E144A forward	**5'**-GCTCTATGTTAGCGG***C***AGATGCGATCAAGGC-**3**'
Ylsu1 E144A reverse	**5'-**GCCTTGATCGCATCT***G***CCGCTAACATAGAGC-**3'**
Ylsu1 D145A forward	**5'-**GCTCTATGTTAGCGGAAG***CG***GCGATCAAGGCAGC**-3'**
Ylsu1 D145A reverse	**5'-**GCTGCCTTGATCGC***CG***CTTCCGCTAACATAGAGC**-3'**
Ylsu1 E144A, D145A forward	**5'-**GCTCTATGTTAGCGG***C***AG***CG***GCGATCAAGG**-3'**
Ylsu1 E144A, D145A reverse	**5'-**CCTTGATCGC***CG***CT***G***CCGCTAACATAGAGC-**3**'

[a] Mutated residues are represented in italics and underlined.

equilibrated with 20 mM HEPES (pH 7.5), 150 mM NaCl and 5 mM β-Me. The protein eluted at a volume corresponding to a dimer, pure fractions were pooled and protein concentration was determined using IR Spectrometry (EMD Millipore Direct Detect). Purification yielded about 2mg/ml of ≥95% pure protein from ~50 gm cells. Molecular weights for WT Ylsu1 and mutant proteins were confirmed by Mass Spectrometry (**Table 3.2**).

3.4.3 Far UV Circular Dichroism:

Pure protein samples of 250-300 µl volume were dialyzed using 3.5 KDa cutoff dialysis membranes (Spectrum Labs) into 1 mM $NaPO_4$ (pH 7.5) buffer of 300 ml volume for 3 hrs at 4^0C with 1 buffer change in between. Spectra were collected at a concentration of both 10 uM and 25 uM using JASCO J-1500 CD spectrometer with a 1 mm pathlength cuvette over a range of 185-260 nm with a scanning speed of 50 nm/minute at room temperature. Prior to data collection, the instrument was baselined without a cuvette to eliminate any background spectral contributions from the instrument. Presented data represent an average of two independent preparations for each protein sample, and each dataset is an average of 8-12 scans. Data were analyzed using the Spectra Analysis software provided by JASCO. Baseline correction

Table 3.2: Masses of Ylsu1 WT and mutants

Sample	Calculated Mass (Da)	Experimental Mass (Da)
WT	15515.9	15514.4[a]
D145A	15471.8	15471[a]
E144A	15457.8	15456.2[a]
E144A D145A	15413.8	15407[b]

[a] Determined by ESI-MS
[b] Determined by Average Mass Spectrometry

was accomplished by subtracting an averaged buffer spectrum from each averaged protein spectrum. Data were fit using the CD Pro fitting program provided by JASCO. Reference databases for soluble proteins namely SP29, 37 and 43 were used and best fits were obtained using the CONTIN method. Fits with the lowest RMSD values were selected and averaged. CD curves were smoothed for display and secondary structure percentages were tabulated from raw unsmoothed data. Standard deviations between averaged runs are denoted in parenthesis

.

3.4.4 Isothermal Titration Calorimetry experiments & analysis:

The binding properties of YIsu1 WT and mutant proteins to Fe(II) and to holo Yfh1WT were tested using ITC. Protein and aqueous ferrous ammonium sulfate solutions were prepared anaerobically in a glove box (Coy Laboratories) in buffer containing 20 mM HEPES (pH 7.5), 150 mM NaCl and 5 mM β-Me. Protein samples were maintained at 4^0C and buffers were extensively degassed prior to sample preparation and loading. Holo Yfh1 was prepared by incubating equimolar amounts of Yfh1WT and Ferrous Ammonium Sulfate solution 15-30 minutes prior to use. ITC data were collected on a TA Instruments Nano ITC calorimeter located within the Coy anaerobic chamber by titrating 1 mM holo Yfh1 WT into a 1.3 ml volume of 50 uM protein solution. Data collection parameters followed a 2 µl initial injection of titrant solution followed by 35 additional injections of 7 µl using a 250 µl syringe. Injections were spaced at 10 minutes each and data was collected at 30^0C with stirring speed set

at 250 rpm. Control experiments of 1 mM holo Yfh1WT titrated into buffer was subtracted from the experimental data to eliminate background heats of dilution. Data analysis was performed utilizing the Nano Analyze software provided by TA instruments using a multiple sites model for curve fitting and analysis. All experiments were performed in duplicate on independent samples to ensure data reproducibility.

3.4.5 Competition Assay:

The affinity of WT YIsu1 and mutants proteins for Fe(II) was determined by competition titrations using Mag-fura-2 (Molecular Probes), a well-known metal chelator that binds ferrous iron. Mag-fura-2 forms a 1:1 complex with most divalent cations and has an absorbance maximum at 366 nm that shifts to 325 nm when metal is bound. The decrease in absorbance at 366 nm as Mag-fura-2 binds increasing amounts of Fe (II) in competition with the protein was monitored on a Shimadzu UV-1800 spectrophotometer using 1 cm pathlength quartz cuvettes. Data were collected at room temperature within an anaerobic chamber (Coy Laboratories). Mag-fura-2 was dissolved in high purity MiliQ water and stored at -80^{0}C in 10 µL aliquots of 2 mM stock concentration. Protein samples and ferrous ammonium sulfate solutions were prepared in buffer containing 20 mM HEPES (pH 7.5) and 150 mM NaCl. Prior to use, protein samples were reduced with 5 mM TCEP. All protein samples, reagents and buffers were allowed to incubate at 4^{0}C overnight in an anaerobic chamber before data collection. For the control reaction, the initial starting solution contained 2-5 μM Mag-fura-2 in 1 ml of reaction buffer, aliquots of Fe (II) of varying volumes were then titrated

until saturation. Each spectrum was collected from 200-800 nm for each 'i'th addition of metal aliquot. Dilution correction was performed by carrying out the same experiment using buffer instead of Fe(II). For protein titrations, the same procedure was followed except that 10-20 μM of protein was mixed with Mag-fura-2 at the beginning of the binding reaction. Metal free Mag-fura-2 concentrations was confirmed using the molecules' molar absorptivity (ε) value at 366 nm that is 29900 $M^{-1}cm^{-1}$ [24]. The dissociation constant of Fe (II)-Mag-fura-2 complex under the above buffer conditions was determined to be 2 (±0.07) µM. Data were fit using the program DYNAFIT [25] with both one and two-site binding models. Our reported K_d values are an average 3 runs.

3.4.6 Differential Scanning Calorimetry experiments & analysis:

Thermal stability of the WT- and mutant YIsu1 samples in the absence and presence of iron were evaluated using a VP Differential scanning calorimeter (TA Instruments) to determine stability parameters associated with the mutants in the apo and holo forms. Protein and iron solutions were prepared anaerobically in 20 mM HEPES (pH 7.5), 150 mM NaCl and 5 mM β-Me. Buffer was extensively degassed prior to sample preparation and loading. Protein concentrations of 1.25 -1.5 mg/ml were used and iron solution was added to obtain samples upto a 1:2 protein:Fe ratio and made up to a final volume of 600 µl. YIsu1 WT remained stable upon addition of Fe, however slight precipitation was observed among the mutants, which was removed by centrifugation, and the change in protein concentration was noted. Scans were run at a

rate of 2^0C per min over a temperature range of 10-90^0C, while pressure was maintained at an excess of 2.95 atm throughout the scan period. Data obtained were analyzed using the Nano Analyze software provided by TA Instruments. Data was baseline subtracted using control runs of buffer alone or buffer with iron at concentrations that matched the amount in protein samples. Peak deconvolution was achieved using the two state scaled mathematical model that incorporates the A_w factor, which accounts for inaccuracies in protein concentration upon denaturation. Data presented represents an average of two independent samples.

3.4.7 Near UV CD for Assembly Activity:

The cluster reconstitution of apo WT YIsu1 and mutants was tested by time course CD spectroscopy. All proteins, reagents and the buffer solution of 20 mM HEPES (pH 7.5), 150 mM NaCl and 5 mM β-Me, were allowed to incubate overnight in an anaerobic chamber. Protein and buffer were maintained at a temperature of 4^0C overnight. All solutions were prepared in the above-mentioned buffer within the anaerobic chamber immediately prior to data collection. The reaction mixture consisted of 100 uM apo YIsu1 WT or mutant, 200 uM ferrous ammonium sulfate solution or 200 uM holo Yfh1 (prepared by incubating equimolar concentrations of Yfh1 and Fe(II) for 15-30 minutes prior to use) and 1 M Na_2S solution made up to a final volume of 1.2 ml. Data was collected on a JASCO J-1500 CD spectrometer at room temperature with a 1 cm pathlength cuvette, which was capped to eliminate any air induction. The instrument

was baseline subtracted without a cuvette prior to data collection to eliminate any background spectral contributions from the instrument. Data was recorded over 300-700 nm and 2 scans were collected at a scanning speed of 100 nm/min; these scans were then averaged. The mixture was subjected to agitation using a magnetic stir bar for 30 seconds prior to data collection. Scan sets were collected every 10 minutes until signal saturation was observed. Data were averaged using the Spectra Analysis software provided by JASCO. The absorbance signal at 435 nm was used for activity plots of absorbance v/s time, plotted using Kaleidagraph.

3.5 Results

3.5.1 Mutant proteins have a similar fold as wild-type (WT) YIsu1:

Far UV CD spectroscopy was used to compare the relative protein fold of WT and mutant Isu1 proteins. WT and mutant YIsu1 proteins were all well folded with a similar secondary structural content. Far UV CD results showed the presence of two predominant secondary structural features: α-helix (positive feature at 192 nm and negative at 208 nm & 222 nm) and β-sheet (negative feature at 218 nm and positive at 196 nm) [26] in WT YIsu1 and to a similar degree in the mutant spectra **(Figure 3.2)**. The wild type protein shows a secondary structural makeup of 20 (± 7)% α-helix, 26 (± 7)% β-sheet, 22 (± 1)% turns and 32 (± 1)% unordered **(Table 3.3)** with an RMSD

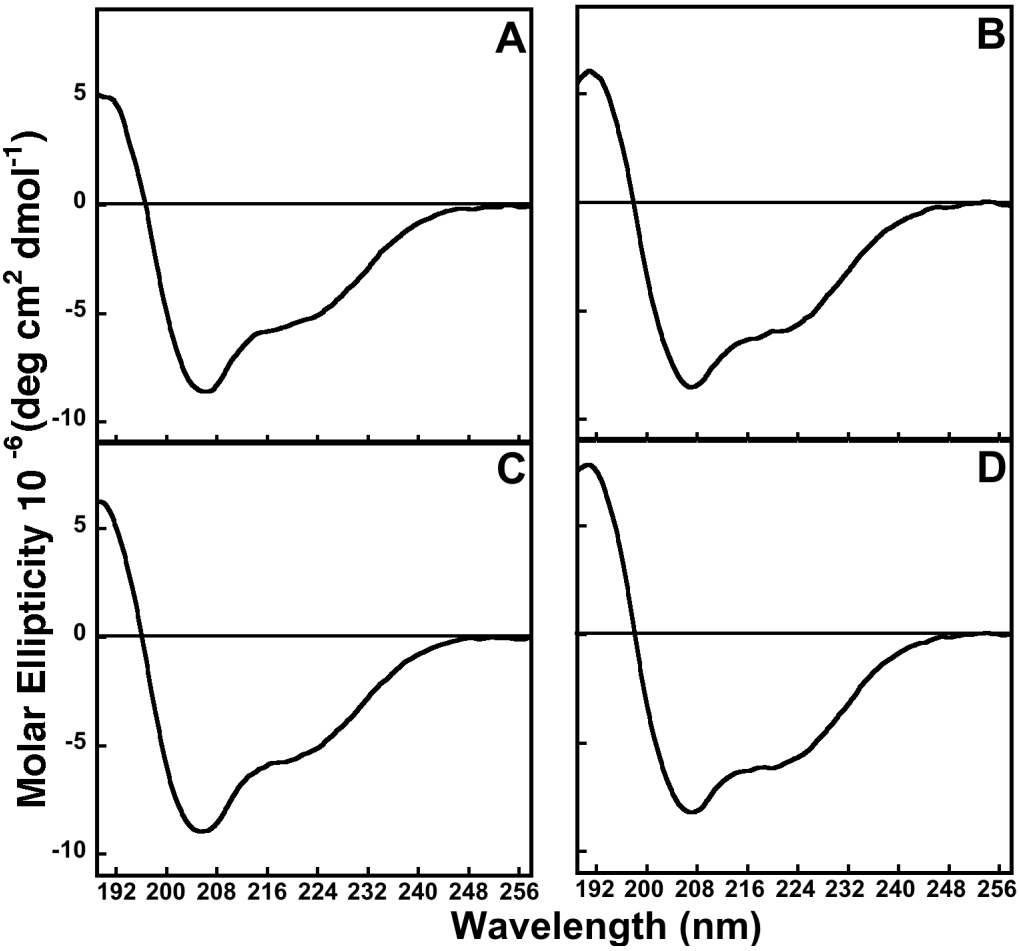

Figure 3.2: Far UV Circular Dichroism spectra of apo YIsu1 WT and mutants. Data were collected at room temperature over a wavelength range of 190-260 nm in 1mM $NaPO_4$ (pH 7.5). The panels below represent: (A) WT (B) E144A (C) D145A (D) E144A, D145A YIsu1 spectra.

Table 3.3: Secondary structural features from simulation of CD spectra for Ylsu1 WT and mutant proteins

Secondary Structure[a]	% Fold with standard deviation			
	WT	E144A	D145A	E144A, D145A
Helix	20(±7)	26(±2)	22	21(±4)
Sheets	26(±7)	20(±2)	23	26(±3)
Turns	22(±1)	23(±1)	23	22
Unordered	32(±1)	31(±1)	32	31(±1)
TOTAL	100	100	100	100
RMSD[b]	0.07	0.07	0.07	0.05

[a] Circular Dichroism data collected in 1mM $NaPO_4$ (pH 7.5) from 190-260nm

[b] % error between experimental and calculated values

between data and simulation of 0.07 ± 0.007 corresponding to an error of ca. 7% which is the difference between the calculated and experimentally determined CD spectrum. Minor differences in simulation parameters observed between WT and mutant proteins include a reduction of up to 6% in β-sheet content for the E144A protein and 3% for the D145A protein with a corresponding increase in α-helical content suggesting a slight change in fold for the mutants. Secondary structural simulations for the double mutant are almost identical to the WT protein.

YIsu1 WT showed the highest standard deviation of approximately 7% between averaged runs for α-helix and β-sheet secondary structures, while the D145A mutant showed no change in secondary structure between averaged runs.

3.5.2 YIsu1 mutants show a decreased Fe(II) binding affinity:

As the environment within a cell contains several potential metal ligands, using chelators that compete with the protein of interest for metal binding has been reported to be a more relevant method of obtaining a more physiological binding constant for protein-metal binding [27]. In this report, we have used the chelator Mag-fura-2 as a competitor for Fe(II) binding with WT YIsu1 and mutant proteins. The metal-free chelator has an absorbance maximum at 366 nm, which decreases upon increasing Fe (II) binding, and this is monitored by UV-Visible spectroscopy [24] **(Figure 3.3, inset)**. Data obtained were fit using the program DYNAFIT [25]. Initial titrations of Fe(II) to Mag-fura-2 were best fit to a one-sites model with a K_D of 2.00 (±0.07) μM under these

experimental conditions. Isu proteins have reported K_D values in the nanomolar to micromolar range [8, 28], therefore a competition between the two ligands for Fe(II) can be envisioned. Using this assay, WT YIsu1 was best fit with a two-sites model with binding affinities in the micromolar range at both sites of K_{D1} 2.38 (±0.85) μM and a K_{D2} of 4.55 (± 2.69) μM. The one-sites fit had large estimated errors **(Table 3.4)**. Previously reported values using isothermal titration calorimetry (ITC) indicate binding affinities for YIsu1 in the nanomolar to micromolar range [8]. However using Trp fluorescence, micromolar binding affinities for *Tm* IscU were reported using a two-site model for fitting [28]. As ITC measures total heat, we speculate the possibility of contributions due to conformational changes in the protein upon substrate binding. The mutant protein E144A was best fit with a two-sites model and showed a slight rise in K_{D1} of 4.95 (± 0.91) and an eight-fold rise in K_{D2} of 38.1 (± 22) compared to the WT protein. Again the one-sites fit had high estimated errors. The D145A mutant showed a similar trend with a slight rise in K_{D1} of 7.60 (± 2.60) and six-fold rise in K_{D2} of 26.2 (± 12.1) compared to WT. This mutant however, yielded an acceptable fit with a one-sites model. Finally, the E144A, D145A mutant was best fit with a one-sites model with a K_D of 3.15 (± 1.43). Fits with a two-sites model yielded high errors. As the single mutant proteins were associated with a significant drop in binding affinities associated with one of the sites, with the other site being largely unaffected, these results suggest the possible loss of one Fe(II) binding site.

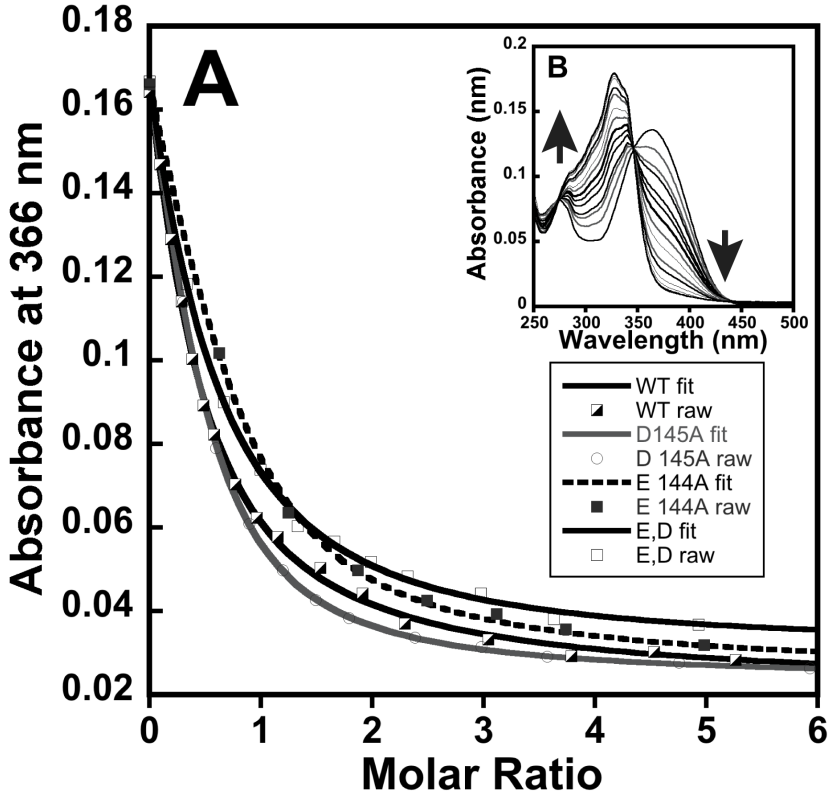

Figure 3.3: Competition Assay between Mag-fura-2 and YIsu1 proteins with Fe(II). **(A)** Data was fit with DYNAFIT. Curves correspond to WT YIsu1 13 μM and 5.5 μM Mag-fura-2; D145A 10.3 μM and 9.4 μM Mag-fura-2; E144A 5.4 μM and 3.9 μM Mag-fura-2; E144A, D145A 8.0 μM and 3.3 μM Mag-fura-2. Fe(II) was titrated in increasing concentrations. **(B) Inset:** Initial absorbance spectra obtained during titration of 5 μM of Mag-fura-2 and 15 μM WT YIsu1 Fe (II) in 20 mM HEPES (pH 7.5), 150 mM NaCl, at 25^{0}C. The arrows denote the direction of the absorbance changes with increasing concentrations of Fe(II).

Table 3.4: K_D values obtained from Mag-fura-2 assay for WT Ylsu1 and mutant proteins. Data was fit to two binding site model using DYNAFIT and average values of (n=3). K_{D1} and K_{D2} are given with errors for Ylsu1 monomer in 20 mM HEPES (pH 7.5) 150mM NaCl and 5 mM TCEP, at 25 ^{0}C.

Ylsu1 Protein	K_{D1} (μM)	K_{D2} (μM)	K_D One -sites
WT	2.38 ± 0.85	4.55 ± 2.69	-[a]
E144A	4.95 ± 0.91	38.1 ± 22.0	12.0 ± 14.0
D145A	7.60 ± 2.60	26.2 ± 12.1	3.96 ± 0.77
E144A,D145A	2.99 ± 0.11	-[a]	3.15 ± 1.43

[a] Error associated with fit were very high.

3.5.3 Thermal Stability of YIsu1 proteins by Differential Scanning Calorimetry (DSC):

The changes observed above in number and affinity of ligand and protein partner binding characteristics of YIsu1 mutants in comparison to WT possibly arise due to changes in energetics at the binding interface with Fe(II) and/ or due to global changes in the stability & dynamics of the C-terminal helix. DSC is a sensitive technique that can be used to study the changes in protein stability and associated energetics upon residue mutation and was applied to study YIsu1 WT and mutants in the absence (Apo) and presence (Holo) of Fe(II). 'Holo' protein refers to protein pre-loaded with two equivalents of Fe(II) to maintain consistency with YIsu1's maximal Fe(II) binding ability. All experiments were performed anaerobically in duplicate with independent protein preparations. Data were fit using the two-state scaled model. The approximation of enthalpy values i.e., ΔH_{cal} (kJ/mol), obtained upon peak integration, to the Van't Hoff enthalpy ΔH_{vH} (kJ/mol), obtained upon model fitting is used an indicator of validity of the model to the system that it is applied to i.e.

$$\Delta H_{cal} = \Delta H_{vH} \text{ or}$$

$$\Delta H_{cal} / \Delta H_{vH} = 1. \quad [29]$$

Apo WT alone, and mutant proteins both; in the apo and holo form were best fit with two two-state transitions possibly corresponding to an equilibrium between structured and disordered states as previously reported for Isu proteins [22]. The apo proteins showed varying percentages of the two states (grey fits, **Figure 3.4**). Holo WT alone was best

fit with a single transition indicating almost a 100% switch in protein structure upon Fe(II) binding. For Apo WT, temperature maximum for the first transition was 47.34 ± 0.38^{0}C and the second transition was 51.36 ± 0.26^{0}C. Holo WT melted at a higher temperature of 54.65 ± 0.06^{0}C indicating a significant increase in stability upon Fe(II) binding with an associated shift in structure that does not significantly disrupt the associated enthalpy or entropy compared to apo WT **(Table 3.4)**. The E144A mutant showed a slight increase in stability of both the apo and holo forms compared to WT. This mutant has previously been reported to stabilize the Isu fold in the structured state in *E.coli* [22]. In the apo form, temperature maximum for the first transition was 51.00 ± 1.20^{0}C and second transition was 53.60 ± 0.90^{0}C, an approximate 3 degree shift toward stability compared to WT. The holo form was more stable, but was fit with a two-state transition, unlike holo WT and appeared to be in equilibrium between two states: a smaller percentage that melted at temperatures similar to holo WT i.e., 54.65 ± 0.06^{0}C while majority of the protein was associated with an even more stable state that melted at 61.07 ± 0.28^{0}C. Holo E144A was also associated with a four-fold rise in enthalpy and entropy compared to the apo form indicating Fe(II) binding was an enthalpically unfavorable, yet entropically favorable reaction. Apo D145A exhibited a melting temperature that was similar to apo WT however, the holo form on the other hand was associated with a decrease in stability. The temperature maximum for holo D145A upon Fe(II) binding dropped to 42.68 ± 0.37^{0}C for the first transition and 49.50 ± 0.16^{0}C for the second transition. Enthalpy and entropy showed a three-fold increase in the holo form

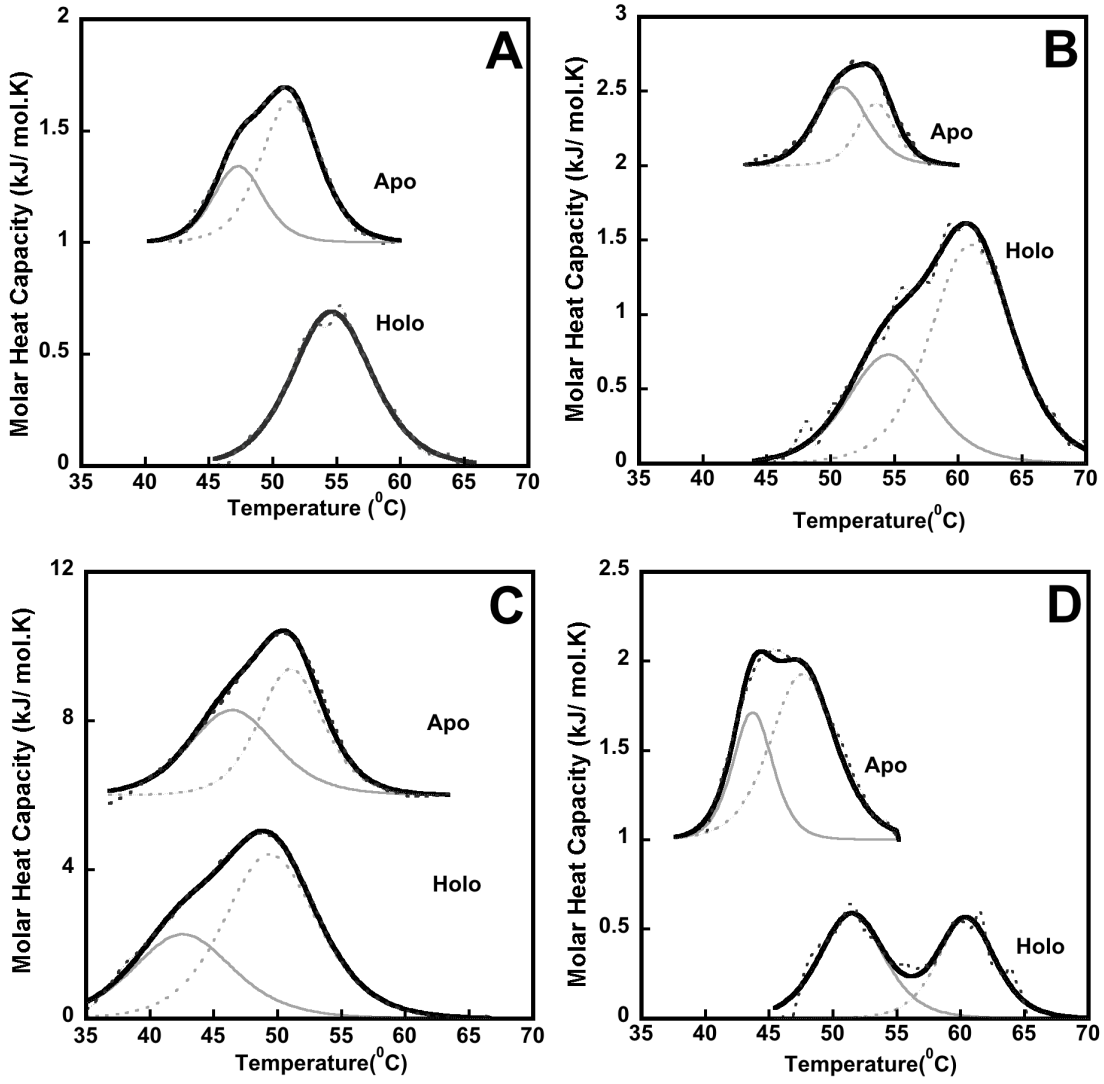

Figure 3.4: Thermal denaturation curves for apo and holo Ylsu1 proteins. Data collected using a Nano DSC instrument over 10-90^{0}C at a scan rate of 2 ^{0}C/ min in 20 mM HEPES (pH:7.5) 150 mM NaCl & 5 mM β-Me at excess pressure of 2.95 atm for WT Ylsu1 (A) and mutants E144A(B), D145A(C) and double mutant E144A, D145A(D). 'Holo' refers to protein pre-loaded with 2 equivalents Fe(II), Apo protein curves are offset for clarity. Black solid lines represent the fit to raw data, black dashed lines represent raw data, and grey solid and dashed lines represent deconvolution of raw data using the two-state scaled model.

Table 3.5: Thermodynamic parameters of melting of WT Ylsu1 and mutant proteins. Tm*fit1* & *2* and represent temperature maximum for each transition fit to raw data. ΔH*vH* represents Van't Hoff enthalpy which is total enthalpy under each fit obtained upon correction with scaling factor Aw. ΔH*cal*, ΔS*cal* and T*max* represent enthalpy, entropy and maximum temperature obtained from peak integration after baseline correction of raw data. Values for ΔH*vH,* ΔH*cal* and ΔS*cal* show a similar trend between datasets.

Ylsu1 variant	State	Tm*fit1* (^{0}C)	Tm*fit2* (^{0}C)	T*Max* (^{0}C)	ΔH*vH* (kJ/mol)	ΔH*cal* (kJ/mol)	ΔH*cal/* ΔH*vH*	*ΔScal* (kJ/mol.K)
A) WT	**Apo**	47.34 ± 0.38	51.36 ± 0.26	51.26	8.40	7.94	0.95	0.025
	Holo	-	54.65 ± 0.06	55.29	5.76	5.10	0.90	0.016
B) E144A	**Apo**	51.00 ± 1.20	53.60 ± 0.90	51.92	4.48	3.97	0.89	0.012
	Holo	54.63 ± 0.58	61.07 ± 0.28	60.82	18.85	18.40	0.98	0.055
C) D145A	**Apo**	48.38 ± 0.50	51.79 ± 0.15	50.86	25.76	25.98	1.01	0.080
	Holo	42.68 ± 0.37	49.50 ± 0.16	48.76	66.33	63.63	0.96	0.200
D) E144A, D145A	**Apo**	43.92 ± 0.43	47.85 ± 0.80	45.32	9.23	8.29	0.90	0.026
	Holo	51.26 ± 0.30	61.72 ± 0.18	61.46	21.35	20.76	0.97	0.018

compared to apo D145A. Both apo and holo D145A proteins were fit with two two-state models with no apparent variation in the percentages of each state. The double mutant E144A, D145A showed a decreased stability in the apo form. Temperature maximum for the first transition was 43.92 ± 0.43^{0}C and the second transition was 47.85 ± 0.80^{0}C. Fe(II) binding showed a melting pattern with an increased stability and was fit with two two-state transitions in a manner similar to that of holo E144A. The holo form, just like the single mutants was associated with an three fold increase in enthalpy compared to its apo form, however, the associated entropy appeared to be similar to that of WT. The rise in molar heat capacity in **Figure 3.4** upon Fe(II) binding in the mutant proteins can be attributed to thermodynamic changes in enthalpy and entropy.

3.5.4: Ylsu1 mutant proteins show altered holo-Yfh1 WT binding:

ITC was performed to study the binding affinity, binding ratio and thermodynamic parameters associated with the interaction between holo-yeast frataxin (Yfh1WT) with WT Ylsu1 and mutant proteins **(Figure 3.5)**. Our previous studies have shown that Yfh1WT and WT Ylsu1 do not interact in the absence of Fe(II), therefore all experiments described below were performed using holo Yfh1WT prepared as described above in the materials & methods section [8]. All data was collected anaerobically on a TA Nano-ITC instrument and in duplicate on independent protein samples to ensure reproducibility. Prior to fitting and analysis, a control experiment of 1 mM holo-Yfh1WT titrated into buffer was subtracted from the raw data. The binding of holo-Yfh1WT to

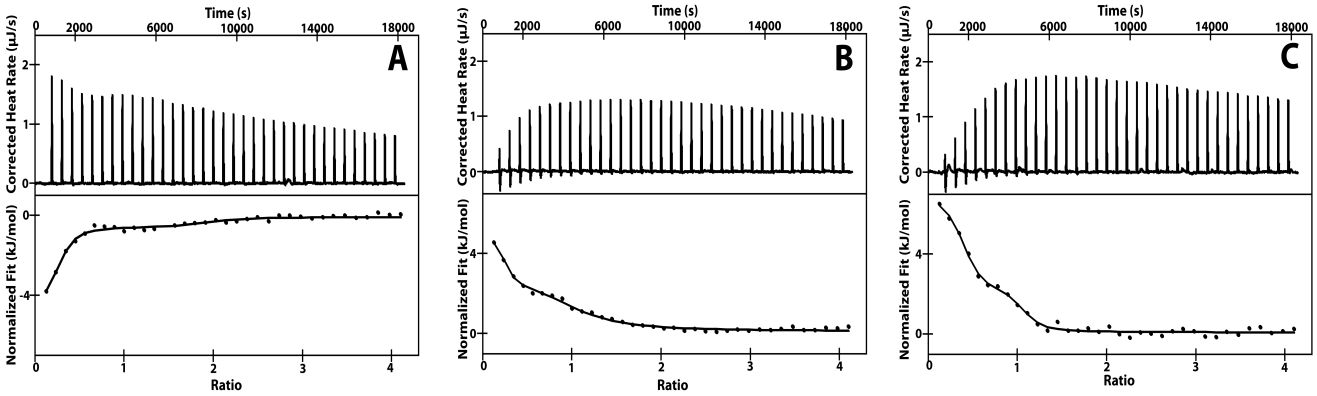

Figure 3.5: Holo-Yfh1 to Ylsu1 protein titrations: Raw ITC data (top) and binding isotherm data after control subtraction (bottom) of holo yeast frataxin (Yfh1WT) binding to (A) Ylsu1 WT (B) Ylsu1 D145A (C) Ylsu1 E144A, D145A. The black solid line in the binding isotherm panel represents the simulated fit to the data after control subtraction.

Table 3.6: Average Simulation Results using ITC Analysis[a] for WT Ylsu1 and mutant proteins

Sample	N_1	K_{D1} (nm)	N_2	K_{D2} (μM)	dH_1 (KJ/mol)	dH_2 (KJ/mol)	dS_1 (J/mol-K)	dS_2 (J/mol-K)
WT -- Fe-Yfh1	0.20 ± 0.07	2.94 ± 1.79	2.13 ± 0.94	0.11 ± 0.06	-1.61 ± 0.46	-0.52 ± 0.50	144 ± 21.51	81 ± 78.17
D145A -- Fe-Yfh1	0.20 ± 0.01	95.2 ± 77.9	0.85 ± 0.07	2.91 ± 2.54	1.01 ± 0.13	1.63 ± 0.67	139 ± 6.93	113 ± 6.36
E144A, D145A -- FeYfh1	0.34 ± 0.02	51.5 ± 15.4	0.68 ± 0.01	0.86 ± 0.02	2.45 ± 0.07	1.26 ± 0.18	148 ± 2.83	120 ± 0.85

[a]Averaged values of stoichiometry v/s the Isu1 monomer.

N_1, N_2, dissociation constants K_{D1}, K_{D2}, enthalpy dH_1, dH_2 and entropy values dS_1, dS_2 are given with errors.

WT Yfh1 follows an exothermic pattern with an initial exponential binding curve followed by a constant heat release pattern consistent with sample dilution in the post saturation stage. Data was best fit using the multiple sites model with a total of two binding molecules at two binding affinities of 2.94 (±1.79) nM and 0.108 (±0.06) µM. This interaction is both enthalpically (dH_1 is -1.61 ± 0.46 KJ/mol and dH_2 is -0.52 ± 0.5 KJ/mol) and entropically favorable (dS_1 is 144 ± 21.51 J/mol.K and dS_2 is 81 ± 78.17 J/mol.K). Binding of holo Yfh1WT to Yfh1 mutant E144A demonstrated a heat release pattern that was similar to the control experiment. Subtraction yielded a flat line with no measurable affinities or thermodynamic parameters (data not shown). In contrast, binding of both: the mutant D145A and the double mutant E144A, D145A yielded an endothermic pattern of heat release and were best fit with a multiple sites binding model with a total binding of approximately one molecule. The D145A mutant showed approximately a thirty-fold decrease in binding affinities at both sites compared to Yfh1 WT of 95.2 (±78) nM and 2.91 (±2.54) µM at the second site. This interaction though not enthalpically favourable (dH_1 is 1.01 ± 0.13 KJ/mol and dH_2 is 1.63 ± 0.67 KJ/mol) was entropically favorable (dS_1 is 139 ± 6.93 J/mol.K and dS_2 is 113 ± 6.36 J/mol.K). The E144A, D145A double mutant showed binding affinities that were decreased, but to a lesser extent as compared to the D145A mutant with K_D values of 51.5 ± 15.4 nM at one site and 0.85 ± 0.02µM at the second site. Again, as in the case of the D145A mutant, this interaction was not enthalpically favorable (dH_1 is 2.45 ± 0.07 KJ/mol and

dH_2 is 1.26 ± 0.18 KJ/mol) but was entropically favorable (dS_1 is 148 ± 2.83J/mol.K and dS_2 is 120 ± 0.85 J/mol.K).

3.5.5 YIsu1 mutant shows altered Fe-S assembly activity:

Protein bound 2Fe-2S clusters yield a characteristic signature spectrum in the near UV region (300-700 nm) using circular dichroism [30]. Owing to its sensitivity, this technique was employed to test the ability of WT YIsu1 and the D145A mutant to synthesize clusters: either in the presence of holo Yfh1WT or just Fe(II) alone**.** A previously published protocol [31] was modified such that the reaction mixture contained 100 µM WT YIsu1 or D145A mutant, 200 µM holo-Yfh1 (prepared as mentioned above) or 200 µM Fe(II) alone. The reaction was initiated by adding 1 mM Na_2S in a final volume of 1.2 mL. The concentration of Na_2S was optimized to minimize contamination by a ferrous sulfide species that forms upon mixing. Controls containing either holo-Yfh1 or Fe (II) alone mixed with Na_2S in buffer and in the absence of YIsu1 was tested and yielded no characteristic spectrum (data not shown). The mixture was slowly agitated by stirring with a magnetic stir bar for 30 seconds in between data collections. A set of two scans were collected over 10 minutes and averaged. Data was collected for approximately 100-120 minutes or until signal saturation was observed. In **Figure 3.5**, panel A shows the activity plot of WT YIsu1 and panel B shows the activity plot of the YIsu1 D145A mutant in the presence of holo Yfh1WT (•) and Fe(II) alone (◆). In the inset are displayed the CD data

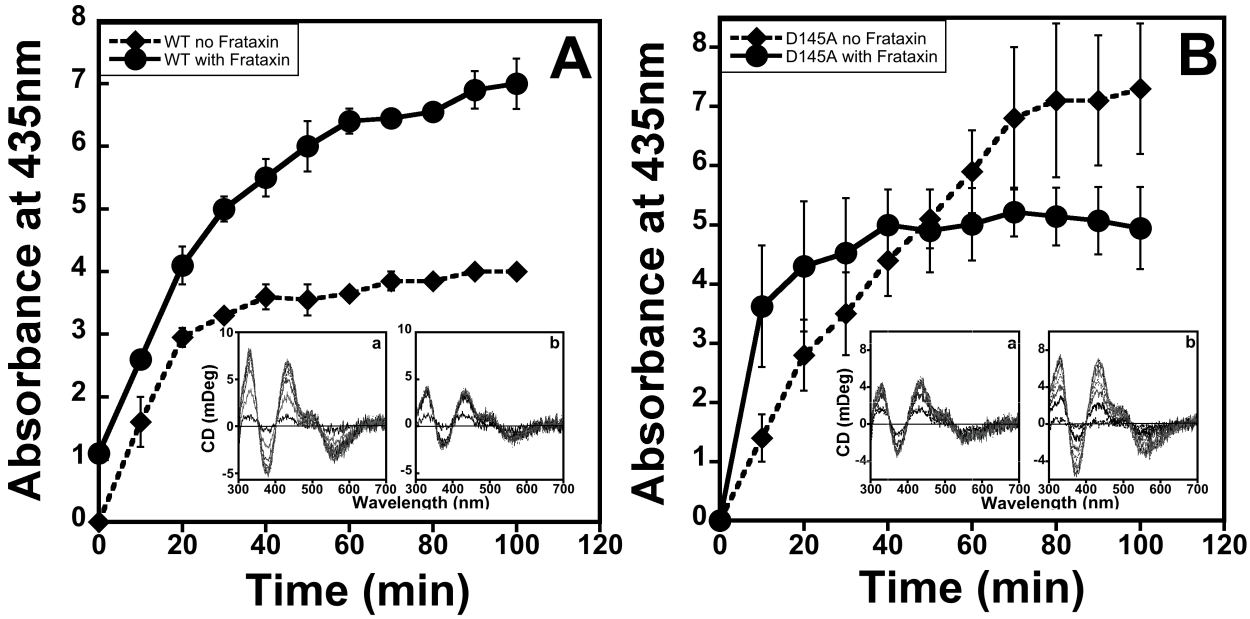

Figure 3.6: Fe-S assembly activity of WT Ylsu1 and mutant D145A: on Ylsu1 WT (A) or the D145A mutant (B) by near UV circular dichroism. The solution contained 100 µM Ylsu1 protein in 20 mM HEPES (pH: 7.5) 150 mM NaCl 5 mM β-Me buffer to which 100 µM Fe (ll) was added either as holofrataxin (• and inset panel 'a') or alone (◆and inset panel 'b'). Reaction progress was monitored from 300-700nm over time until saturation. CD data at 435nm was plotted over time to obtain activity plots. Error bars represent average values at each time point from two independent reproducible experiments collected.

collected in the presence of holo Yfh1 WT, panel 'a' and in the presence of Fe(II) alone, panel 'b'. In the presence of holo Yfh1 WT, YIsu1 shows activity that is approximately two fold higher than its activity in the presence of Fe(II) alone. The reaction with Frataxin also appears to proceed at a faster rate compared to that with Fe(II), evident from the initial phase of the reaction (initial 20 mins.) which occurs on a shorter time scale. This clearly indicates a stimulation of YIsu1 WT activity in the presence of holo Yfh1WT. In contrast, the D145A mutant showed a higher activity in the presence of Fe (II) alone. The reaction, although slower was more active in the synthesis of clusters than the reaction with Frataxin alone which reached saturation earlier. This phenomenon could be due to diminished interaction of the D145A mutant with Yfh1WT and altered energetics associated with the synthesis of Fe-S clusters.

3.6 Discussion:

There has been much speculation over the role of Frataxin in the ISC multiprotein complex. So far, its functions that have been described include a role as the Fe chaperone for iron-sulfur cluster synthesis where it functions in delivering iron to ISU for cluster assembly [8, 31, 32] and as a modulator of the cysteine desulfurase enzyme in Fe-S assembly [33]. Frataxin and ISU are known to be stable binding partners within and outside of the ISC complex [8, 10, 32-34]. This interaction has been demonstrated both genetically and *in vitro* and has been shown to be iron dependent [8, 35]. However, the initial events of Fe acceptance by ISU and its subsequent incorporation

into Fe-S clusters are yet unclear. In this study we further examine the interaction between Frataxin and ISU with a focus on ISU. Unpublished XAS and Mössbauer results from our lab carried out on four ISU orthologs namely yeast, human, fly and *Thermatoga* all show that Fe (II) is bound in a 6-coordinate oxygen/nitrogen ligand environment [8] indicating that the Fe delivery/acceptance occurs at a site that is different from ISU's cysteine rich active site. The presence of alternative metal binding and substrate binding sites on the same protein has previously been described for Ferrochelatase, the enzyme that inserts Fe into heme [21]. ISU is a molten globule protein with a hydrophobic interior and it has been previously described that the synthesized Fe-S cluster is buried within a solvent inaccessible region in the multiprotein complex [8] possibly precluding a release of reaction intermediates that may endanger the mitochondrion. Under such circumstances, the occurrence of a separate metal binding site in a region that is accessible to solvent and/or protein binding partners is feasible. The assembly of Fe-S clusters by ISU involves changes in fold within the protein. The Markley group has demonstrated that bacterial IscU exists in an equilibrium between structured (S) and disordered (D) states and that the (D) state is the substrate for cysteine desulfurase binding [22]. Using fluorescence anisotropy, research from our group has reported structural changes in yeast Isu1 upon binding of Fe and S^{2-} [8]. These results indicate that substrate binding drives structural changes in ISU. This fact has been further corroborated by the crystal structure of IscU from the

bacterium *A. aeolicus* which shows an increase in order of fold of the C-terminus upon cluster assembly [20].

In this study we replaced conserved, charged residues E144 and D145 on YIsu1's C-terminal helix with an uncharged alanine residue by site directed mutagenesis. We have previously shown by NMR that charged residues on frataxin's α1/β1 acidic ridge along with a portion of its β-sheet forms the interface of frataxin with ISU [8]. These regions also include frataxin's Fe binding residues [36]. A closer look at the IscU-IscS crystal structure from the Cygler group shows that IscU interacts with IscS in the proximity of its active site, leaving the c-terminal helix open and solvent exposed. Predictive modeling of CyaY on the IscU-IscS structure showed that CyaY possibly binds IscS in a region close to the IscU binding site and appears to be in a region that also overlaps the IscU C-terminus [9]. Charged residues on IscU's c-terminus would provide a complementary charged binding surface to frataxin promoting electrostatic interactions that could aid Fe delivery.

Far UV circular dichroism did not show major deviations in secondary structure between the wild type protein and mutants. Compared to the wild type protein, the E144A and D145A single mutants both showed a slight increase in helical content of 6% and 3% respectively with a corresponding drop in β–sheet content indicating a possibility that these mutants have a greater helical fold compared to the WT protein and that in the WT protein, these mutants possibly destabilize the C-terminal helix. The fact that the E144A mutant stabilizes the protein fold has been previously shown by the

Markley group in bacterial IscU (corresponding residue E111A) [22]. A double mutation in the area appears to restore WT folds as indicated by the E144A**,** D145A mutant**.**

Competition binding assays with Mag-fura-2, used to test the Fe(II) binding ability of WT YIsu1 and mutant proteins showed binding affinities in the micromolar range for both sites. Using isothermal titration calorimetry, we observe nanomolar to micromolar binding affinities when YIsu1 binds Fe(II) [8]. As ITC measures total heat, we speculate the occurrence of contributions from heats due to conformational changes on Isu in addition to heat released upon Fe(II) binding. As the mutant proteins all showed a drop in binding affinities at one of the sites with the second site being only marginally affected, we can conclude that these residues are possibly involved in Isu's initial iron binding site.

The thermal stability and associated energetics of the apo- and holo-forms of WT and mutant proteins were also tested by differential scanning calorimetry. Melting curves of the apo forms of both WT and mutant proteins showed two distinct transition temperatures, which could possibly correspond to denaturation of the structured and disordered forms of the protein [22]. The holo form of WT YIsu1 alone could be fit with a single transition state indicating almost 100% shift to a higher, single melting temperature brought about by a stabilizing change in protein structure accompanied by Fe(II) binding. The melting of the protein at two distinct temperatures during denaturation has been recently reported by the Pastore group in as-purified bacterial IscU at a 30 fold EDTA excess, in addition, a stabilizing change accompanied with a

shift to a higher melting upon Zn binding was also shown [37]. Among the mutant proteins, apo D145A melted at a temperature similar to WT, while the holo form underwent a destabilizing change upon Fe(II) binding evident by a shift to lower melting temperature. The E144A mutant was intrinsically more stable, the apo form melted at a temperature that was three degrees higher that WT. Holo E144A appeared to be in equilibrium between two stable states, one at a temperature similar to holo WT YIsu1 and another at a higher temperature. As previously described, the E144A mutant has been described as a mutant that stabilizes the S-state [22], which possibly is a reason for the observed higher than WT stability. The apo form of the E144A, D145A mutant had a lower stability than WT, however Fe(II) binding was associated with a stabilizing switch to higher temperatures in a manner similar to the E144A single mutant possibly reflecting the stabilizing change observed in the single mutant. These results clearly indicate a stabilizing change in YIsu1 structure upon substrate, Fe(II) binding. In addition, the inability of the D145A mutant to make the switch to a more stable fold would implicate this residue in in metal binding. Thermodynamic parameters associated with the unfolding of WT YIsu1 showed that denaturation of holo WT YIsu1 was not accompanied by any significant changes in enthalpy and entropy indicating that the structural change possibly balanced out energetic changes associated with Fe(II) binding. The denaturation of apo D145A was associated with an increased enthalpy compared to apo WT indicating a possible intrinsic change within the protein structure. However, the denaturation of the holo forms of all the mutant proteins was accompanied

by significant increases in both enthalpy and entropy indicating an enthalpically unfavorable yet entropically favorable process, distinct from WT YIsu1.

The holo Yfh1WT binding ability of WT YIsu1 and mutant proteins was also tested by isothermal titration calorimetry. Binding of WT YIsu1 to holo Yfh1WT was associated with much tighter binding affinities than those previously published for Fe(II) alone [8], indicating a strong binding interaction with holo Yfh1WT. Binding affinities, unlike the UV-Vis method were of two distinct types: a tighter nanomolar affinity and a lower micromolar affinity. Compared to WT, binding of mutant proteins D145A and E144A, D145A was associated with a decrease in binding affinity of up to 30-fold in the D145A mutant and approximately 20-fold in the double mutant at the higher affinity site. The lower affinity site was also associated with decreased affinities, however to a less severe extent. In addition, decreased binding affinities were associated with a decrease in stoichiometry of binding indicating a weak interaction. For E144A binding to holo Yfh1WT, the binding isotherm was similar to the buffer control yielding no measurable binding affinity upon buffer subtraction. Mutant proteins D145A and E144A, D145A binding holo-Yfh1 followed an endothermic trend as opposed to the exothermic trend observed with WT YIsu1 binding. Associated changed with thermodynamic parameters were also observed. WT YIsu1 binding holo Yfh1 was enthalpically favorable however mutant binding to holo frataxin was associated with a rise in enthalpy i.e. was an enthalpically unfavorable change. Entropy and free energy values for both WT and mutant YIsu1 however, remained similar. These results indicate a) that holo Yfh1WT

binding is an enthalpically favorable process possibly characterized by electrostatic interactions and hydrogen bonding, an enthalpically favorable process has also been described for holo *Drosophila* frataxin binding Isu1 [31] and that b) these residues, particularly the D145A mutant is required for both Fe binding, and holo-Yfh1 interaction, possibly forming the interface between Yfh1WT and WT YIsu1 and c) mutations at these regions are associated with a change in thermodynamic properties associated with Fe(II) binding that are enthalpically unfavorable.

Finally, the ability of WT YIsu1 and the D145A mutant to synthesize clusters was tested by time course far UV circular dichroism spectroscopy in the presence of either Fe(II) alone or holo Yfh1WT. WT YIsu1 showed a twofold increase in cluster synthesis in the presence of holo Yfh1WT, indicating a direct stimulation of YIsu1 activity in keeping with its role as an Fe chaperone. In contrast, the D145A mutant showed an increase in activity in the absence of holo Yfh1WT, though the reaction progressed at a slower pace. Fe(II) binding experiments showed a decrease in affinity at one site while the second site which is possibly the active site, appeared to retain binding properties which could explain the ability of the mutant to synthesize clusters. ITC experiments of holo-Yfh1 binding to the D145A mutant showed a weak interaction with altered energetics associated with binding. In the presence of holo Yfh1, the reaction with D145A reached equilibrium faster possibly due to saturation of the active site by additional interactions mediated by frataxin. In the absence of frataxin, one can envision the active site being

populated at a slower pace in the absence of the initial binding site hence, saturates later.

These results lead us to postulate a model for the initial binding events of Fe-S cluster assembly.

1) Holo-frataxin appears to activate Fe-S assembly therefore an iron dependent interaction between frataxin & ISU appears to be essential for efficient cluster synthesis.
2) Initial metal binding is facilitated by electrostatic interactions between charged residues at the interface of holo-frataxin and ISU at Isu's c-terminus, and is an enthalpically favorable process. The D145A residue appears to play a critical role in this process.
3) This is followed by a structural change in ISU that possibly favors hydrophobic interactions within the protein and facilitates Fe-S synthesis.

3.7 Acknowledgements:

Funding for this research comes from NIHR01DK068139 (TLS), AHA12PRE11720005 (AVR), AHA14PRE18830036 (SPD) and the Friedreich's Ataxia Research Alliance. The authors would also like to acknowledge Dr. Michael Mathews (TA Instruments) for helpful discussions regarding differential scanning calorimetry and Dr. Andrew Dancis (University of Pennsylvania) for providing the WT YIsu1 plasmid.

3.8 References

1. Lill, R., *Function and biogenesis of iron-sulphur proteins.* Nature, 2009. **460**(7257): p. 831-8.
2. Beinert, H., R.H. Holm, and E. Munck, *Iron-sulfur clusters: nature's modular, multipurpose structures.* Science, 1997. **277**(5326): p. 653-9.
3. Switzer, R.L., *Non-redox roles for iron-sulfur clusters in enzymes.* Biofactors, 1989. **2**(2): p. 77-86.
4. Grodick, M.A., et al., *DNA-Mediated Signaling by Proteins with 4Fe–4S Clusters Is Necessary for Genomic Integrity.* Journal of the American Chemical Society, 2014.
5. Rouault, T.A., *The role of iron regulatory proteins in mammalian iron homeostasis and disease.* Nat Chem Biol, 2006. **2**(8): p. 406-14.
6. Meyron-Holtz, E.G., M.C. Ghosh, and T.A. Rouault, *Mammalian tissue oxygen levels modulate iron-regulatory protein activities in vivo.* Science, 2004. **306**(5704): p. 2087-90.
7. Rouault, T.A., *Biogenesis of iron-sulfur clusters in mammalian cells: new insights and relevance to human disease.* Dis Model Mech, 2012. **5**(2): p. 155-64.
8. Cook, J.D., et al., *Molecular details of the yeast frataxin-Isu1 interaction during mitochondrial Fe-S cluster assembly.* Biochemistry, 2010. **49**(40): p. 8756-65.

9. Shi, R., et al., *Structural basis for Fe-S cluster assembly and tRNA thiolation mediated by IscS protein-protein interactions.* PLoS Biol, 2010. **8**(4): p. e1000354.

10. Iannuzzi, C., et al., *The role of CyaY in iron sulfur cluster assembly on the E. coli IscU scaffold protein.* PLoS One, 2011. **6**(7): p. e21992.

11. Bridwell-Rabb, J., et al., *Effector role reversal during evolution: the case of frataxin in Fe-S cluster biosynthesis.* Biochemistry, 2012. **51**(12): p. 2506-14.

12. Rawat, S. and T.L. Stemmler, *Key players and their role during mitochondrial iron-sulfur cluster biosynthesis.* Chemistry, 2011. **17**(3): p. 746-53.

13. Sheftel, A., O. Stehling, and R. Lill, *Iron-sulfur proteins in health and disease.* Trends Endocrinol Metab, 2010. **21**(5): p. 302-14.

14. Radisky, D.C., M.C. Babcock, and J. Kaplan, *The yeast frataxin homologue mediates mitochondrial iron efflux. Evidence for a mitochondrial iron cycle.* J Biol Chem, 1999. **274**(8): p. 4497-9.

15. Campuzano, V., et al., *Friedreich's ataxia: autosomal recessive disease caused by an intronic GAA triplet repeat expansion.* Science, 1996. **271**(5254): p. 1423-7.

16. Rotig, A., et al., *Aconitase and mitochondrial iron-sulphur protein deficiency in Friedreich ataxia.* Nat Genet, 1997. **17**(2): p. 215-7.

17. Mochel, F., et al., *Splice mutation in the iron-sulfur cluster scaffold protein ISCU causes myopathy with exercise intolerance.* Am J Hum Genet, 2008. **82**(3): p. 652-60.

18. Olsson, A., et al., *Myopathy with lactic acidosis is linked to chromosome 12q23.3-24.11 and caused by an intron mutation in the ISCU gene resulting in a splicing defect.* Hum Mol Genet, 2008. **17**(11): p. 1666-72.

19. Garland, S.A., et al., *Saccharomyces cerevisiae ISU1 and ISU2: members of a well-conserved gene family for iron-sulfur cluster assembly.* J Mol Biol, 1999. **294**(4): p. 897-907.

20. Shimomura, Y., et al., *The asymmetric trimeric architecture of [2Fe-2S] IscU: implications for its scaffolding during iron-sulfur cluster biosynthesis.* J Mol Biol, 2008. **383**(1): p. 133-43.

21. Kohno, H., et al., *Site-directed mutagenesis of human ferrochelatase: identification of histidine-263 as a binding site for metal ions.* Biochim Biophys Acta, 1994. **1209**(1): p. 95-100.

22. Kim, J.H., M. Tonelli, and J.L. Markley, *Disordered form of the scaffold protein IscU is the substrate for iron-sulfur cluster assembly on cysteine desulfurase.* Proc Natl Acad Sci U S A, 2012. **109**(2): p. 454-9.

23. Cai, K., et al., *Human mitochondrial chaperone (mtHSP70) and cysteine desulfurase (NFS1) bind preferentially to the disordered conformation, whereas*

co-chaperone (HSC20) binds to the structured conformation of the iron-sulfur cluster scaffold protein (ISCU). J Biol Chem, 2013. **288**(40): p. 28755-70.

24. Walkup, G.K. and B. Imperiali, *Fluorescent chemosensors for divalent zinc based on zinc finger domains. Enhanced oxidative stability, metal binding affinity, and structural and functional characterization.* Journal of the American Chemical Society, 1997. **119**(15): p. 3443-3450.
25. Kuzmic, P., *Program DYNAFIT for the analysis of enzyme kinetic data: application to HIV proteinase.* Anal Biochem, 1996. **237**(2): p. 260-73.
26. Greenfield, N.J., *Analysis of the kinetics of folding of proteins and peptides using circular dichroism.* Nature protocols, 2007. **1**(6): p. 2891-2899.
27. Waldron, K.J. and N.J. Robinson, *How do bacterial cells ensure that metalloproteins get the correct metal?* Nat Rev Microbiol, 2009. **7**(1): p. 25-35.
28. Nuth, M., T. Yoon, and J.A. Cowan, *Iron-sulfur cluster biosynthesis: characterization of iron nucleation sites for assembly of the [2Fe-2S]2+ cluster core in IscU proteins.* J Am Chem Soc, 2002. **124**(30): p. 8774-5.
29. Grzesiak, A., et al., *Substitutions at the P(1) position in BPTI strongly affect the association energy with serine proteinases.* J Mol Biol, 2000. **301**(1): p. 205-17.
30. Mapolelo, D.T., et al., *Monothiol glutaredoxins and A-type proteins: partners in Fe-S cluster trafficking.* Dalton Trans, 2013. **42**(9): p. 3107-15.
31. Kondapalli, K.C., et al., *Drosophila frataxin: an iron chaperone during cellular Fe-S cluster bioassembly.* Biochemistry, 2008. **47**(26): p. 6917-27.

32. Yoon, T. and J.A. Cowan, *Iron-sulfur cluster biosynthesis. Characterization of frataxin as an iron donor for assembly of [2Fe-2S] clusters in ISU-type proteins.* J Am Chem Soc, 2003. **125**(20): p. 6078-84.

33. Tsai, C.L. and D.P. Barondeau, *Human frataxin is an allosteric switch that activates the Fe-S cluster biosynthetic complex.* Biochemistry, 2010. **49**(43): p. 9132-9.

34. Shan, Y., E. Napoli, and G. Cortopassi, *Mitochondrial frataxin interacts with ISD11 of the NFS1/ISCU complex and multiple mitochondrial chaperones.* Hum Mol Genet, 2007. **16**(8): p. 929-41.

35. Stemmler, T.L., et al., *Frataxin and mitochondrial FeS cluster biogenesis.* J Biol Chem, 2010. **285**(35): p. 26737-43.

36. He, Y., et al., *Yeast frataxin solution structure, iron binding, and ferrochelatase interaction.* Biochemistry, 2004. **43**(51): p. 16254-62.

37. Iannuzzi, C., et al., *The role of zinc in the stability of the marginally stable IscU scaffold protein.* Protein Sci, 2014. **23**(9): p. 1208-19.

CHAPTER 4
DROSOPHILA FRATAXIN CRYSTAL STRUCTURE, RESONANCE ASSIGNMENTS AND PUTATIVE IRON BINDING RESIDUES

4.1 Prelude

Friedreich's ataxia (FRDA) is caused by a patient's inability to produce a viable form of the mitochondrial protein frataxin. Frataxin's involvement in cellular iron regulation became evident by the observed accumulation of large amounts of iron in actively metabolizing cells of individuals suffering from FRDA. Frataxin has since been shown to participate in several capacities related to regulating cellular iron homeostasis: as an iron chaperone for iron-sulfur cluster and heme synthesis, as a modulator of protein partners in the Fe-S cluster assembly pathway and as an iron storage protein within the mitochondria in a manner similar to cytosolic Ferritin but, only under conditions of oxidative stress. Analysis of the activity and structure of two eukaryotic frataxin orthologs (yeast and human) has been constrained by autodegradation and aggregation. In contrast, the *Drosophila* frataxin homolog (Dfh) is stable making it a perfect molecule for structure based functional characterization studies.

In this report, we describe the crystal structure and NMR assignments of apo Dfh. In addition, using nuclear magnetic resonance (NMR) spectroscopy, we report potential Fe(II) binding residues on this protein. A previous graduate student (Dr. Swati Rawat) who completed backbone chemical shift assignments for Dfh, initiated this work. My contributions include sample preparation, ^{15}N HSQC data collection and processing, and development of the crystallization for the apo-protein. Contributors include Dr.

Joseph Brunzelle (APS, Argonne National Laboratory) who crystallized Dfh and solved the structure, Lindsey Thompson and John Rotondo who aided with protein purification and Jefferson Plegaria (Pecoraro lab, University of Michigan) who aided with NMR data processing. The text below is being prepared for publication in the journal Biochemistry.

4.2 Abstract:

Friedreich's ataxia, the most prevalent hereditary ataxia is caused by a patient's inability to produce a viable form of the protein frataxin [1-3]. Frataxin is a nuclear encoded protein transported to the mitochondrial matrix [1, 4] and believed to serve as an iron chaperone/regulator of the Fe-S cluster (ISC) assembly pathway [5-9]. Frataxin's role as an iron chaperone is controversial and atomic details of its interaction with partner proteins are still unknown. While the in vitro studies on the human and yeast orthologs have been plagued by the poor stability of the proteins, the *Drosophila* homolog appears to resist autodegradation. Thus, a structural clarification of Dfh would serve as a useful starting point for further studies into the molecular and atomic details of frataxin's function at a molecular level. With this goal in mind, we report the crystal structure of Dfh, nearly complete NMR chemical shift assignments of the mature apo-protein and the identification of Dfh iron binding residues, obtained by NMR. The crystal structure of the mature apo-Dfh suggests the protein is well folded with an alpha/beta sandwich motif structure in agreement with the published structures for related orthologs

[6, 10-12]. This work provides a starting point for further characterization of metal binding and partner protein interaction sites in the stable fly system.

4.3 Introduction:

Friedreich's ataxia (FRDA), a cardio- and neurodegenerative disorder affecting 1 in 50,000, is caused by an inability to produce the mitochondrial protein "frataxin" [1]. Protein deficiency in FRDA patients is typically the result of an atypical GAA trinucleotide intronic expansion in the frataxin gene that disrupts transcription, although a subset of patients have frataxin single point mutations [3]. Phenotypes of the disorder include Fe-S cluster (ISC) deficiency, as well as mitochondrial iron overload coupled to cell death. This is a result of reactive oxygen species (ROS) induced oxidative stress that occurs when the iron chemistry within the mitochondria is unregulated [13, 14]. Current treatment strategies for the disorder have suffered due to a lack of specific knowledge regarding the exact role frataxin plays in regulating cellular iron homeostasis [15]. Such functional knowledge at the molecular level would be extremely beneficial, since it would provide an additional focal point to target new alternative drug treatment strategies.

A large amount of work in the frataxin field has been performed using the yeast and human model systems. These studies have revealed valuable insight into the biochemistry of the protein and its role in the molecular pathogenesis of FRDA [6, 16-19]. However, FRDA research has suffered due to deficiencies in the proteins within

these model systems. Instability of human frataxin with N-terminal autodegradation and the high susceptibility for oxidation induced protein aggregation in the yeast ortholog has plagued studies with both eukaryotic proteins [10, 20, 21]. Recently, our laboratory fortuitously discovered that the frataxin homolog from *Drosophila melanogaster* (Dfh) is much more stable than the other orthologs [8]. Thermal denaturation profiles showed that Dfh melted at a temperature of 59^0C, compared to Yeast ortholog which melted at a temperature of 44^0C [8]. Greater stability would make the fly system a perfect model for structure/function characterization.

In addition to issues of protein stability, Dfh makes an excellent model system for studying frataxin function since Dfh shares a high degree of sequence homology with other frataxin orthologs (for example, 53% with the human protein) [22]. It also plays a direct role in controlling cellular oxidative stress, with activity towards aconitase repair and stability [23-26]. Under anaerobic conditions, Dfh exists as a stable iron-loaded protein monomer which is arguably the functional form of the protein under normal cellular conditions. We have shown Dfh prevents reactive oxygen species-induced oxidative damage to DNA in the presence of both Fe (II) and H_2O_2, so the protein has additional functions beyond possible iron delivery. Finally, the fact that Dfh mediates Fe(II) delivery to yeast Isu, promoting Fe-S cluster assembly *in vitro* in the process, has implications for protein activity (and the potential for teasing out mechanistic details) between species [8]. Given the direct correlation between frataxin's function and ISC biosynthesis, the fly model could therefore be exploited to provide real insight into Fe-

cofactor bioassembly.

In this report we compare the structures of human, yeast and fly frataxin orthologs, which are similar in fold and function, but exhibit subtle differences which possibly form the basis for the extraordinary stability of Dfh. Finally, we identify Dfh residues that may play a role in iron binding.

4.4 Materials & Methods:

4.4.1 Labeling, expression, and purification of Drosophila Frataxin

The Dfh construct was expressed in the *E. coli* BL21 (DE3) strain transformed with a modified pET 101/D-TOPO vector DNA. ^{15}N-labeled and $^{13}C/^{15}N$ doubly labeled *Drosophila* frataxin, spanning amino acids 59–190, were obtained from bacteria grown in M9 minimal medium with $^{15}NH_4Cl$ and $^{13}C_6$ D-glucose as the sole nitrogen and carbon sources, respectively. Unlabelled protein was overexpressed and isolated from bacteria grown in Luria-Bertani broth. For unlabelled protein expression, cells were grown at 37°C followed by induction at OD_{600} of 0.6 with 1 mM IPTG for 6 hours. For labeled protein expression, as cells grew at a slower pace in minimal media, growth was continued overnight (16-18 hrs.) at 25^0C and then harvested. Cell pellets were stored at -80^0C until use.

All protein isolation steps were carried out at 4^0C. Cell pellets re-suspended in buffer containing 25 mM TRIS (pH: 8.0), 10mM EDTA, 5 mM β-Me (5 ml buffer/g cells) in the presence of lysozyme (100 µg/µl), complete EDTA free protease inhibitor (1

tablet/ 50 ml, Roche), DNAse (10 µg/ml) and $MgCl_2$ (5 mM) were allowed to incubate for ~15mins. Cells were lysed by three passes through a high-pressure homogenizer (Emulsiflex C3, Avestin) and centrifuged at 21,000 rpm for one hour. The supernatant was separated and filtered through a 0.2 µm filter and the crude soluble fraction was subjected to two ammonium sulfate precipitation steps: salting in at 40% ammonium sulfate followed by recovery of supernatant, and precipitation at 65% ammonium sulfate, followed by resolubilization in lysis buffer. This partially purified preparation was then dialyzed twice against a 1:200 volume dilution of Buffer A (25 mM Tris-HCl (pH: 8.0), 10 mM EDTA, 5 mM β -Me) for a minimum of 6 - 12 hours at 4^0C with one buffer change in between to remove Ammonium Sulfate. Following dialysis, protein was filtered and subjected to anion exchange chromatography using a Q-Sepharose column (Pharmacia) equilibrated in Buffer A, and eluted using a salt gradient made with buffer B (25 mM Tris-HCl (pH: 8.0), 10 mM EDTA, 1 M NaCl, 5 mM β-Me) up to a final concentration of 1 M NaCl. Dfh eluted at a sodium chloride concentration of 500 mM. Fractions containing Dfh were pooled and dialyzed against buffer A to remove NaCl. The dialyzed protein was then made up to 1 M Ammonium Sulfate, filtered and loaded onto a Phenyl-Sepharose column (Pharmacia) using Buffer A and a reverse 1 M ammonium sulfate gradient in Buffer C (25 mM Tris-HCl (pH:8.0), 10 mM EDTA, 1M Ammonium Sulfate, 5 mM β-Me). Dfh eluted at 800 mM ammonium sulfate. Fractions containing Dfh were pooled and concentrated to 1 ml followed by a final purification step by size-exclusion through a Sephacryl-75 column (GE) equilibrated with 20 mM HEPES

(pH 7.5), 150 mM NaCl, 5 mM β−Me. Dfh eluted at a volume corresponding to a monomer [8]. Isolated protein was concentrated and stored anaerobically in a glove box (Coy Labs) at 4^0C or flash frozen in liquid nitrogen and stored at -80^0C. Typical yields were 50mg/L of growth medium.

4.4.2 Crystallization and determination of apo-Dfh structure:

Purified unlabelled apo Dfh at ~2 mM concentration in 20 mM HEPES (pH: 7.5) 150 mM NaCl and 5 mM β−Me **(Figure 4.1)** was crystallized and the structure was solved in collaboration with Dr. Joseph Brunzelle at the Advanced Photon Source, Argonne National Laboratory.

Crystals of native Dfh were obtained by sitting drop vapor diffusion by mixing 1:1 ratio of 7.2 mg/mL protein with 0.1 M citric acid (pH 5.0) and 1.6 M ammonium sulfate grown at 20ºC. Crystals were harvested, soaked in the mother liquor with 25% glycerol and flash frozen in liquid nitrogen. Data were collected on the 21-ID-G beam line (LS-CAT Sector-21) at the Advanced Photon Source (Argonne National Labs, Argonne IL). A 1.405 Å data set was processed and scaled with autoPROC [27]. The structure was solved by molecular replacement using PHENIX autoMR [28] with the atomic coordinates of 1EKG, which was further built and refined manually using Coot [29] and Phenix refine with TLS refinement [30], respectively. The final model was validated in MolProbity [31]. Data collection and refinement statistics are provided in **Table (4.1).**

Figure 4.1: SDS-PAGE gel showing Dfh purity. Unlabelled Dfh samples were run on an SDS-PAGE gel after purification through a phenyl sepharose column. The lane to the extreme right represents the protein marker and the lanes to the left represent Dfh at varying concentrations. Protein obtained was >95% pure and was used for crystallization.

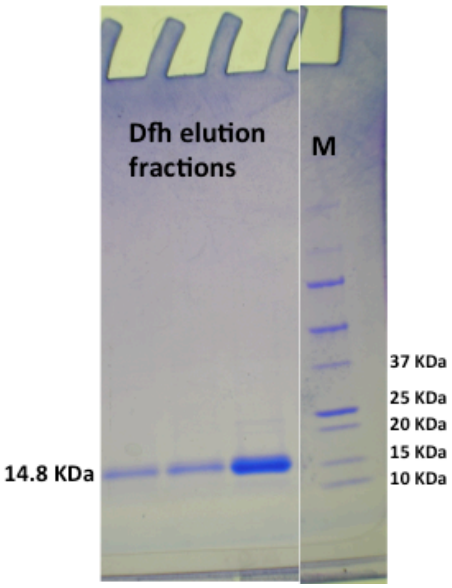

Table 4.1: Dfh crystallography data collection & refinement statistics.

Data collection

Wavelength (Å)	0.979
Space group	*C2*
Cell dimensions (Å)	a = 78.90, b = 38.51, c = 46.30, β = 123.45°
Resolution (Å)[a]	37-1.405 (1.41-1.405)
Observed reflections	74,124
Unique reflections	21,840
R_{merge} (%)[a,b]	3.7 (32.8)
Multiplicity[a]	3.4 (2.1)
Completeness (%)[a]	95.9 (75.6)

Refinement statistics

Resolution range (Å)	37–1.405
R_{factor} (%)[c]	15.24
R_{free} (%)[d]	17.39
No. of protein atoms	1986
No. of non-protein atoms	10
No. of water molecules	140
Molprobity score	3.92
Ramachandran plot (%)[e]	97.0/3.0/0.0
Average B factor (Å^2)	
Protein	20.9
Non-Protein	46.2
Waters	31.4
Overall	21.7
RMSDs	
Bond lengths (Å)	0.008
Bond angles (°)	1.191

[a] The values in parentheses are for the highest resolution shell. [b] $R_{merge} = \Sigma_{hkl} \Sigma_i |I(hkl)_i - \langle I(hkl)\rangle| / \Sigma_{hkl} \Sigma_i I(hkl)_i$, where $I(hkl)$ is the intensity of reflection hkl, and $\langle I(hkl)\rangle$ is the average intensity over all equivalent reflections. [c] $R_{factor} = \Sigma||F_o| - |F_c|| / |F_o|$, where $|F_o|$ and $|F_c|$ are the observed and calculated structure factor amplitudes, respectively. [d] R_{free} is the same as the R_{factor} but for a 5% subset of all reflections that were not used in the refinement. [e] Core/allowed/disallowed.

4.4.3 NMR Spectroscopy on Apo and Holo Dfh:

NMR spectra were acquired at 298 K on a Varian INOVA 720 MHz spectrometer (National High Field Magnet Laboratory, Tallahassee FL) and on a Varian INOVA 600 MHz spectrometer (Wayne State University). The 720 MHz spectrometer was equipped with a triple resonance gradient room temperature probe while the 600 MHz spectrometer utilized a Varian triple resonance gradient cold probe. Frataxin samples used in the backbone assignments were prepared at 1.2 mM concentration in NMR buffer (20 mM HEPES, 150 mM NaCl, pH 7.5, 90% H_2O /10% D_2O). Backbone assignments were made using the following experiments: ^{15}N-HSQC, HNCO, HNCACB and CBCA(CO)NH [32]. HNCACB spectra provide Cα and Cβ chemical shifts for the amino acid of interest, as well as from the residue immediately N-terminal in the protein's sequence. CBCA (CO) NH spectra are used to verify chemical shifts of the N-terminal residue. When combined, these data allow one to make sequential assignments for the backbone of a protein. All spectra were analyzed according to established lab protocols [6] using the processing programs NMRPipe [33] and nmrView [34]. CSI analysis was performed using a program provided by nmrView using backbone Cα, Carbonyl carbon and Nitrogen atoms only. Secondary structure prediction based on backbone atom chemical shift suggests that mature Dfh contains 2 alpha helices and 6 beta sheets in agreement with that of the crystal structure.

NMR amide chemical shift perturbation experiments were used to identify amino acids affected by the presence of iron under solution conditions that stabilize the

monomeric iron loaded Dfh protein. ^{15}N labeled apo Dfh protein at ~0.7 mM concentration was prepared in the NMR buffer listed above: 20 mM HEPES (pH 7.5) 150 mM NaCl 5 mM β-mercaptoethanol, 90%H_2O/ 10% D_2O. Protein sample was pre-incubated in the glove box overnight at 4^0C followed by transfer to NMR tubes, which were sealed with airtight septa. Ferrous ammonium sulfate was also prepared anaerobically within the glove box in the NMR buffer. For the holo Dfh sample, ferrous ammonium sulfate at a concentration of 6mM was anaerobically titrated in 70 uL volumes into the protein, to a final concentration of 1:1 Dfh to Fe(II). Protein concentration after addition of Fe(II) was ~0.63 mM. Spectra were collected on a Varian INOVA 600 MHz spectrometer under conditions identical to backbone assignment experiments outlined above. Samples were allowed to equilibrate to 25 ^0C within the spectrometer prior to data collection. Full $^1H/^{15}N$ heteronuclear single quantum coherence (HSQC) spectra were collected at each titration point using a ^1H sweep width of 7804 Hz (2048 points and 64 transients) and a ^{15}N sweep width of 2500 Hz (512 increments). Spectra were transformed as mentioned above using NMRPipe and peak positions were calculated using SPARKY [35].

4.4.4 Assignments and data deposition

Residue assignments for the mature (59-190) *Drosophila* frataxin protein are provided in the high-resolution ^{15}N-HSQC spectrum for the protein **(Figure 4.4).** Full backbone assignment was achieved for 128 out of 133 residues. Five proline residues

in the protein remain unassigned. For further reference, the residue sequence for full-length *Drosophila* frataxin can be found at http://www.uniprot.org/uniprot/Q9W385. Chemical shift assignments are deposited in the Biological Magnetic Resonance Bank (http://www.bmrb.wisc.edu/) under the accession code BMRB- 17135.

4.5 Results:

4.5.1 Crystal structure of Drosophila Frataxin homolog (Dfh):

Crystallographic results indicate that Dfh has an overall fold that is highly similar to the characterized ortholog structures [21]. The protein has an alpha-beta sandwich motif comprising two α−helices that form one plane, with a succession of five β-strands that are sandwiched between the α−helices forming the second plane of the molecule [21]. A sixth β-strand intersects the two planes, thus forming the characteristic α-β sandwich motif that is shared between the frataxin family of proteins **(Figure 4.2 A)**. The number of β-strands is variable between orthologs: yeast frataxin and the bacterial homolog CyaY have six β-strands while a seventh strand has been reported only in the human ortholog [21]. Sequence identity between proteins measured by clustal−ω sequence alignment are 54% and 38% with the human and yeast proteins respectively and 22% with the bacterial homolog CyaY **(Figure 4.3)**. RMSD values between Dfh and orthologs in regions of secondary structure are 1.13 Å and 1.44 Å respectively with the human and yeast orthologs (measured using the 'align' tool on PyMoL [36]).

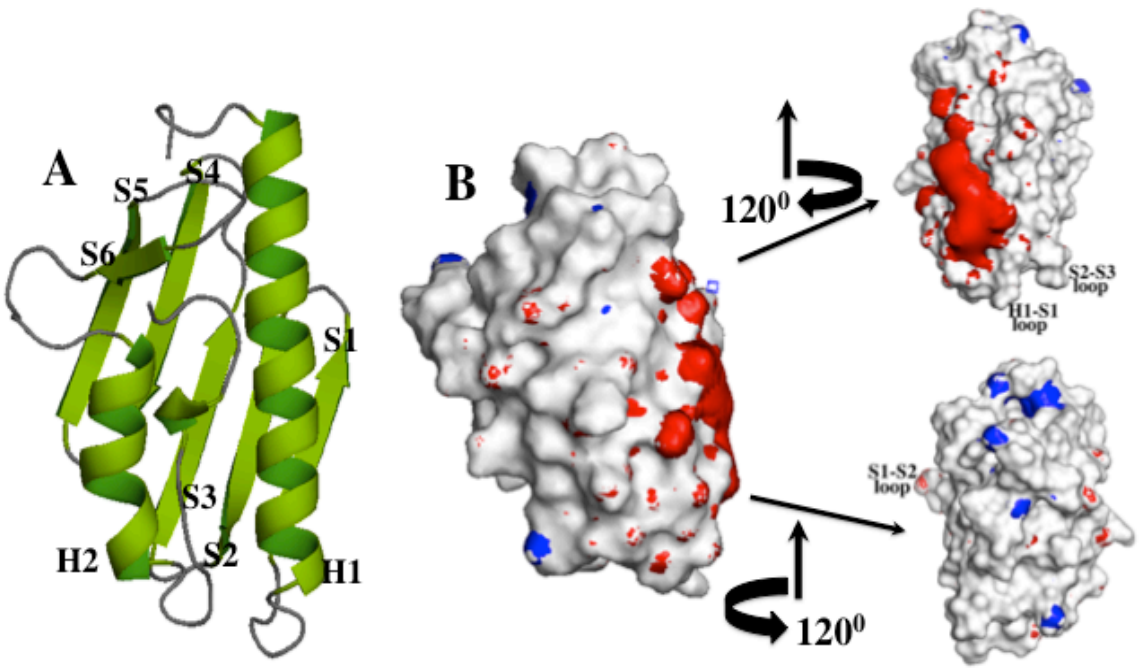

Figure 4.2: The crystal structure of *Drosophila* frataxin homolog Dfh. (A) Ribbon structure and (B) Surface electrostatic potential plots for Dfh at three different orientations around the vertical axis. (A) Labels for the different secondary structural elements are marked adjacent to the corresponding helix or strand. (B) To the left is a surface electrostatic potential plot for Dfh at an orientation that corresponds to the ribbon structure. Electrostatic surface plots were calculated using the free PDB2PQR software* and modeled with the APBS plugin* for PyMoL using a solvent radius of 1.4 Å and a contour value of 10 kT/e for both charged isoforms. Secondary structural landmarks on the rotated structures are labeled for clarity. **[37, 38]

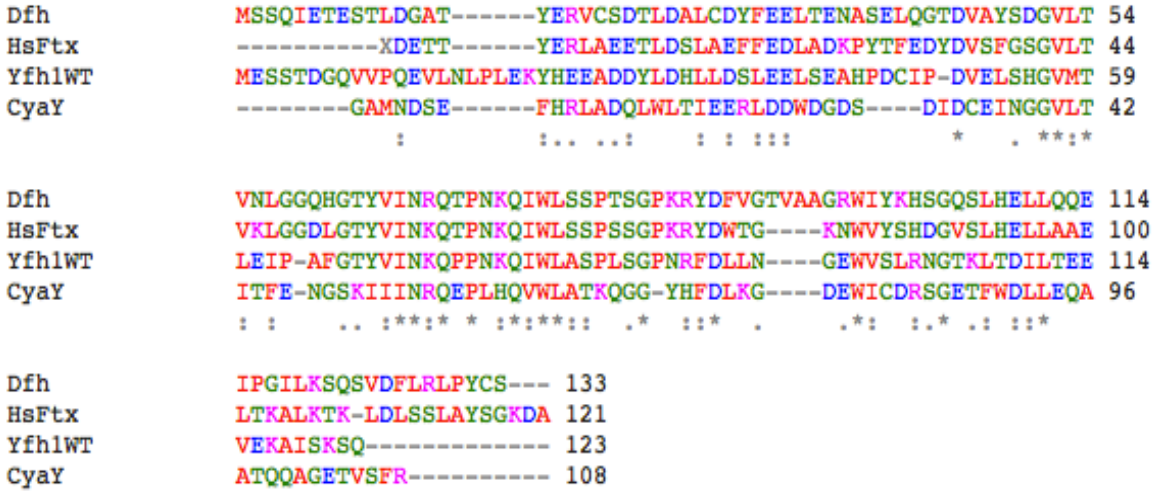

Figure 4.3: Clustal-ω sequence alignment between Frataxin orthologs: *D. melanogaster* (Dfh), *H. sapien* (HsFtx), *S. cerevisiae* (Yfh1WT) and *E. coli* (CyaY). Fully conserved residues are indicated by an asterisk (*) under the residue.

Structural instability associated with the human and yeast frataxins have been attributed to their relatively unfolded N-terminus, prior to the helix-1, which leads to protein autodegradation [21]. Mature human frataxin extends from residue 75-210 with a total of 18 N-terminal residues and [10, 20], mature yeast frataxin spans residues 52-174 [6] and, like the human ortholog has 18 N-terminal residues. On the other hand, the structure of Dfh spans residues 65-190 and appears to have a relatively short unfolded N-terminus comprising 5 residues only **(Figure 4.2 A).** In addition, frataxin's C-terminal residues past the helix-2 have been reported to be an additional determinant of protein stability. Melting temperature studies on yeast frataxin correlated a longer C-terminus to greater stability [21]. Human frataxin has a relatively long C-terminus of 16 residues, while the yeast ortholog has only 3 residues terminal to helix-2. The C-terminus of Dfh on the other hand comprises 18 residues, a part of which appears to be folded into a 3_{10} helix and in addition, makes contact with helix-1 possibly providing added stability. A combination of a relatively shorter N-terminus with a longer C-terminus, both of which are attributes to greater stability are possibly factors that contribute to the resistance of Dfh to degradation.

Figure 4.2 (B) shows the electrostatic surface plot of Dfh. The red region that spans the first α-helix and first β-strand region represents the acidic patch that consists of conserved, surface exposed acidic residues. This acidic patch is common to frataxin proteins and has been identified to be crucial for frataxin's iron binding ability and interaction with partner proteins [21].

4.5.2 Dfh backbone resonance assignments:

In order to exploit structural information regarding Dfh, we present the assignment of the backbone atom chemical shifts, obtained by Nuclear Magnetic resonance (NMR) spectroscopy, in this report. Dispersion of amide resonances in the ^{15}N HSQC spectra of the 59-190 residues of fly frataxin construct **(Figure 4.4)** confirm the majority of residues exist in a structured region. In order to avoid referencing errors, LACS (Linear Analysis of Chemical Shift) analysis of the protein residues was performed. LACS analysis is used to detect the referencing errors. Linear regression plots between the secondary shifts of the alpha and difference between the secondary shifts of the alpha and beta carbons for residue 'i' of protein pass through the origin from two directions, suggesting correct referencing. A total of 128 out of 133 residues of the mature Dfh protein were assigned. The structure of Dfh was predicted using the Chemical Shift Indices (CSI) program based on the backbone atom assignments. CSI is a program that predicts protein's secondary structure. CSI measures the deviation of the obtained chemical shift value assigned to each backbone atom in the molecule of interest to values from an averaged library for atoms in a random coil, helix and strand. The sign and magnitude of these deviations can then be used to correlate the predicted secondary structure type that the residue is found in, providing a rough estimate of the probable secondary structure profile of the molecule from just the chemical shift assignments. Prediction of secondary structural elements for Dfh in solution using chemical shift indices (CSI) analysis within the program nmrView [34]

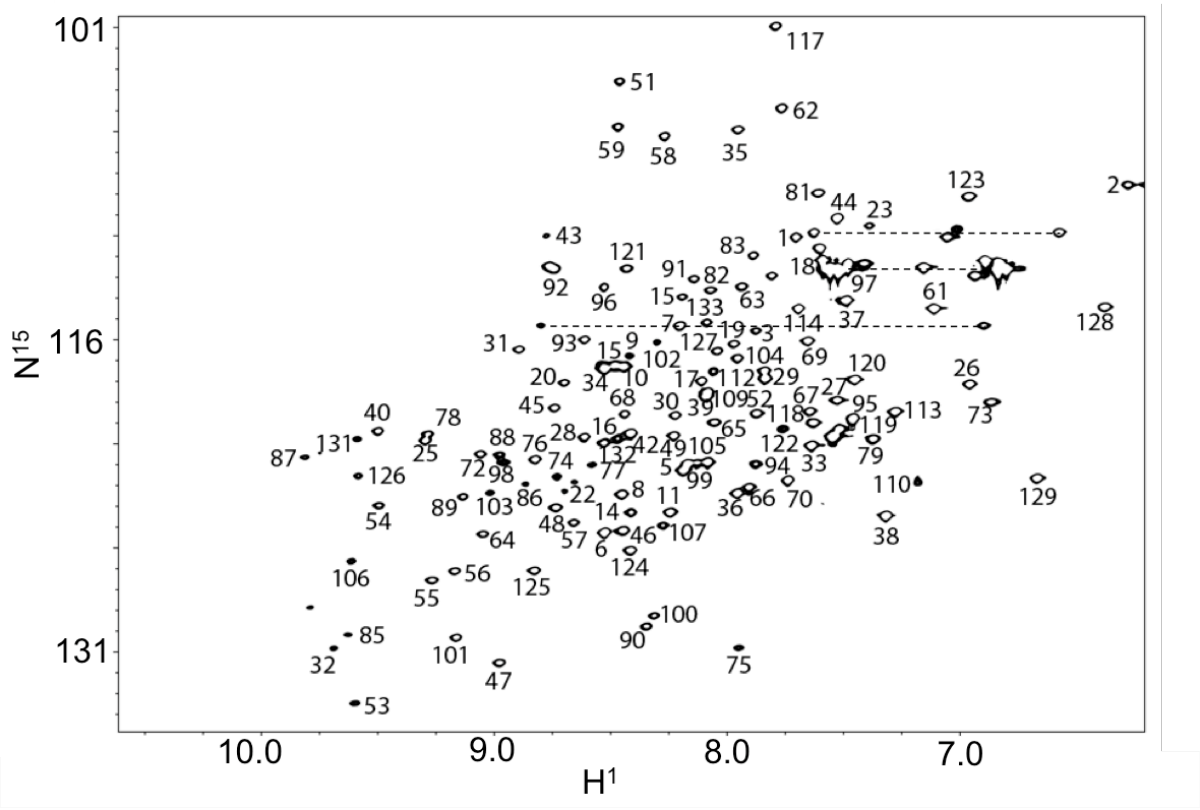

Figure 4.4. Assigned ^{15}N HSQC spectrum of Dfh. Data was collected on the National Magnet Laboratory's Varian INOVA 720 MHz spectrometer at 298 K and at in house INOVA 600 MHz

suggests the protein secondary structural elements are highly conserved between orthologs, and the structure most likely exists as an α/β sandwich motif family member **(Figure 4.5)**. The predicted Dfh secondary structure lacks the N-terminal 3^{10} helix observed in the yeast frataxin structure [6] but it shows the presence of a beta strand before the helix-1, suggesting the Dfh structure is little different than the human frataxin N-terminal extension protein [11, 39]. Based on the predicted structural regions of the protein using the highly reliable C_a, N and CO data, the structure of Dfh consists of helices formed by the [residues 13-37 (H1) and 108-120 (H2)] and seven β-strands covering residues 10-12 (S1), 46-48 (S2), 53-57 (S3), 72-74 (S4), 77-79 (S5), 88-93 (S6) and 96-100 (S7).

The CSI predicted structure of Dfh suggests that it consists of 27% beta strand and 36% helical content. Based on this predicted structure Isu binding residues on the Dfh structure were determined. In case of yeast frataxin (Yfh1), the Isu binding residues have been assigned. The corresponding residues of Dfh include Glu 32, Thr 35 (lie on helix 1 region); Val 52, Leu 53, Thr 54, Val 55, Leu 57 (lie on beta sheet 1 surface); Gln 105, Gly 117 and Ser 119 (lie on loop and helix 2 surface). Thus most of the functionally important residues of frataxin lie on the same region on predicted protein as in case of yeast frataxin.

The backbone atom chemical shift assignments of Dfh provides a control for future experiments directed at monitoring structural changes on the protein coupled with Fe (II) and partner protein binding. Using the predicted secondary structure model, we

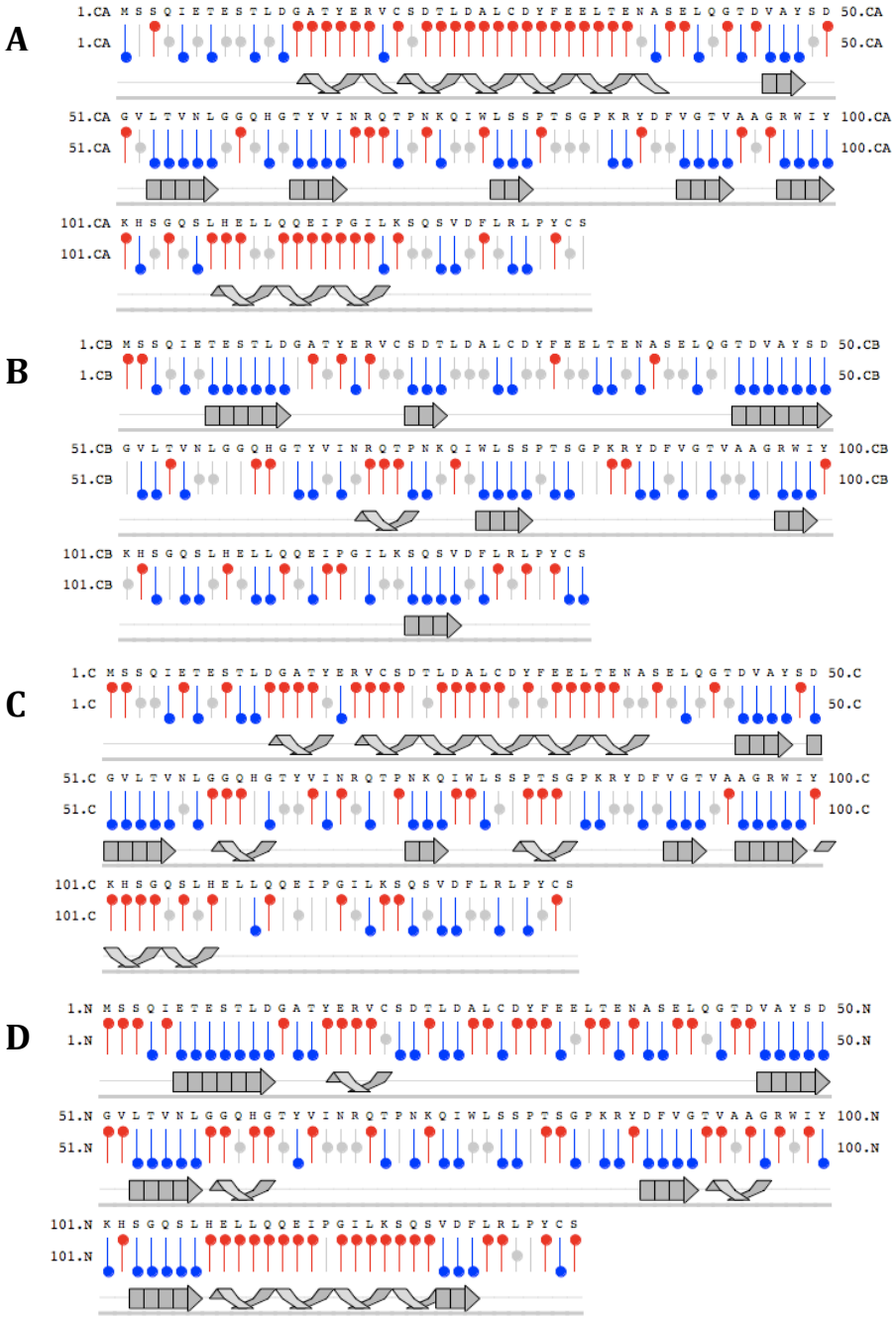

Figure 4.5. Summary of proposed secondary structural elements for Dfh: based on A) Cα, B) Cβ, C) Carbonyl carbon and D) N, in solution obtained from CSI analysis using NMRView. Single letter residue designations are provided (top) with predicted secondary structural elements displayed in red (helix), blue (strand) or grey (unfolded).

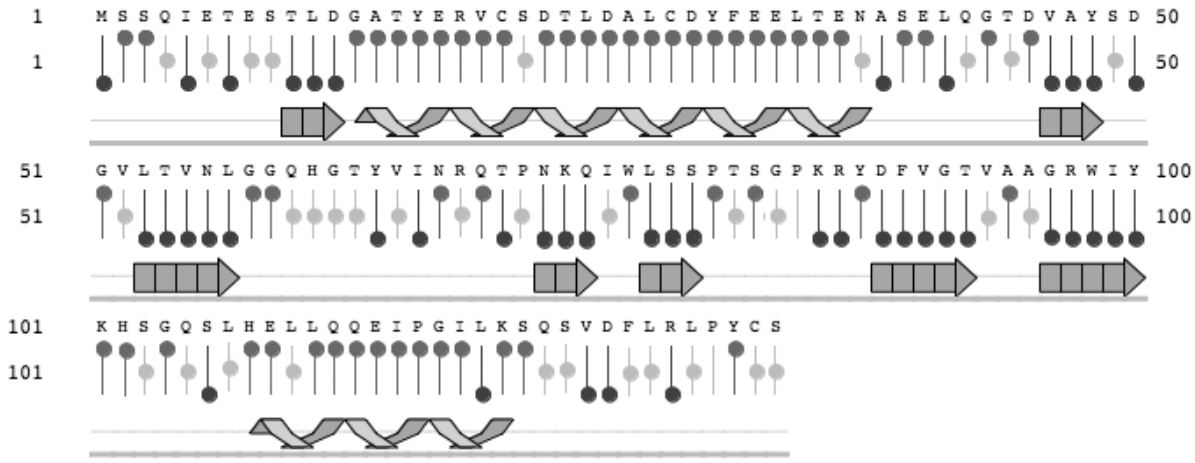

Figure 4.6. Consensus secondary structure prediction. This structure is predicted using the secondary structure prediction for Cα, N and Carbonyl carbon. Prediction is made manually by using consensus where two of the three values points the same prediction.

found most of the corresponding residues in the yeast frataxin iron binding site (Ala 26, Asp 29, Glu 36, Asn 37, Ala 47 and Tyr 48 - based on Dfh numbering) lie on the helix-1 and strand-2 portion of the molecule [5].

4.5.3 Mapping the putative iron binding residues on Dfh

NMR spectroscopy was used to identify frataxin amino acids that are influenced by the presence of ferrous iron. A series of ^{1}H-^{15}N HSQC spectra were collected by titrating anaerobic ferrous ammonium sulfate at a final ratio of 1:1 protein to Fe(II). This ratio was in keeping with previously reported Isothermal Titration Calorimetry results, which showed that Dfh bound 1 atom of iron [8]. Both protein and Fe(II) solutions were prepared under strict anaerobic conditions to prevent any chances of oxidation. Data was collected under conditions identical to those of the backbone assignment experiments. Our control apo-Dfh spectrum was identical to that obtained observed in Figure 4.4, enabling a direct comparison of the reproducible protein samples. An overlay of backbone amide chemical shifts in the apo and holo forms revealed 10 residues on Dfh underwent substantial chemical shift changes **(Figure 4.7)**. Residues that are shifted include D25, A26, E36, N37, D45, T54, V55, N56, H61 and E114. In addition, residues that disappeared upon addition of iron include Y30, E33, S52, F88, G100, V103, and Y105, the disappearance is a possible indication of residues being in close proximity to the paramagnetic metal. The positions on the apofrataxin structure that are affected by the presence of iron are shown in **(Figure 4.8)**.

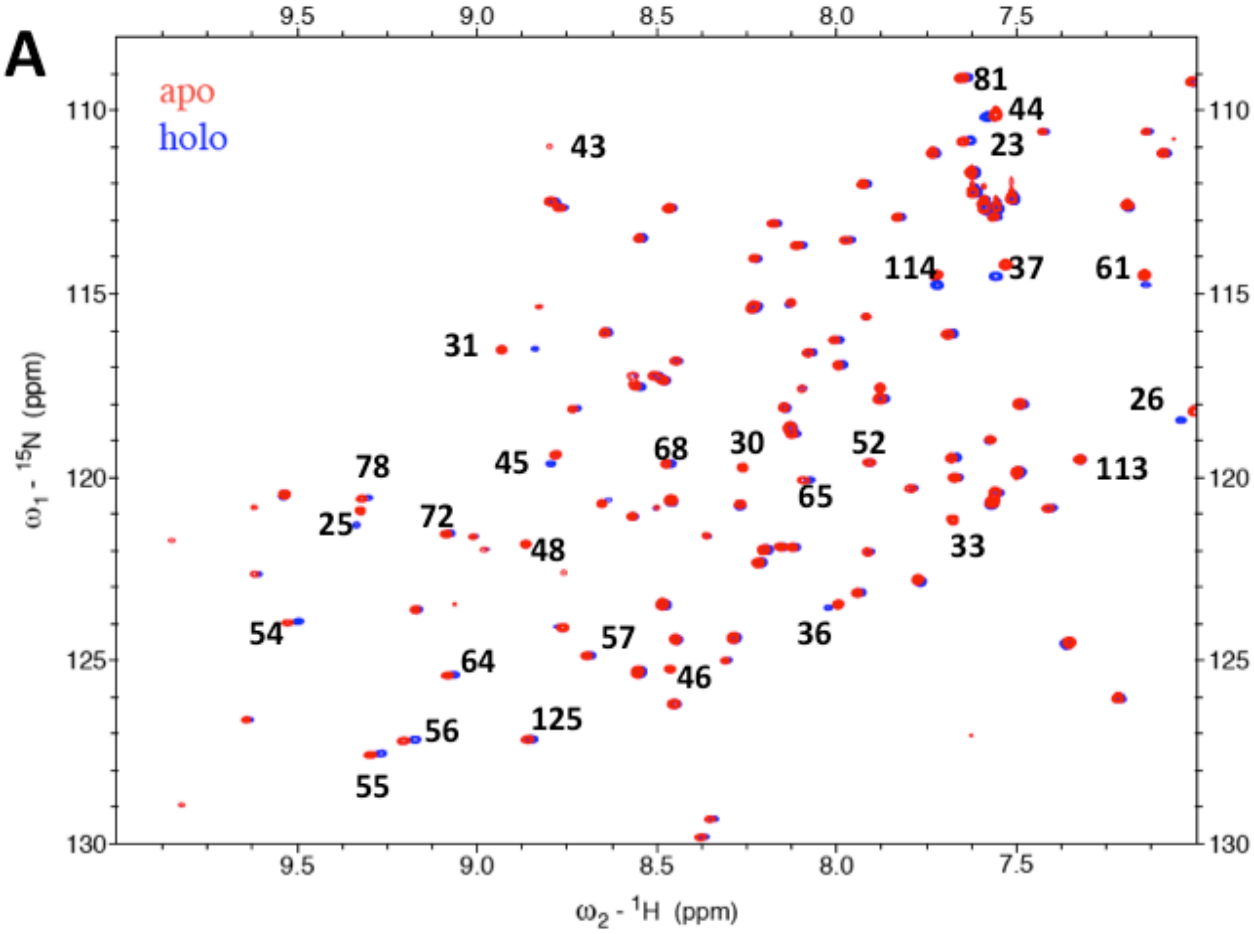

Figure 4.7. Overlay of 2D ^{1}H-^{15}N HSQC spectra for Dfh. (Zoomed in for clarity**).** Apo protein peaks are shown in red and holo protein peaks in blue. Spectra were collected on a Varian Inova 600 MHz spectrometer at 25 ^{0}C in 20 mM HEPES (pH: 7.5) 150 mM NaCl and 5 mM β-mercaptoethanol. Peaks that showed substantial chemical shift perturbations were identified by comparison to the map of assigned Dfh backbone resonances (Figure 4.4).

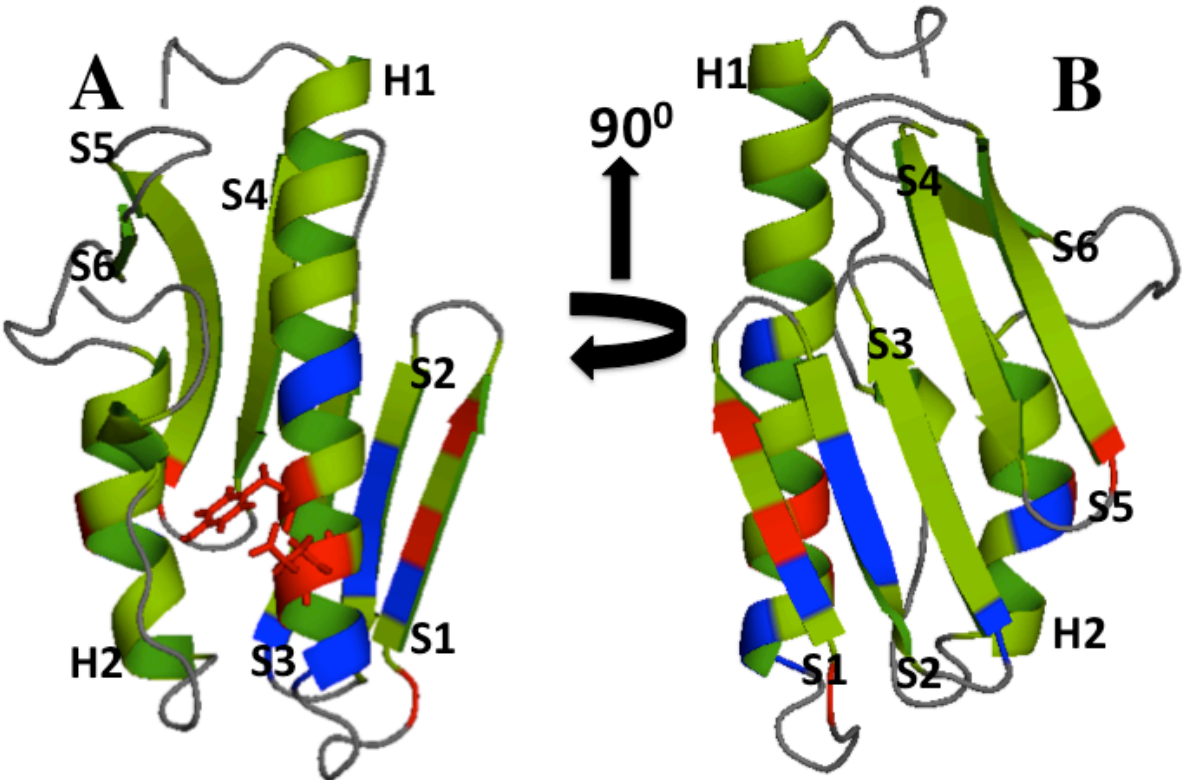

Figure 4.8 Perturbed residues upon Fe (II) titration into Dfh. Determined by 2D ^{1}H-^{15}N HSQC NMR spectroscopy and modeled on PyMoL [36]. (**A)** Orientation 1 showing the helix-1and strand-1 acidic patch & **(B)** Orientation 2 showing the plane formed by helices & strands. Residues that showed a perturbation upon iron addition (colored blue) include D25, A26, E36 and E37 on helix-1; D45 on strand-1; T54, V55 and N56 on strand-2; H61 on the strand 2, 3 loop and E114 on helix-2. Residues that disappeared upon iron addition (colored red) include Y30, F31, E33 located on the helix-1 region; G43 on the helix, strand-1 loop; V46 and Y48 on strand-1; S52 on the strand 4, 5 loop and Q113 on helix-2.

4.6: Discussion:

Similarity between frataxin orthologs and determinants of stability:

All the characterized frataxins so far (Human, yeast, bacterial and fly) share a common structural fold comprising a characteristic α-β sandwich motif with a characteristic acidic patch in the region spanning helix-1 and strand-1 [21]. This region also contributes to the characteristic acidic *p*I of the protein: Dfh has a theoretical *p*I of 4.65 which matches those of the human (4.98), yeast (4.34) and *E. coli* (4.24) proteins [6]. Surface exposed and charged residues in this acidic patch have been shown to be responsible for the iron binding properties of the Frataxin family [21].

Although the structures are similar with a well folded globular C-terminus, the human and yeast proteins have been reported to be inherently unstable due to a high susceptibility to autodegradation. One of the main reasons that contribute to autodegradation is the relatively long and unfolded N-terminal region, prior to helix-1. Both the yeast and human proteins have an 18 residue long N-terminus in the mature form [21] . The function of this unfolded N-terminus is unclear. In the human ortholog, it has been reported to function in binding Isu and also in binding iron [40, 41]. For Dfh, the presence of a mitochondrial targeting sequence has been reported [22] however; *in vivo* details of processing intermediates in the formation of mature Dfh are not yet available. Our crystal structure spanning residues 65-190 of the open reading frame shows the presence of a relatively shorter N-terminus of 5 residues. An additional structural feature that possibly contributes to the stability of Dfh is its long C-terminus,

which extends past helix-2, comprising 18 residues in length. A longer C-terminus has been associated with a higher melting temperature and stability. Thermal denaturation experiments have shown that Dfh melts at 59^0C, while the human and yeast orthologs melt at 60^0C and 44^0C respectively. Human frataxin has a 16 residue spanning C-terminus while yeast has only three residues. However, the increased susceptibility of human frataxin's N-terminus to autodegradation possibly contributes to its overall instability [21].

Iron binding properties of Drosophila Frataxin:

Data was collected at a stoichiometry of 1:1 protein to iron in keeping with previous results from isothermal titration calorimetry [8]. Even at a 1:1 Fe:protein concentration, substantial chemical shift perturbations were observed, along with peak disappearance suggestive of residues in the vicinity of paramagnetic metal (see Figures 4.7, 4.8). Iron predominantly binds charged oxygen or nitrogen based amino acids, and to a lesser extent, thiols [6]. Most of these residues are located in the conserved helix-1, strand-1 acidic patch and are predominantly oxygen/nitrogen based, which fits well with our published XAS data on Dfh which shows Fe(II) bound in an octahedral complex formed by oxygen/ nitrogen based ligands [8]. The resonance shifted residues are a good indicator of iron proximity, and on helix-1 the charged residues include Y30 and E33 were line broadened. Both these residues are solvent exposed indicating a possible role in iron binding. An additional F31 was also line broadened possibly due to its

proximity to the above residues. On strand-1, Y46 was line broadened, however not solvent exposed. An additional charged residue that was line broadened is Q113 on helix-2. Residues that were perturbed appear to flank the sides of the line broadened residues. The occurrence of perturbed residues in clusters on helix-1 and on strand-1 indicates the possibility of greater than one iron-binding site, as observed in the case of yeast frataxin which binds two iron atoms at sites located on helix-1 and strands-1& 2 [5]. Human frataxin has been shown to bind up to 6 atoms of iron [42]. In addition, a cluster of residues in the region around the loops of strands-2 &3; strands-4 & 5 and the helix-2 could indicate a molecular rearrangement in structure as a result of metal binding or an additional metal binding site of a different functional significance. Experiments are currently underway to collect holo Dfh data at sub-stoichiometric and at higher concentrations to obtain more accurate information on residues that are shifted and stoichiometry of Fe (II) binding. A final confirmation of the possible iron binding sites would be site directed mutagenesis followed by tests for iron binding.

Biological Significance:

This study provides a complete description of the crystal structure of the Drosophila frataxin homolog (Dfh) from *D. melanogaster.* In addition we completed backbone resonance assignments for Dfh residues using NMR. These backbone assignments were used to determine putative residues involved in Fe (II) binding. Our studies show that Dfh is a well-folded protein with a fold similar to those of characterized

orthologs in the Frataxin family. The monomeric form of the protein was used in all experiments and was shown to be able to bind iron, at sites that are predominantly located in the helix-1, strand-1 region just as in the case of the human and yeast frataxins indicating an iron chaperone role for Dfh is possible [21]. Though similar in its structure and function to related orthologs, Dfh appears to be far more stable against autodegradation. Experiments are currently underway to map binding interfaces between Dfh & DIsu and additional binding partners.

4.7 Acknowledgements

The authors acknowledge the National High Magnetic Field Laboratory (NHMFL) in Tallahassee, FL. for 720 MHz NMR time as part of their user's program. The INOVA 600 MHz spectrometer (Wayne State University) with cold probe was purchased through NIH support (Grant-1S10RR1662601). The authors also acknowledge members of the Life Science Collaborative Access Team of the Advanced Photon Source (APS) for assistance in data collection at the beam lines of sector 21, which is in part funded by the Michigan Economic Development Corporation and the Michigan Technology Tri-Corridor (Grant 085P1000817). Use of APS was supported by the Office of Science of the US Department of Energy, under Contract No. DE-AC02-06CH11357. This work was supported by the National Institutes of Health (Grant - R01DK068139, TLS), the American Heart Association (Grant-AHA12PRE1172005, AVR) and the Friedreich's Ataxia Research Alliance.

4.8 References

1. Campuzano, V., et al., *Friedreich's ataxia: autosomal recessive disease caused by an intronic GAA triplet repeat expansion.* Science, 1996. **271**(5254): p.1423-7.
2. Cossee, M., et al., *Inactivation of the Friedreich ataxia mouse gene leads to early embryonic lethality without iron accumulation.* Hum Mol Genet, 2000. **9**(8): p. 1219-26.
3. Delatycki, M.B., R. Williamson, and S.M. Forrest, *Friedreich ataxia: an overview.* J Med Genet, 2000. **37**(1): p. 1-8.
4. Babcock, M., et al., *Regulation of mitochondrial iron accumulation by Yfh1p, a putative homolog of frataxin.* Science, 1997. **276**(5319): p. 1709-12.
5. Cook, J.D., et al., *Monomeric yeast frataxin is an iron-binding protein.* Biochemistry, 2006. **45**(25): p. 7767-77.
6. He, Y., et al., *Yeast frataxin solution structure, iron binding, and ferrochelatase interaction.* Biochemistry, 2004. **43**(51): p. 16254-62.
7. Adinolfi, S., et al., *Bacterial frataxin CyaY is the gatekeeper of iron-sulfur cluster formation catalyzed by IscS.* Nat Struct Mol Biol, 2009. **16**(4): p. 390-6.
8. Kondapalli, K.C., et al., *Drosophila frataxin: an iron chaperone during cellular Fe-S cluster bioassembly.* Biochemistry, 2008. **47**(26): p. 6917-27.
9. Yoon, T. and J.A. Cowan, *Iron-sulfur cluster biosynthesis. Characterization of frataxin as an iron donor for assembly of [2Fe-2S] clusters in ISU-type proteins.* J. Am. Chem. Soc., 2003. **125**: p. 6078-84.

10. Dhe-Paganon, S., et al., *Crystal structure of human frataxin.* J Biol Chem, 2000. **275**(40): p. 30753-6.

11. Kondapalli, K.C., et al., *NMR assignments of a stable processing intermediate of human frataxin.* Biomol NMR Assign. **4**(1): p. 61-4.

12. Nair, M., et al., *Solution structure of the bacterial frataxin ortholog, CyaY: mapping the iron binding sites.* Structure (Camb), 2004. **12**(11): p. 2037-48.

13. Muhlenhoff, U., et al., *The yeast frataxin homolog Yfh1p plays a specific role in the maturation of cellular Fe/S proteins.* Hum Mol Genet, 2002. **11**(17): p. 2025-36.

14. Rotig, A., et al., *Aconitase and mitochondrial iron-sulphur protein deficiency in Friedreich ataxia.* Nat Genet, 1997. **17**(2): p. 215-7.

15. Santos, R., et al., *Friedreich ataxia: molecular mechanisms, redox considerations, and therapeutic opportunities.* Antioxid Redox Signal, 2010. **13**(5): p. 651-90.

16. Cavadini, P., et al., *Assembly and iron-binding properties of human frataxin, the protein deficient in Friedreich ataxia.* Hum Mol Genet, 2002. **11**(3): p. 217-27.

17. Cook, J.D., et al., *Molecular Details of the Yeast Frataxin-Isu1 Interaction during Mitochondrial Fe-S Cluster Assembly.* Biochemistry, 2010.

18. Yoon, T. and J.A. Cowan, *Frataxin-mediated iron delivery to Ferrochelatase in the final step of Heme biosynthesis.* J Biol Chem, 2004. **279**(25): p. 25943-6.

19. Park, S., et al., *Yeast frataxin sequentially chaperones and stores iron by coupling protein assembly with iron oxidation.* J. Biol. Chem, 2003. **278**: p. 31340-51.

20. Musco, G., et al., *Towards a structural understanding of Friedreich's ataxia: the solution structure of frataxin.* Structure, 2000. **8**(7): p. 695-707.

21. Bencze, K.Z., et al., *The structure and function of frataxin.* Crit Rev Biochem Mol Biol, 2006. **41**(5): p. 269-91.

22. Canizares, J., et al., *dfh is a Drosophila homolog of the Friedreich's ataxia disease gene.* Gene, 2000. **256**(1-2): p. 35-42.

23. Anderson, P.R., et al., *RNAi-mediated suppression of the mitochondrial iron chaperone, frataxin, in Drosophila.* Hum Mol Genet, 2005. **14**(22): p. 3397-405.

24. Anderson, P.R., et al., *Hydrogen peroxide scavenging rescues frataxin deficiency in a Drosophila model of Friedreich's ataxia.* Proc Natl Acad Sci U S A, 2008. **105**(2): p. 611-6.

25. Llorens, J.V., et al., *Causative role of oxidative stress in a Drosophila model of Friedreich ataxia.* Faseb J, 2007. **21**(2): p. 333-44.

26. Runko, A.P., A.J. Griswold, and K.T. Min, *Overexpression of frataxin in the mitochondria increases resistance to oxidative stress and extends lifespan in Drosophila.* FEBS Lett, 2008.

27. Vonrhein, C., et al., *Data processing and analysis with the autoPROC toolbox.* Acta Crystallographica Section D: Biological Crystallography, 2011. **67**(4): p. 293-302.

28. McCoy, A.J., et al., *Phaser crystallographic software.* Journal of applied crystallography, 2007. **40**(4): p. 658-674.

29. Emsley, P. and K. Cowtan, *Coot: model-building tools for molecular graphics.* Acta Crystallographica Section D: Biological Crystallography, 2004. **60**(12): p. 2126-2132.

30. Adams, P.D., et al., *PHENIX: a comprehensive Python-based system for macromolecular structure solution.* Acta Crystallographica Section D: Biological Crystallography, 2010. **66**(2): p. 213-221.

31. Davis, I.W., et al., *MolProbity: all-atom contacts and structure validation for proteins and nucleic acids.* Nucleic acids research, 2007. **35**(suppl 2): p. W375-W383.

32. Cavanagh, J., et al., *Protein NMR spectroscopy: principles and practice*. 1995: Academic Press.

33. Delaglio, F., et al., *NMRPipe: a multidimensional spectral processing system based on UNIX pipes.* J Biomol NMR, 1995. **6**(3): p. 277-93.

34. Blevins, B.A.J.a.R.A., *NMRView: A computer program for the visualization and analysis of NMR data.* J. Biomol. NMR 1994. **4**(5): p. 11.

35. Goddard T.D., K.D.G., *Sparky 3.* University of California.

36. Schrodinger, LLC, *The PyMOL Molecular Graphics System, Version 1.3r1*. 2010.

37. Dolinsky, T.J., et al., *PDB2PQR: an automated pipeline for the setup of Poisson-Boltzmann electrostatics calculations.* Nucleic Acids Res, 2004. **32**(Web Server issue): p. W665-7.

38. Baker, N.A., et al., *Electrostatics of nanosystems: application to microtubules and the ribosome.* Proc Natl Acad Sci U S A, 2001. **98**(18): p. 10037-41.

39. Prischi, F., et al., *The N-terminus of mature human frataxin is intrinsically unfolded.* FEBS J, 2009.

40. Yoon, T., E. Dizin, and J.A. Cowan, *N-terminal iron-mediated self-cleavage of human frataxin: regulation of iron binding and complex formation with target proteins.* J Biol Inorg Chem, 2007. **12**(4): p. 535-42.

41. Gentry, L.E., et al., *His86 from the N-terminus of frataxin coordinates iron and is required for Fe-S cluster synthesis.* Biochemistry, 2013. **52**(35): p. 6085-96.

42. Yoon, T. and J.A. Cowan, *Iron-sulfur cluster biosynthesis. Characterization of frataxin as an iron donor for assembly of [2Fe-2S] clusters in ISU-type proteins.* J Am Chem Soc, 2003. **125**(20): p. 6078-84.

CHAPTER 5
SUMMARY, CONCLUSIONS AND FUTURE DIRECTIONS

5.1 Significance of Iron in health:

Iron is the most common transition metal in the earth's crust and the most abundantly used transition metal among living organisms [1]. Its biological significance is largely attributed to its ability to undergo reversible oxidation-reduction chemistry that enables its participation in electron transfer reactions [2]. However, as a cofactor associated with proteins, its functions are not limited to electron transfer alone, but also include oxygen binding (hemoglobin) [3], catalysis (aconitase) [4], free-radical generation (SAM enzymes) [5] among many more. Its versatility in function allows iron to participate in various processes that sustain life such as oxygen transport, oxidative metabolism, xenobiotic metabolism, ribonucleotide reduction during DNA synthesis, and for DNA repair [1, 2, 6]. Considering its biological significance, understanding its metabolism is crucial to maintaining a healthy population.

As essential as it is for survival, iron in excess can be detrimental. In the reaction described as 'Fenton Chemistry', ferrous iron participates in the generation of deadly hydroxyl radicals that can cause widespread damage to DNA, protein, membrane lipids and cellular constituents leading to cell death [7]. Iron-induced free radical damage has been implicated in the pathology of diseases of iron overload such as Friedreich's Ataxia, a genetic disorder characterized by an accumulation of iron in actively metabolizing tissues ultimately leading to cardio- and neuro- degeneration and cell

death [8, 9]. In addition, neurodegenerative disorders such as Alzheimer's and Parkinson's disease are also associated with pathology caused by iron accumulation [10, 11]. At the other end of the spectrum, a deficiency of iron is associated with anemia [12] and has been reported to have deleterious effects on neurotransmission, myelination, and dopamine receptor and transporter functions [2]. Anemia is the most prevalent nutritional disorder worldwide, affecting about 30% of the world's population according to the NIH. In addition, we do not fully understand the role of iron in neurodegenerative disorders [13]. Therefore, iron metabolism has become an important research directive at national funding agencies.

5.2 Summary & Future Directions

Cellular iron metallochaperones are an important aspect of metal homeostasis. They are often small diffusible molecules that bind metal preventing any incidence of free radical generation [14]. The first chapter of my thesis is a review article that outlines the roles of two potential cellular iron chaperones, the mitochondrial iron chaperone Frataxin and the cytosolic PCBP family of proteins. Frataxin plays a key role in iron homeostasis, evident from pathogenesis associated with the debilitating disease Friedreich's Ataxia, described above, caused by an inability to synthesize this single protein. Frataxin has been shown by numerous groups to be a part of the iron-sulfur cluster (ISC) multicomplex, where it functions in the capacity of a potential iron provider and an allosteric modulator of both the cysteine desulfurase and scaffold protein Isu [15-

17]. Other roles have been described, including an ability to oligomerize in the presence of oxygen and a ferroxidase ability that enables storage of ferric iron in a manner similar to ferritin [2, 7]. The role of frataxin needs to be clarified to assist in the development of improved research strategies for treating FRDA.

The first chapter also outlines the role of the cytosolic PCBP family and describes its role in chaperoning iron to Ferritin for storage. The iron binding and thermodynamic properties of PCPB have been established [18] but a structural characterization of the protein and residues involved in iron binding are still lacking. Further clarification of the activity of the PCBP protein family will provide additional insight into cellular iron distribution strategies.

The second and third chapters of my thesis are focused on understanding the initial events of iron loading onto the iron-sulfur cluster scaffold protein. The second chapter describes the Fe(II) binding properties of ISU using four orthologs (human, fly, yeast and from the thermophile *Thermatoga*). By ITC, the ISU proteins were found to bind Fe(II) with a nanomolar to micromolar affinity. Using XAS, the Stemmler laboratory characterized the ISU-Fe(II) bound complex in these orthologs and found that ISU appears to bind iron in a 6 coordinate oxygen/nitrogen ligand environment. The absence of any thiol ligation to metal indicates iron loading onto ISU occurs at a site distinct from its cysteine rich active site. These findings were confirmed by Mössbauer spectroscopy. This would suggest that if Frataxin interacts with ISU to deliver iron, it may interact with the protein at this distinct metal-loading site.

The third chapter of my thesis builds off of the results of chapter 2 and is directed at elucidating the initial Fe(II) loading site on ISU, using the yeast model system. The C-terminal helix of ISU has a high percentage of charged residues (approx. 50% based on the modeled structure of YIsu1) and appears to undergo an increase in order of fold upon substrate binding, similar to the transition demonstrated by the crystal structure of ISU in *A. aeolicus* [19]. Based on the crystal structure of *E. coli* IscU-IscS and predictive modeling of the Frataxin ortholog CyaY docking to the complex [20], the C-terminus of IscU appears to be in a perfect orientation to bind CyaY and its charged surface would provide a complementary surface to Frataxin's charged surface that has been implicated in iron binding and Isu interaction in yeast. Yeast Isu1 residues E144A, and D145A and a double mutant E144A, D145A located on the protein's C-terminal α-helix, were mutated by site directed mutagenesis. Among these, using competition assays, E144A, D145A and double mutants confirmed a drop in affinity for Fe(ll) at one site, while the affinity at the other site was only marginally decreased. Binding of mutant proteins E144A and D145A to holo-Yfh1, measured by ITC followed an endothermic pattern of binding and was accompanied by a rise in enthalpy indicating an enthalpically unfavorable process. Binding of holo-Yfh1 to WT YIsu1, on the other hand was an enthalpically favorable process. This indicates that a mutation of the D145A residue perturbs the interaction between frataxin and YIsu1. In addition, thermal denaturation experiments using DSC performed on holo WT YIsu1 was associated with a shift to higher temperature indicating a stabilizing change upon Fe(ll) binding. In contrast,

however, the holo D145A mutant shifted to a lower temperature indicating destabilization upon iron binding. Thermodynamics associated with denaturation of the holo forms of the mutant proteins were associated with a rise in enthalpy and entropy, while holo YIsu1 showed no significant change in associated thermodynamics compared to the apo form. This possibly indicates that the stabilizing change in structure in WT YIsu1 balances changes in energetics upon binding Fe(II). The ability of YIsu1 WT and the D145A mutant to synthesize Fe-S clusters was also tested by an Fe-S assembly assay using Near UV circular dichroism in the presence of either Fe(II) or holo-Yfh1. WT YIsu1 showed a clear rise in activity in the presence of holo Frataxin compared Fe(II) alone. On the other hand, the D145A mutant showed a higher activity in the presence of Fe(II) alone via a reaction that was slower than that in the presence of holo Yfh1, which was a reaction that appeared to reach saturation quickly. This is consistent with the ITC results obtained with holo-Yfh1, which showed a weak binding of holo-Yfh1WT with D145A and thus, a weaker interaction. In addition the mutant reaction with Yfh1WT possibly saturated faster due to a loss of an iron-binding site. As iron binding is clearly facilitated by holo-Yfh1WT, in its absence, the mutant protein would take longer to bind iron and saturate the active site. These results collectively indicate that the c-terminal charged residue D145A on Isu could be a possible ligand for holo frataxin interaction.

An additional study that could further confirm that residues on YIsu1's C-terminus are involved in frataxin binding is currently underway in the Stemmler laboratory, in

collaboration with Dr. Andrew Dancis (University of Pennsylvania). Three constructs have been synthesized with a cleavable thrombin-His tag and with 10, 17 and 22 C-terminal residues deleted. Experiments are currently underway to determine which of these constructs show perturbations with frataxin binding. **Figure 5.1** shows an amino acid sequence alignment of these constructs after DNA isolation and sequencing.

Obtaining a crystal structure of holo Yfh1WT and WT YIsu1 would be the final confirmation of the initial binding site. Attempts, however, at crystallization have been plagued by poor stability of the yeast proteins and the redox activity of iron. As an alternative method, the *Drosophila* proteins are also being tested for crystallization. Since *Drosophila* frataxin appears easily crystallizable, and, as we now have its crystal structure as a starting point, there is some indication that we may have the same success with DIsu.

The final chapter of my thesis is a structural characterization of the *Drosophila* frataxin homolog Dfh. Dfh was crystallized and the structure of the protein was determined by Dr. Joseph Brunzelle (APS, Argonne National Laboratories). Like its yeast and human homologs, Dfh is well-folded with an α-β sandwich motif comprising two α-helices and six β-strands sandwiched between the two helices [21, 22]. The Dfh protein does not have a long unstructured N-terminal region like that seen in the yeast and human proteins [7, 23], and it has a considerably longer C-terminal tail; two factors that could contribute to its extraordinary stability. Electrostatic potential surface plots show the presence of the conserved acidic patch at the α1-β1region on Dfh. This acidic

```
YIsuWT      ----------MGSSHHHHHHSSGL-VPRGS----HMYHPKVIEHYTHPRNVGSLDKKLPNVG-47
YIsu_Δ22    ----------MGSSHHHHHHSSGL-VPRGS----HMYHPKVIEHYTHPRNVGSLDKKLPNVG-47
YIsu_Δ17    ----------MGSSHHHHHHSSGL-VPRGS----HMYHPKVIEHYTHPRNVGSLDKKLPNVG-47
YIsu_Δ10    ----------MGSSHHHHHHSSGL-VPRGS----HMYHPKVIEHYTHPRNVGSLDKKLPNVG-47
                      **********.*****.---* * **************************
YIsuWT      TGLVGAPACGDVMRLQIKVNDSTGVIEDVKFKTFGCGSAIASSSYMTELVQGMTLDDAAK-107
YIsu_Δ22    TGLVGAPACGDVMRLQIKVNDSTGVIEDVKFKTFGCGSAIASSSYMTELVQGMTLDDAAK-107
YIsu_Δ17    TGLVGAPACGDVMRLQIKVNDSTGVIEDVKFKTFGCGSAIASSSYMTELVQGMTLDDAAK-107
YIsu_Δ10    TGLVGAPACGDVMRLQIKVNDSTGVIEDVKFKTFGCGSAIASSSYMTELVQGMTLDDAAK-107
            ************************************************************
YIsuWT      IKNTEIAKELSLPPVKLHCSMLAEDAIKAAIKDYKSKRNTPTMLSGTLE -156
YIsu_Δ22    IKNTEIAKELSLPPVKLHCSMLA----------------------------------------130
YIsu_Δ17    IKNTEIAKELSLPPVKLHCSMLAEDAIK-------------------------------------135
YIsu_Δ10    IKNTEIAKELSLPPVKLHCSMLAEDAIKAAIKDYK-----------------------------142
            **********************
```

Figure 5.1: Multiple sequence alignments of YIsu1 c-terminal truncation mutants after DNA isolation and sequencing: YIsu1 Δ10, Δ17 and Δ22 aligned with the YIsu1WT construct.

patch has been described to be important for the function of the frataxin proteins [7]. ^{15}N HSQC experiments performed on Dfh in the presence of iron show that the majority of the perturbed residues lie on the α helix-1 and β-strands 1 & 2 region; this is in the region of the conserved acidic patch indicating an Fe chaperone role for Dfh. Additional studies directed at characterizing the Dfh iron binding site involve collecting ^{1}H-^{15}N HSQC data upon titrating Fe(II) into the protein at sub-stoichiometric and excess Fe to get insight into both residues that are perturbed and line broadened which would give an accurate estimate of the Fe binding site. It will also provide some insight into stoichiometry, as upon excess Fe(II) titration, protein aggregation alters the peak dispersion pattern. As a future direction, mutation of these perturbed residues would be a good confirmation of their role in iron binding.

Determining the structure of the multiprotein complex would provide real insight into how the complex functions. This is a major goal of our lab, through collaboration with Dr. Amy Rosenzweig's laboratory (Northwestern University). As the Dfh protein has been found to be much more stable than its yeast and human counterparts, it would serve as a great starting point to attempt to crystallize the cysteine desulfurase/Isd11/Isu/Frataxin (SDUF) proteins in the *Drosophila* system considering the poor stability of the yeast proteins.

5.3 Conclusion

One of the main goals of the Stemmler laboratory is to provide insight into role of the mitochondrial iron binding protein Frataxin in cellular iron homeostasis. There is much speculation over the role of Frataxin as a possible iron chaperone for iron-sulfur cluster assembly. Our work, along with others, have shown that Frataxin binds iron, and binds Isu, in a stable complex that appears to enhance iron-sulfur cluster assembly on Isu, a behavior consistent with that of a metal chaperone [15, 24, 25]. The bulk of my thesis was to characterize the initial Fe delivery site by Frataxin/Fe(II) acceptance site on Isu. Residues on the C-terminus of Isu, upon mutagenesis to alanine, show a perturbation upon iron and holo-Yfh1WT binding. A crystal structure would confirm these being the ligands of the 6-coordinate Isu-Fe (II) complex determined by XAS. In addition, this would reveal the residues that form the protein-protein interface. This would serve as a good starting point for drug design of molecules that can mimic Frataxin's activity as there is yet no cure for Friedreich's Ataxia (FRDA) [8]. On the same note, the crystal structure of Dfh along with its extraordinary stability would serve as a good starting point for crystallization of holo Dfh-DIsu and holo SDUF.

REFERENCES:

1. Theil, E.C. and K.N. Raymond, *Transition-metal storage, transport and biomineralization*. 1994, University Science Books: Mill Valley, CA. p. 1-37.
2. Mackenzie, E.L., K. Iwasaki, and Y. Tsuji, *Intracellular iron transport and storage: from molecular mechanisms to health implications.* Antioxidants & redox signaling, 2008. **10**(6): p. 997-1030.
3. Collman, J.P., et al., *Structure of an iron(II) dioxygen complex; a model for oxygen carrying hemeproteins.* Proc Natl Acad Sci U S A, 1974. **71**(4): p. 1326-9.
4. Switzer, R.L., *Non-redox roles for iron-sulfur clusters in enzymes.* Biofactors, 1989. **2**(2): p. 77-86.
5. Layer, G., et al., *Structure and function of radical SAM enzymes.* Current opinion in chemical biology, 2004. **8**(5): p. 468-476.
6. Grodick, M.A., et al., *DNA-Mediated Signaling by Proteins with 4Fe–4S Clusters Is Necessary for Genomic Integrity.* Journal of the American Chemical Society, 2014.
7. Bencze, K.Z., et al., *The structure and function of frataxin.* Crit Rev Biochem Mol Biol, 2006. **41**(5): p. 269-91.
8. Santos, R., et al., *Friedreich ataxia: molecular mechanisms, redox considerations, and therapeutic opportunities.* Antioxid Redox Signal, 2010. **13**(5): p. 651-90.
9. Pandolfo, M., *Friedreich's ataxia: clinical aspects and pathogenesis.* Semin Neurol, 1999. **19**(3): p. 311-21.

10. Zecca, L., et al., *Iron, brain ageing and neurodegenerative disorders.* Nature Reviews Neuroscience, 2004. **5**(11): p. 863-873.

11. Crichton, R.R., D.T. Dexter, and R.J. Ward, *Brain iron metabolism and its perturbation in neurological diseases*. 2012: Springer.

12. Przybyszewska, J. and E. Zekanowska, *The role of hepcidin, ferroportin, HCP1, and DMT1 protein in iron absorption in the human digestive tract.* Prz Gastroenterol, 2014. **9**(4): p. 208-13.

13. Lovejoy, D.B. and G.J. Guillemin, *The potential for transition metal-mediated neurodegeneration in amyotrophic lateral sclerosis.* Front Aging Neurosci, 2014. **6**: p. 173.

14. Finney, L.A. and T.V. O'Halloran, *Transition metal speciation in the cell: insights from the chemistry of metal ion receptors.* Science, 2003. **300**(5621): p. 931-6.

15. Cook, J.D., et al., *Molecular details of the yeast frataxin-Isu1 interaction during mitochondrial Fe-S cluster assembly.* Biochemistry, 2010. **49**(40): p. 8756-65.

16. Kondapalli, K.C., et al., *Drosophila frataxin: an iron chaperone during cellular Fe-S cluster bioassembly.* Biochemistry, 2008. **47**(26): p. 6917-27.

17. Tsai, C.L. and D.P. Barondeau, *Human frataxin is an allosteric switch that activates the Fe-S cluster biosynthetic complex.* Biochemistry, 2010. **49**(43): p. 9132-9.

18. Shi, H., et al., *A cytosolic iron chaperone that delivers iron to ferritin.* Science, 2008. **320**(5880): p. 1207-10.

19. Shimomura, Y., et al., *The asymmetric trimeric architecture of [2Fe-2S] IscU: implications for its scaffolding during iron-sulfur cluster biosynthesis.* J Mol Biol, 2008. **383**(1): p. 133-43.

20. Shi, R., et al., *Structural basis for Fe-S cluster assembly and tRNA thiolation mediated by IscS protein-protein interactions.* PLoS Biol, 2010. **8**(4): p. e1000354.

21. He, Y., et al., *Yeast frataxin solution structure, iron binding, and ferrochelatase interaction.* Biochemistry, 2004. **43**(51): p. 16254-62.

22. Musco, G., et al., *Towards a structural understanding of Friedreich's ataxia: the solution structure of frataxin.* Structure, 2000. **8**(7): p. 695-707.

23. Musco, G., et al., *Assignment of the 1H, 15N, and 13C resonances of the C-terminal domain of frataxin, the protein responsible for Friedreich ataxia.* J Biomol NMR, 1999. **15**(1): p. 87-8.

24. Kondapalli, K.C., et al., *NMR assignments of a stable processing intermediate of human frataxin.* Biomol NMR Assign, 2010. **4**(1): p. 61-4.

25. Tsai, C.L., J. Bridwell-Rabb, and D.P. Barondeau, *Friedreich's ataxia variants I154F and W155R diminish frataxin-based activation of the iron-sulfur cluster assembly complex.* Biochemistry, 2011. **50**(29): p. 6478-87.

ABSTRACT

CHARACTERIZATION OF INITIAL IRON BINDING LOCATION AND THE STRUCTURE/IRON BINDING SITE ON *S. CEREVISIAE* ISU AND ON *D. MELANOGASTER* FRATAXIN

by

ANDRIA RODRIGUES

May 2015

Advisor: Prof. Timothy L. Stemmler, PhD.

Major: Biochemistry and Molecular Biology

Degree: Doctor of Philosophy

Iron-induced free radical damage has been implicated in the pathology of diseases of iron overload such as Friedreich's Ataxia, a genetic disorder characterized by an accumulation of iron in actively metabolizing tissues ultimately leading to cardio- and neuro- degeneration and cell death. It is caused by an inability to synthesize the mitochondrial protein, frataxin. Frataxin has been shown by numerous groups to be a part of the iron-sulfur cluster (ISC) multicomplex, where it functions in the capacity of a potential iron provider and an allosteric modulator of both the cysteine desulfurase and scaffold protein ISU. My research has been focused on studying the interaction between frataxin and ISU, particularly the mechanism of iron binding/ iron acceptance by ISU from frataxin. Using XAS, the Stemmler laboratory characterized the ISU-Fe(II) bound complex in four orthologs and found that ISU appears to bind iron in a 6 coordinate oxygen/nitrogen ligand environment. The absence of any thiol ligation to metal indicates iron loading onto ISU occurs at a site distinct from its cysteine rich active

site. Using site directed mutagenesis, followed by biochemical and biophysical analysis of the mutant proteins in the yeast system, we demonstrate that charged residues E144A and D145A possibly form the interface between iron loaded frataxin and ISU and are involved in initial iron acceptance by ISU.

In this thesis, we also describe the crystal structure of Frataxin in D. melanogaster (Dfh). Dfh is well-folded with an α-β sandwich motif comprising two α-helices and six β-strands sandwiched between the two helices like its yeast and human homologs. The Dfh protein does not have a long unstructured N-terminal region like that seen in the yeast and human proteins and it has a considerably longer C-terminal tail; two factors that could contribute to its extraordinary stability. ^{15}N HSQC experiments performed on Dfh in the presence of iron show that the majority of the perturbed residues lie on the α helix-1 and β-strands 1 & 2 region; this is in the region of the conserved acidic patch shared by frataxin proteins indicating an iron binding/ chaperone role for Dfh. As the Dfh protein has been found to be much more stable than its yeast and human counterparts, it would serve as a great starting point to attempt to crystallize the cysteine desulfurase/Isd11/Isu/frataxin (SDUF) proteins in the *Drosophila* system considering the poor stability of the yeast proteins.

AUTOBIOGRAPHICAL STATEMENT

I was born and raised in the city of Dubai, United Arab Emirates, when it was still a small city sans the skyscrapers it is famous for today. I am however, a native of the state of Goa, India well known for its coconut palms and beautiful beaches facing the Arabian Sea. I received my Bachelor of Science degree from Bangalore University, India and my Master's degree in Biochemistry from Manipal University, India. I moved to Detroit in the Fall of 2009 to pursue a doctoral degree in Biochemistry & Molecular Biology at Wayne State University's School of Medicine. In addition to science, I enjoy reading and art.

PUBLICATIONS:

- **Rodrigues AV**, Kandegedara AS, Rotondo JA, Dancis A and Stemmler TL: Iron loading site on the Fe-S cluster assembly scaffold protein is unique from the active site, Biometals, submitted
- Rhine MA, **Rodrigues AV**, Urbauer R, Urbauer J, Stemmler TL and Harrop TC: *Proton Induced Reactivity of NO from a {CoNO}8 Complex*, J. Am. Chem. Soc., Sep 10; 136(36): 12560-3
  PMID: 25073017
- Subramanian P, **Rodrigues AV**, Ghimire – Rijal S and Stemmler TL: *Iron chaperones for mitochondrial Fe-S cluster biosynthesis and ferritin iron storage,* Current Opinion in Chemical Biology, Vol. 15: 1 – 7, 2011.
  PMID: 21288761
- M Prakash, JK Shetty, L Rao, S Sharma, **A Rodrigues**, R Prabhu*: Serum paraoxonase activity and protein thiols in chronic renal failure patients,* Indian Journal of Nephrology, Vol. 18: 13 -16, 2008.
  PMID: 20368914

FELLOWSHIPS/ AWARDS:

- Midwest Affiliate Pre-doctoral Fellowship (American Heart Association, 2012-14)
- Third place award, poster presentation (Graduate Exhibition, WSU, 2014)
- Dr. C.P. Lee Travel Award (Dept. of Biochemistry & Molecular Biology, WSU, 2014)
- Dissertation Research Support (Graduate School, WSU, 2012)
- Vice President for Research Award for obtaining external funding (WSU, 2012)
- Graduate School Award for obtaining external funding (WSU, 2012)
- Interdisciplinary Biomedical Sciences Graduate Program Fellowship (WSU – SoM, 2009-2011)